

1. Report No. FHWA/VA-93-R13	2. Government Accession No.	3. Recipient's Catalog No.	
4. Title and Subtitle <i>Field Instrumentation and Measured Response of the I-295 Cable-Stayed Bridge: Part 2—Field Study of Thermal Responses</i>		5. Report Date December 1992	6. Performing Organization Code
		8. Performing Organization Report No. VTRC 93-R13	
7. Author(s) Paul S. Duemmel, Thomas T. Baber, Furman W. Barton, Wallace T. McKeel, Jr.		10. Work Unit No. (TRAIS) HPR Research Study No. 68	
9. Performing Organization Name and Address Virginia Transportation Research Council Box 3817, University Station Charlottesville, Virginia 22903-0817		11. Contract or Grant No.	
		13. Type of Report and Period Covered Final Report – Part B	
12. Sponsoring Agency Name and Address Virginia Department of Transportation 1401 E. Broad Street Richmond, Virginia 23219		14. Sponsoring Agency Code	
		15. Supplementary Notes None	
16. Abstract <p>This report describes the results of a field study of the thermal responses of a cable-stayed bridge. Data were gathered from the I-295 James River Bridge, a precast segmental concrete bridge with a cable-stayed main span consisting of twin box girders connected by delta frames.</p> <p>The thermal gradient and associated thermal strains in the box girders and pylons were measured using an extensive array of thermocouples and strain-gaged reinforcing bars installed at selected locations in the main-span box girder and south pylon. The temperature and strain response data were compared with that predicted from detailed finite element models of the structure using both frame and plate elements. Comparison revealed a complex three-dimensional strain pattern dependent on the wind direction and the angle of solar incidence. Simplified beam element models were unable to predict many of the observed local variations in thermal strain, which are influenced by wind direction, solar heating direction, proximity to the web, and the existence of parapets monolithic with the deck. Three-dimensional finite element models appear to be more capable of predicting the kind of three-dimensional strains observed, but quantitative agreement with the observed thermal strains was limited at best.</p>			
17. Key Words Thermal tests, prestressed concrete, cable-stayed bridges, field testing.		18. Distribution Statement No restriction. This document is available to the public through the National Technical Information Service, Springfield, VA 22161.	
19. Security Classif. (of this report) Unclassified	20. Security Classif. (of this page) Unclassified	21. No. of Pages 86	22. Price



**FINAL REPORT**

**FIELD INSTRUMENTATION AND MEASURED RESPONSE  
OF THE I-295 CABLE-STAYED BRIDGE:  
PART 2—FIELD STUDY OF THERMAL RESPONSES**

**Paul S. Duemmel  
Graduate Research Assistant**

**Thomas T. Baber  
Faculty Research Scientist**

**Furman W. Barton  
Faculty Research Scientist**

**Wallace T. McKeel, Jr.  
Research Manager**

(The opinions, findings, and conclusions expressed in this report are those of the authors and not necessarily those of the sponsoring agencies.)

**Virginia Transportation Research Council  
(A Cooperative Organization Sponsored Jointly by the  
Virginia Department of Transportation and  
the University of Virginia)**

**In Cooperation with the U.S. Department of Transportation  
Federal Highway Administration**

**Charlottesville, Virginia**

**December 1992  
VTRC 93-R13**

**BRIDGE RESEARCH ADVISORY COMMITTEE**

C. A. NASH, Chairman, Suffolk District Administrator, VDOT

W. T. MCKEEL, Executive Secretary, Senior Research Scientist, VTRC

G. W. BOYKIN, Suffolk District Materials Engineer, VDOT

N. W. DILLON, Salem District Structures & Bridge Engineer, VDOT

M. T. KERLEY, Salem District Structures and Bridge Engineer, VDOT

T. F. LESTER, Structures and Bridge Division, VDOT

L. L. MISENHEIMER, Staunton District Bridge Engineer, VDOT

C. NAPIER, Structural Engineer, Federal Highway Administration

W. L. SELLARS, Lynchburg District Bridge Engineer, VDOT

D. B. SPRINKEL, Culpeper District Structures and Bridge Engineer, VDOT

J. F. J. VOLGYI, JR., Structures and Bridge Division, VDOT

L. R. L. WANG, Professor of Civil Engineering, Old Dominion University

R. E. WEYERS, Professor of Civil Engineering, VPI & SU

**FINAL REPORT**  
**FIELD INSTRUMENTATION AND MEASURED RESPONSE**  
**OF THE I-295 CABLE-STAYED BRIDGE:**  
**PART 2—FIELD STUDY OF THERMAL RESPONSES**

**Paul S. Duemmel**  
**Graduate Research Assistant**

**Thomas T. Baber**  
**Faculty Research Scientist**

**Furman W. Barton**  
**Faculty Research Scientist**

**Wallace T. McKeel, Jr.**  
**Research Manager**

**INTRODUCTION**

**Cable-Stayed Bridges**

Two relatively recent developments in bridge technology, segmentally erected, prestressed, concrete box girders and cable-stayed support systems, were employed on the James River Bridge near Richmond, Virginia. These innovations result in speedy erection and efficient use of high-strength materials, as well as pleasing aesthetics.

Until the early 1970s, concrete was not used extensively in cable-stayed bridges because of its relatively low strength-to-weight ratio, but recent design simplifications have helped make it more competitive (Muller & McCallister, 1988). Segmental construction, by means of the cantilever method, is ideally suited to the stay cable support system (Mathivat, 1983). The cable-stayed segmental bridge scheme provides a number of benefits, in addition to some economic advantages. Concrete superstructures are well suited to stay cable configurations because the horizontal component of cable-stay forces produces prestressing in the deck. Concrete bridges also have favorable vibration damping characteristics, and their small live load-to-dead load ratio limits live load deflections. Today, cable-stayed segmental bridges are competitive for intermediate spans that had previously been constructed using variable depth box girders. The James River Bridge, with a main span of 630 ft, is in this category.

Cable-stayed, segmentally erected, prestressed bridges are challenging to analyze and design. The typical arrangement of several continuous spans with

multiple supporting cables makes these structures highly statically indeterminate. In addition to the complications introduced by multistage post-tensioning, stay cable nonlinearity, and time-dependent deformations, and the complexity of the load deformation response, the bridge behavior under complicated time-varying systems of thermal and mechanical loads must be determined. In particular, serious problems have been attributed to the underestimation of thermal stresses and lack of consideration or the underestimation of the effects of thermal gradients (Elbadry & Ghali, 1986).

Numerous methods for analyzing segmental prestressed and cable-stayed bridges have been developed. Although these computational methods can estimate structural response to a variety of thermal and mechanical loadings, the information is meaningful only if it models the actual behavior of the bridge. Thermal effects on bridge superstructures have not been clearly established, and further information concerning the effects of temperature differentials is necessary in order to evaluate modifications in bridge design specifications (Imbsen et al., 1985). Field testing of complex bridge designs is therefore essential to allow the insight needed to construct valid computer models and gain insight into the actual behavior of bridges built using new and innovative structural technology.

### James River Bridge

The I-295 James River Bridge is a segmentally erected, precast, post-tensioned, cable-stayed box girder bridge located approximately 15 miles southeast of Richmond, Virginia. The bridge has 28 spans, including approach spans. The focus of this study was a 7-span continuous section, which includes the 630-ft main (river crossing) span and three 150-ft approach spans at each end. The main span and the two adjacent spans on each side of the river are supported by a system of 52 cable stays arranged in a single plane harp configuration. The stays emanate from a pair of 290-ft pylons located on either side of the river. An elevation drawing of the bridge is shown in Figure 1.

The bridge deck is composed of twin box girders joined by a closure pour along the center line of the structure. The forces from the cable stays are transferred to the twin box girders through a series of precast delta frame assemblies located between the girders at each stay location, as shown in Figure 2. The main span of the bridge was constructed by the cantilever method, with each side built outward from the pylon and connected by a closure pour at midspan. The segments are joined by epoxy cement and post-tensioning strands within the girders. The box girders are externally post-tensioned by a system of multiple tendons anchored within the girder segments. Figure 3 shows the cross-sectional dimensions of the main span segments, which are 10 ft long and weigh approximately 70 tons each. The bridge superstructure is supported on precast, segmental piers. The pylons are cast in place below deck level and are precast and segmental beginning 6 ft above the deck. Figure 4 shows the twin box girders at the main pier/pylon locations.

The James River Bridge was completed in April 1990. It is the first cable-stayed bridge in Virginia and the first to employ the twin parallel box girder

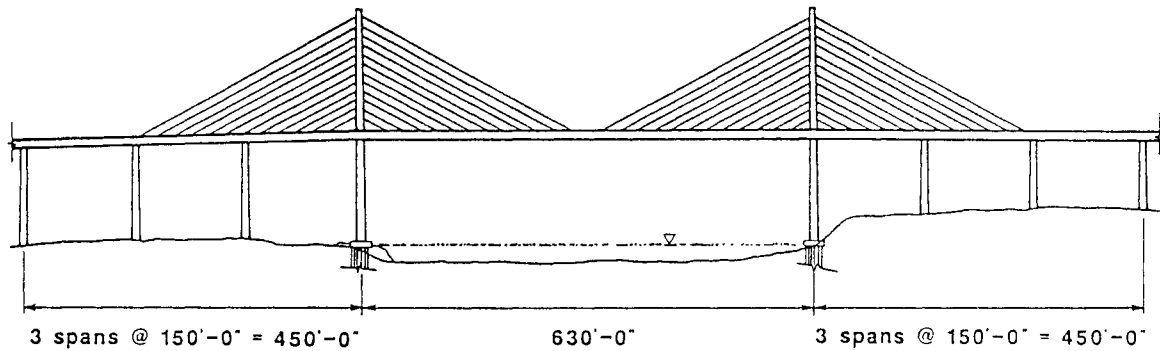


Figure 1. Central Spans of the I-295 Bridge.

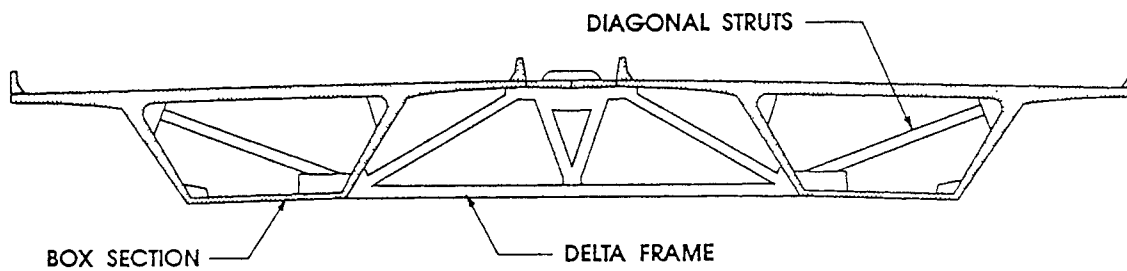


Figure 2. Cross Section of Twin Box Girder Showing Typical Delta Frame.

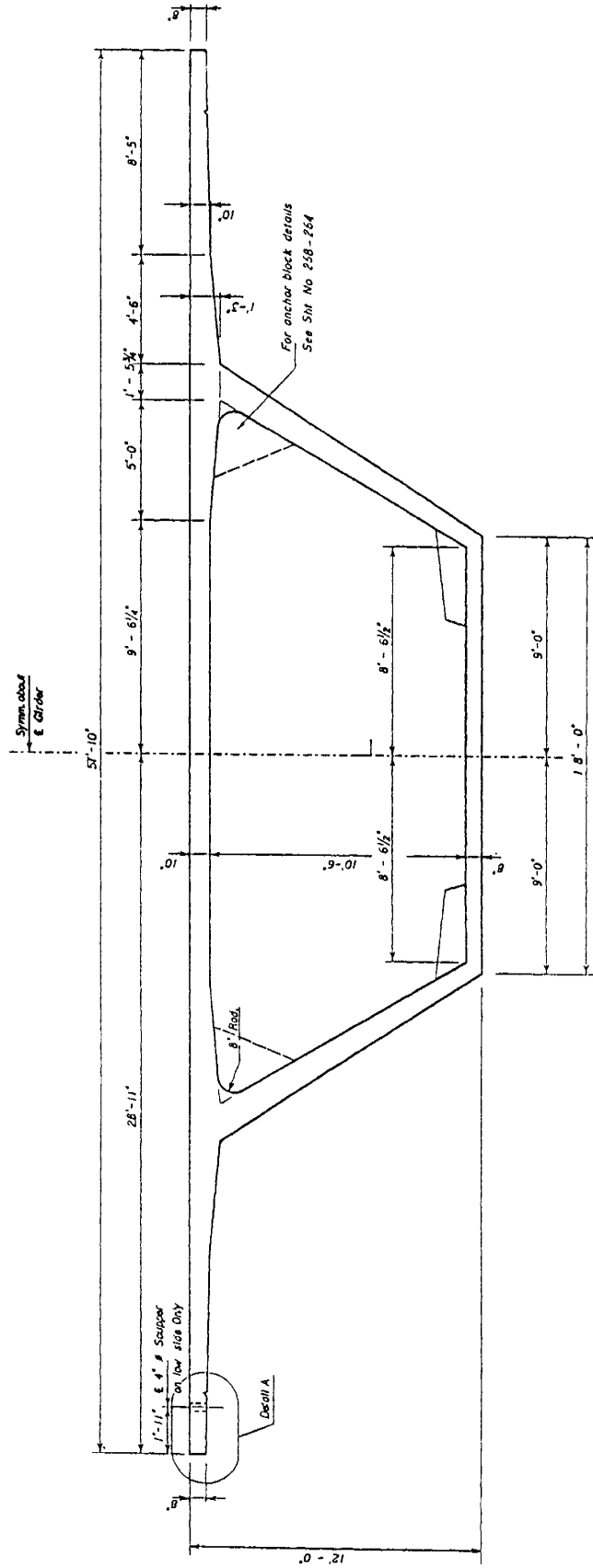


Figure 3. Dimensions of Box Girder Cross Section.

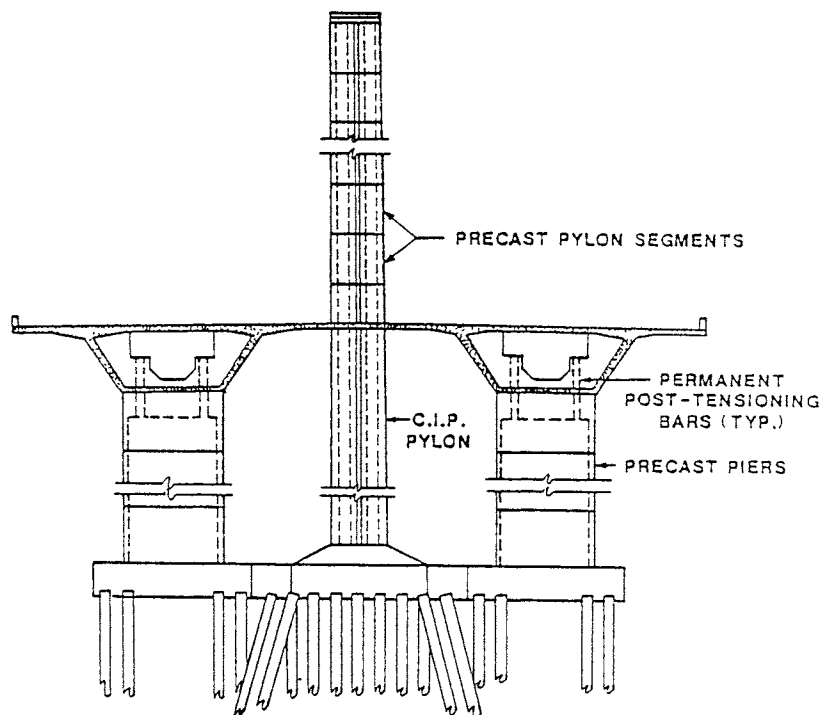


Figure 4. Bridge Section at Main Pier/Pylon Locations. CIP = cast in place.

deck supported by a single plane of cable stays. This innovative scheme required less material than a single box girder of the same width, and the need for special construction equipment was significantly reduced (Muller & McCallister, 1988).

## PURPOSE AND SCOPE

A research team from the University of Virginia (UVa) and the Virginia Transportation Research Council (VTRC) conducted the current field study of the thermal responses of a segmental, cable-stayed, box girder bridge. A companion report describes a study of live load responses carried out concurrently with this study (Duemmel et al., 1992).

The overall objective of the UVa/VTRC study was to determine the important stresses of the James River Bridge during construction by the measurement of field responses. Previous work included measurement of strains in the box girders and cable stays during construction (Barton et al., 1991; Mohr, 1989). The objective of the present research was to investigate the thermal gradient and resulting thermal stresses in the box girders and pylons. To meet this objective, three tasks were undertaken:

1. A literature review was conducted of the methods used to conduct thermal analyses of box girder bridges.

2. The thermal response of the structure was measured over a 10-day period by thermocouples and strain-gaged reinforcing bars installed in box girder and pylon segments.
3. Measured temperature distributions were used in conjunction with finite element models (frame and plate) to predict the daily variations in strain recorded at the instrumented segments. The strains computed from each of the models were compared with those measured in the field.

## LITERATURE REVIEW

Bridge structures are continuously subjected to temperature changes because of varying climatic conditions. Differential heating and cooling of box girder and pylon sections cause deformations, which, when restrained, result in complex states of stress. Thermally induced stresses may be on the same order of magnitude as those attributable to applied vehicle loading, emphasizing the need to consider thermal effects on concrete bridges (Waldron et al., 1990). Serious cracking in concrete bridges has been attributed to thermal stresses resulting from temperature gradients within box girder bridges (Podolny, 1985).

A comprehensive study of thermally induced stresses in prestressed concrete bridge superstructures conducted by the American Association of State Highway and Transportation Officials (AASHTO) illustrated the lack of a unified approach to thermal gradient effects in design at both domestic and international levels (Imbsen et al., 1985). Current AASHTO specifications have provisions for uniform temperature variation in bridge decks but do not provide guidance for temperature variations within members. The Post-Tensioning Institute's (PTI) *Precast Segmental Box Girder Bridge Manual* (1978) provides methods for considering differential temperatures, as do some international codes, but variations are considerable. Surveys of state bridge officials indicate few cases of thermal distress, even though the effects of thermal gradients are often ignored. The lack of serious problems does not suggest that design procedures are adequate, but it has led to skepticism among bridge designers as to the need for accurate but complicated thermal design procedures.

The AASHTO study stated that measured thermal gradients and resulting thermal stresses in concrete box girder bridges were sufficiently large to warrant consideration by designers. Theoretical stresses calculated from measured temperature gradients were often inconsistent with observed bridge performance, however. This suggests the possibility that thermally induced stresses may not be as high as predicted or that bridge structures may have higher inherent strength than is thought. Since most thermal-related problems affect serviceability rather than strength, more information will be needed to convince designers of the need for elaborate thermal design procedures. Although problems are not critical with present bridge designs, the trend toward cross-section optimization in long superstructures increases the need for accurate and consistent thermal gradient design methods (Imbsen et al., 1985).

The distribution of temperature throughout the cross section of a box girder bridge is governed by three principal heat transfer mechanisms: radiation (which includes reradiation), conduction, and convection. These mechanisms are, in turn, influenced by a number of factors, including bridge geometry, orientation, and geographic location; variations of solar radiation; ambient temperature; wind; and thermal properties of bridge materials (Waldron et al., 1990). Previous studies have shown that the temperature distributions within concrete box sections are nonlinear because of the continuously varying thermal environment and the relatively poor thermal conductivity of the concrete itself. Thermal gradients occur through the depth of the box girder, as well as through the thickness of the flanges and webs. Large thermal gradients have been shown to cause severe cracking in a number of box girder bridges (Podolny, 1985; Priestly, 1978). Numerical methods, such as finite difference and finite element methods, have been used in transient heat flow analyses to predict temperature distributions within box girders accurately using measured climatic data as input (Elbadry & Ghali, 1983; Potgieter & Gamble, 1983; Rao, 1986).

A nonlinear temperature distribution through the depth of a box girder member will result in a comparable nonlinear strain distribution since the level of strain in each fiber is proportional to the temperature at that location. The free thermal strain distribution can be separated into three components: uniform, linear, and nonlinear, shown in Figure 5. If the section is unrestrained, it may elongate and bend because of the uniform and linear strain components. The remaining nonlin-

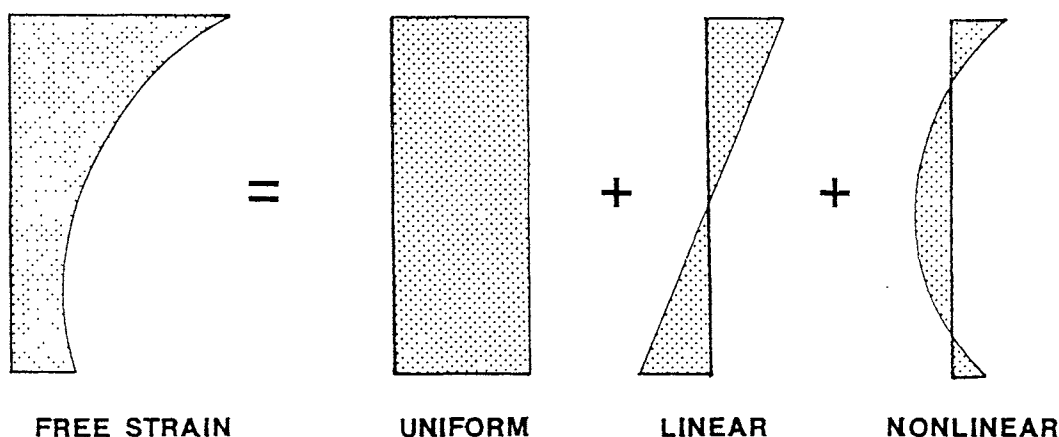


Figure 5. Components of Nonlinear Thermal Strain Distribution.

ear strain results in self-equilibrating stresses; i.e., the net resultant axial force and bending moment are zero. This situation is shown in Figure 6.

If the section is fully restrained, the temperature-induced deformations cannot occur, resulting in a system of stresses having the same distribution as the free strain in Figure 5. The restraint of the thermally induced deformations causes additional stresses in the member. Multi-ply indeterminate bridges, such as the cable-stayed bridge in this study, provide significant restraint and are thus subjected to stresses not present in bridges with simply supported spans.

Transverse thermal gradients occur through the thickness of the walls of a box girder section and result in strain distributions similar to those shown in Figure 5. If the girder is heated uniformly, the walls of the section will expand equally and no additional stresses will be developed. If differential heating occurs on the top flange, for example, the cross section will deform as shown in Figure 7. The section acts as a frame in resisting this deformation, generating significant transverse stresses, which are usually ignored in design (Waldron et al., 1990).

Little work has been conducted toward measuring temperature variations and thermal stresses in concrete pylon structures. As with box girders, differential heating will result in a thermal gradient across the pylon's cross section. The pylon sections are more massive than the box girders, however, and the thickness of the exterior walls will limit the thermal variations within their core. In effect, the exterior walls of the pylon, especially those with southern and western exposures, will be subjected to large changes in temperature. The temperatures within the section

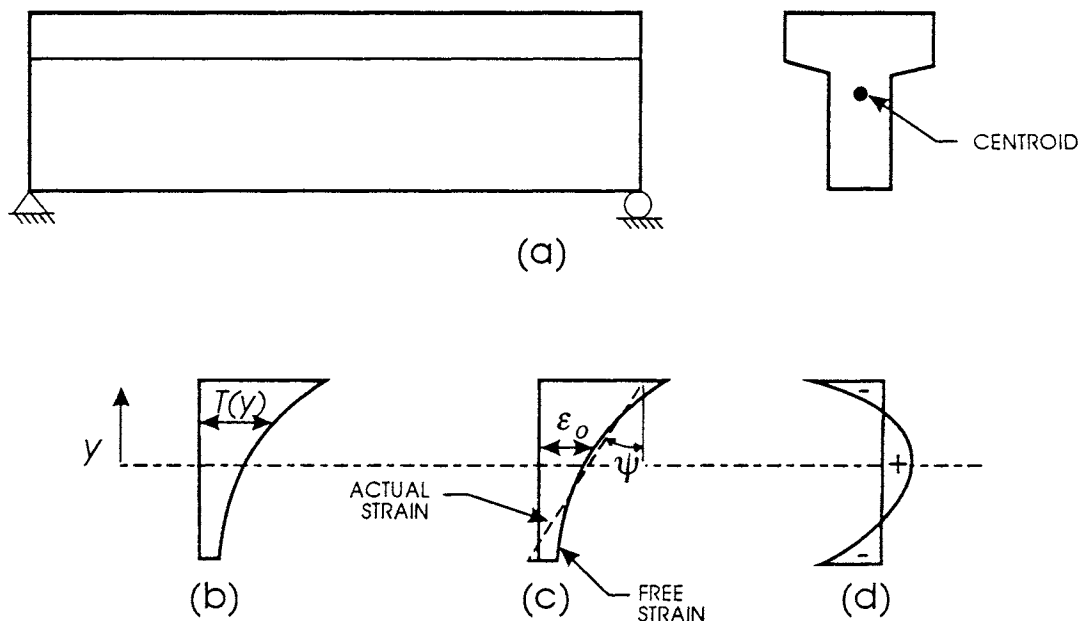


Figure 6. Stresses in Simply Supported Beam Due to Nonlinear Temperature Distribution. CIP = cast in place.

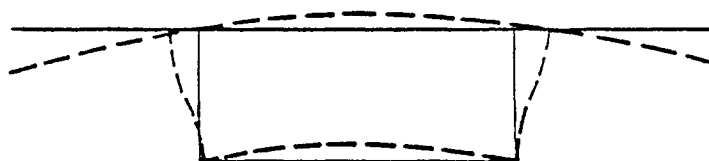


Figure 7. Local Cross-Sectional Thermal Section Distortion.

will vary more slowly. These differences in temperature will result in a complex state of thermal strain and will affect the overall behavior of the bridge.

Analytical methods have been implemented for analysis of box girder bridges subject to thermal loading and varying climatic conditions. Dilger et al. (1983) employed a one-dimensional finite difference program to predict temperature distributions in composite box girder bridges, which considered the effects of geometry, material, and environment. A parametric study was performed to find extreme temperature differences by varying bridge orientation, cantilever length, and girder depth for each season. Temperature distributions were then used as input for a finite element analysis to obtain thermal stress distributions for a two-span continuous bridge.

Potgieter and Gamble (1983) presented a thorough review of the literature concerning the theoretical prediction and experimental measurement of heat flow in bridge superstructures. They developed programs for linear heat flow analysis and subsequent thermal stress analysis. The accuracy of the analytical models was assessed in a field study of a segmental box girder bridge. Theoretical temperature distributions and stress results showed good agreement with field measurements. The authors used weather data from a number of U.S. cities as input for the heat flow model to estimate the variation in temperature distributions in different parts of the country and identify the effects of specific climatic parameters. The thermal response of various cross sections, including 18 existing box girder bridges, was also studied. As a result, specific span configurations at high risk for cracking under

thermal loads were identified, and simplified expressions for determining bridge thermal response were developed.

Churchward and Sokel (1980) used measured temperature data from a box girder bridge to develop an analytical procedure for determining temperature distributions in bridges with similar cross sections. Thermocouples measured temperatures throughout the cross section, and environmental parameters such as ambient temperature, solar radiation, and wind speed were recorded simultaneously. Empirical expressions were developed from the observed nonlinear temperature distributions and were correlated with the environmental parameters. The results showed that temperatures could be predicted reasonably well using a function that considered the maximum temperature differential across the section as the dependent variable. The authors reiterated the need for additional thermal data as well as strain and deflection measurements from other bridges.

Imbsen et al. (1985) conducted a comprehensive study of thermally induced stresses in reinforced and prestressed concrete bridge superstructures. Field measurements of temperature distributions and associated stresses have been documented by numerous investigators. The thermal design provisions in bridge design codes from the United States and abroad were surveyed. Typical design thermal gradients were determined from representative codes and applied to a group of U.S. box girder bridges. Both longitudinal and transverse effects were studied, and the results showed significant differences in calculated stresses depending on the temperature gradient used. Large transverse stresses were identified, although these effects are virtually ignored in practice. The authors suggested design guidelines for thermal effects based on their findings.

Elbadry and Ghali (1983) formulated a solution for heat flow in concrete box girders using the finite element method. A two-dimensional thermal analysis procedure was implemented in a computer program, FETAB, which has the capability of modeling material, solar, wind, and seasonal effects. A parametric study was conducted on a two-span continuous bridge, which yielded extreme temperature variations and thermal stress distributions. Significant stresses were found to develop on summer days having large variations of ambient temperature. Elbadry and Ghali (1986) investigated transverse thermal stresses and discussed the effects of thermal stresses on cracking of concrete box girders.

Rao (1986) formulated a series solution for heat flow in concrete box girders, which was developed into a finite strip thermal analysis program. The effects of different climatic data on temperature distributions and stresses were analyzed, and results were compared with those of the finite difference method. The author's method was shown to be simpler and converged more rapidly than the finite difference solution. Results of a parametric study again showed the significance of high solar radiation and large ambient temperature variations on box girder stresses.

Waldron, Ramezankhani, and Woodman (1990) used a time step thermal finite element analysis based on the work of Elbadry and Ghali to investigate temperature distributions in a box girder bridge located in South Wales, U.K. Their

model measured climatic data as input to establish time-varying boundary conditions. Transverse thermal stresses were obtained using the calculated temperature distributions in a two-dimensional plane strain model. Significant daily stress variations in the webs of the two girder bridges were observed. Results were compared with field data, and the analytical method showed good agreement with measured values. A parametric study was also performed to investigate the effects of cross-sectional configuration on temperature-induced transverse stresses.

## METHODS

### Overview

Thermal gradients and thermally induced stresses were measured within the box girder and pylon members. Measured temperature distributions were used in conjunction with a frame finite element model to predict the daily variations in strain recorded at the instrumented segments. Analysis results from a plate element model of the structure were compared with the measured and predicted thermal response data.

Ideally, thermal response data should be taken during the early summer months, during which large ambient temperature changes and high solar radiation cause the largest thermal gradients within the bridge superstructure. The data analyzed for this report were taken over a 10-day period in November 1989. During this period, the bridge had not been opened to normal traffic and cable-stay retensioning operations were underway. Consequently, some of the strain data were subject to the effects of the changes in cable-stay stresses as well as construction-related traffic on the bridge. During a weekend period, however, there was no construction activity, allowing the thermal response of the bridge to be measured alone. The thermal response data presented in this study were taken during the period from Friday, November 17, through Sunday, November 19, 1989.

### Strain Gage Instrumentation

An extensive array of electrical resistance strain gages mounted on dummy reinforcing bars were installed during construction. Each strain gage was mounted on a 4-ft length of No. 5 reinforcing bar by use of a high-grade epoxy resin cured at an elevated temperature. The gages were waterproofed by use of a layer of epoxy resin followed by a polysulfide compound designed for protection of electronic equipment. An instrumented reinforcing bar is shown in Figure 8. The gaged dummy rebars were tied into the deck and pylon segment reinforcing cages prior to their placement into the precasting forms. Lead wires, jacketed with TFE Teflon for waterproofing, were run along the cages to blockouts in the walls of the segments. After the segment was cast and placed, the lead wires were retrieved and connected directly to the data acquisition system.

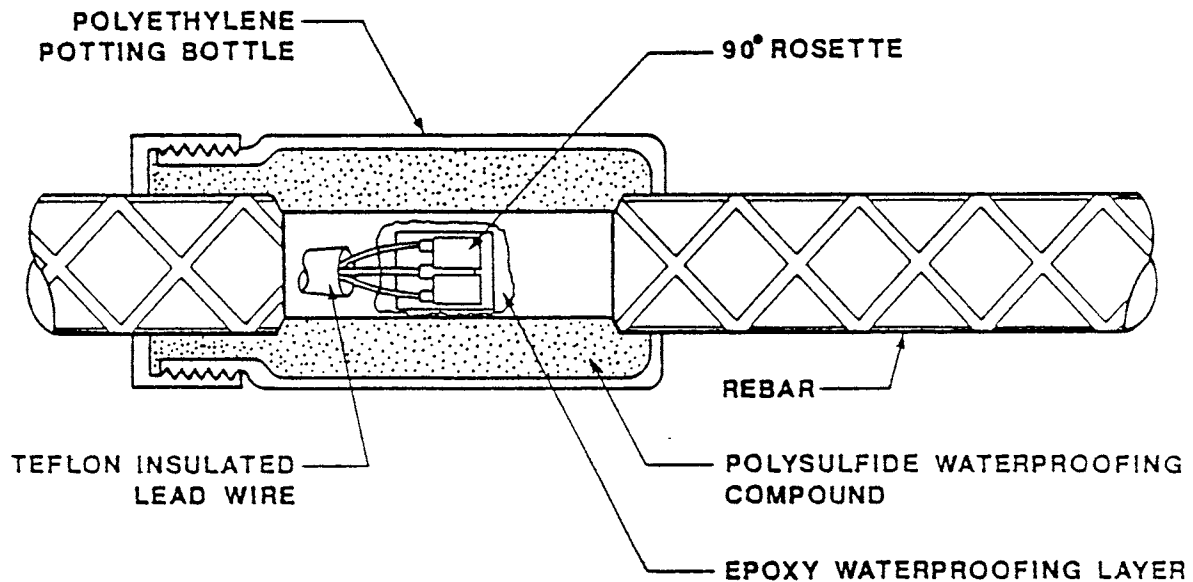


Figure 8. Instrumented Dummy Reinforcing Bar.

In the field, changes in temperature result in apparent strains in addition to the mechanical strains measured by the strain gages. To compensate for these temperature effects, 90-degree rosette gages, consisting of gages oriented parallel and transverse to the axis of the bar, were used. The transverse portion of the rosette then underwent a Poisson strain as well as a compensating thermal strain. When the gages are wired in a Wheatstone half bridge, a small temperature correction appeared but was not significant for the range of temperatures expected during the study.

The gages were mounted along the curve of the rebar rather than on a flat surface, which would have necessitated extra machining. Although mounting the gages on a curve avoids the uncertainties in strain measurement associated with a reduction of bar area, an additional temperature-induced strain is introduced by the curvature of the transverse gage. This apparent strain is a function of the radius of the curved surface, the thicknesses of the gage backing and adhesive, and temperature change. An approximate correction was given by Measurements Group, Inc. (1983) as:

$$\Delta\epsilon_{APP} = \frac{1}{R} [(1 + 2\nu_{A-B})(h_A\alpha_A + h_B\alpha_B) - 2\nu_{A-B}\alpha_S(h_A + h_B)] \Delta T \quad [1]$$

where  $\epsilon_{APP}$  = apparent strain induced by curvature

$R$  = radius of curvature

$\nu_{A-B}$  = Poisson's ratio of adhesive and backing

$h_A, h_B$  = adhesive and backing thickness, respectively

$\alpha_A, \alpha_B$  = thermal expansion coefficients of adhesive and backing, respectively

$\alpha_S$  = thermal expansion coefficient of specimen

$\Delta T$  = temperature change.

Strain gages were installed in three deck segments located in the main span of the bridge. Specifically, the north and southbound lanes of main-span box girder segments 33, 48, and 62 were instrumented with single longitudinal gages and three gage rosettes. Figure 9 shows the locations of the instrumented segments with respect to the south pylon/pier and the center line of the main span. Segment

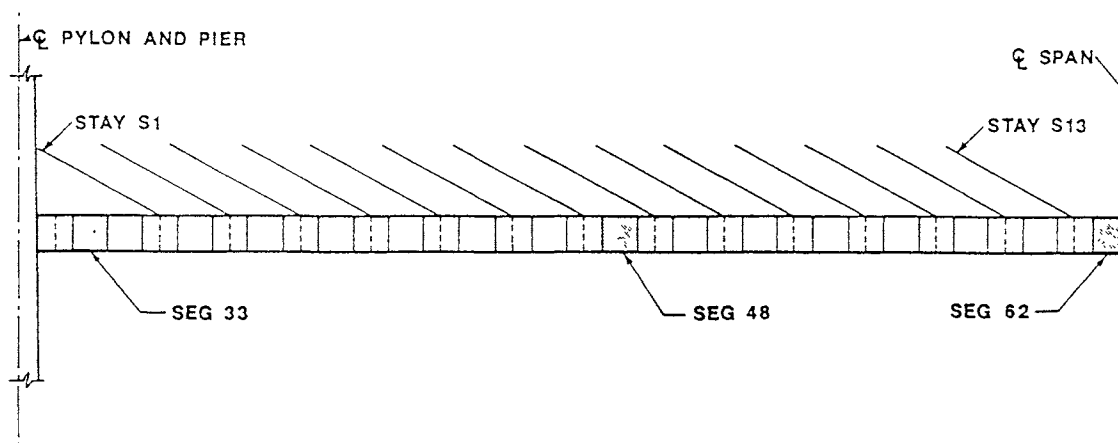


Figure 9. Location of Box Girder Segments Instrumented with Strain Gages.

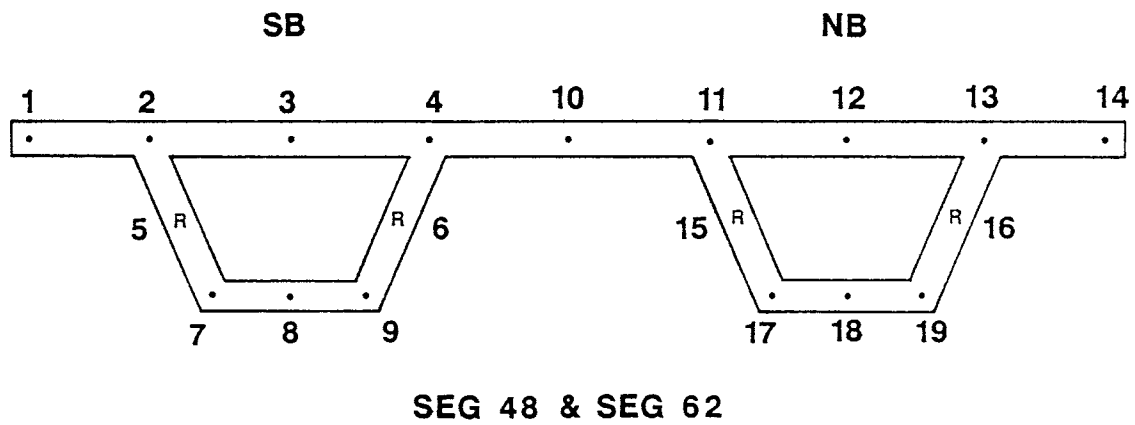
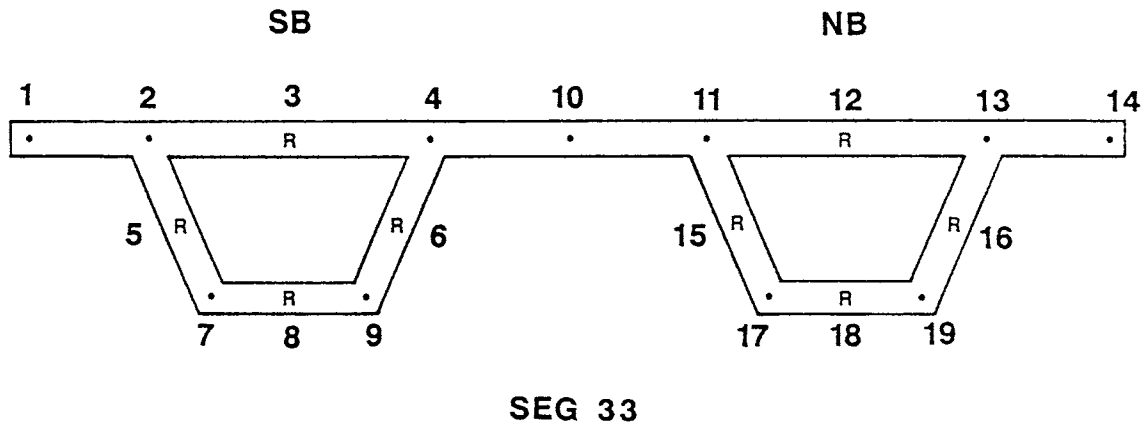


Figure 10. Location of Strain Gages in Instrumented Box Girder Segments.  
 SB = southbound; NB = northbound; • = single gage oriented parallel to the long axis of the bridge; R = strain rosette.

33 is adjacent to the pier, segment 48 is near the quarter span, and segment 62 is at midspan. The locations of the strain gages within each of the segments are shown in Figure 10, where a *dot* represents a single gage oriented parallel to the long axis of the bridge, and an *R* represents the location of a strain rosette. The rosettes consist of three gaged rebars arranged at 45-degree angles and were installed to measure shear strains. Rosette gages were placed in the webs of each instrumented segment. As can be seen in Figure 10, additional rosettes were placed in the top and bottom flanges of segment 33. Readers will wish to refer to Figures 9 and 10 to assist in interpreting the discussion of the field study data.

In view of the complexity of behavior anticipated for box girders, complete instrumentation was not feasible, so the strain gages were arranged to provide data concerning the gross cross-sectional deformations only. The instrumented segments were not connected to delta frames so as to avoid the local cross-sectional distortions likely in these areas. The gage pattern shown in Figure 10 allows the gross cross-sectional flexural strains and the shear strains acting in the four webs to be determined. The additional rosettes in the flanges of segment 33 provide additional information concerning the torsional shear strains at that location.

Two sections of the south pylon were also instrumented with strain-gaged reinforcing bars. The gages were placed vertically in the uppermost cast-in-place section, just above deck level, and in precast segment D6, located beneath cable stay S7. The locations of these sections are shown in Figure 11. Figure 12 depicts the

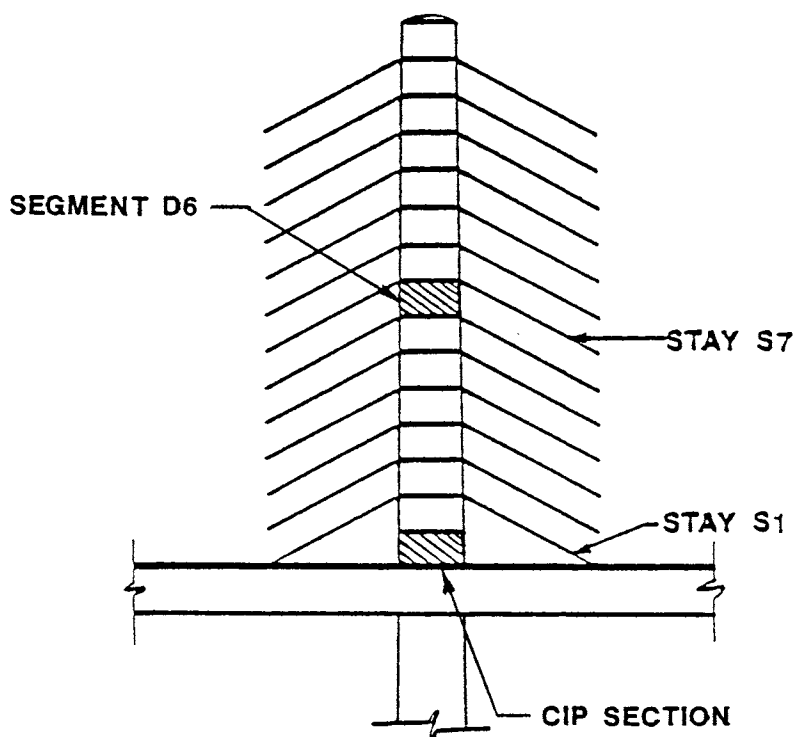


Figure 11. Location of Pylon Segments Instrumented with Strain Gages. CIP = cast in place.

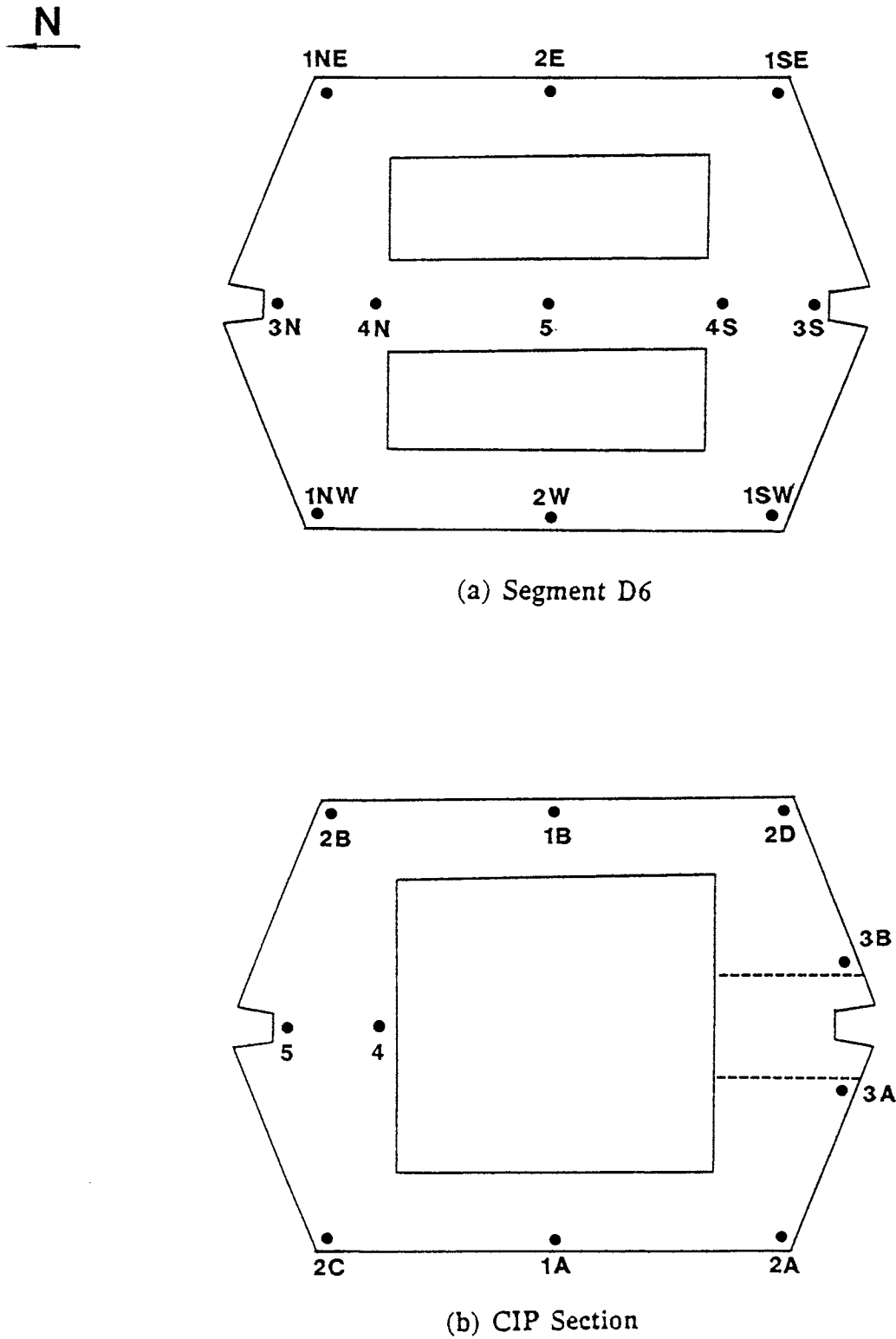


Figure 12. Location of Strain Gages in Instrumented Pylon Segments.  
CIP = cast in place.

locations of the strain gages within the instrumented pylon segments. Readers will wish to refer to Figures 11 and 12 to assist in interpreting the field study data.

### Thermocouple Instrumentation

Thermocouples were installed in the box girder and pylon to measure the temperature variations within these members. Previous research has shown that little variation in temperatures occurs along bridge spans, and the present bridge is essentially straight, except for a small vertical curvature, so a single twin box section of the main span was chosen for instrumentation. Type T thermocouples were placed in the top and bottom flanges of main-span segment 46, as shown in Figure 13. Thermocouples offered sufficient precision for the current study and are less expensive and more rugged than thermistors. Several thermocouples were installed through the thickness of each flange to measure thermal gradients that occurred through the depth of the box girders. Thermocouples were located across the section to determine the differential thermal effects resulting from eastern versus western exposure. The locations of the thermocouples within box girder segment 46 are shown in Figure 14.

Precast pylon segment D6 was also instrumented with an array of thermocouples to correlate data from the strain gages installed at that location. The instrumented pylon segment is shown in Figure 15. Figure 16 shows the locations of

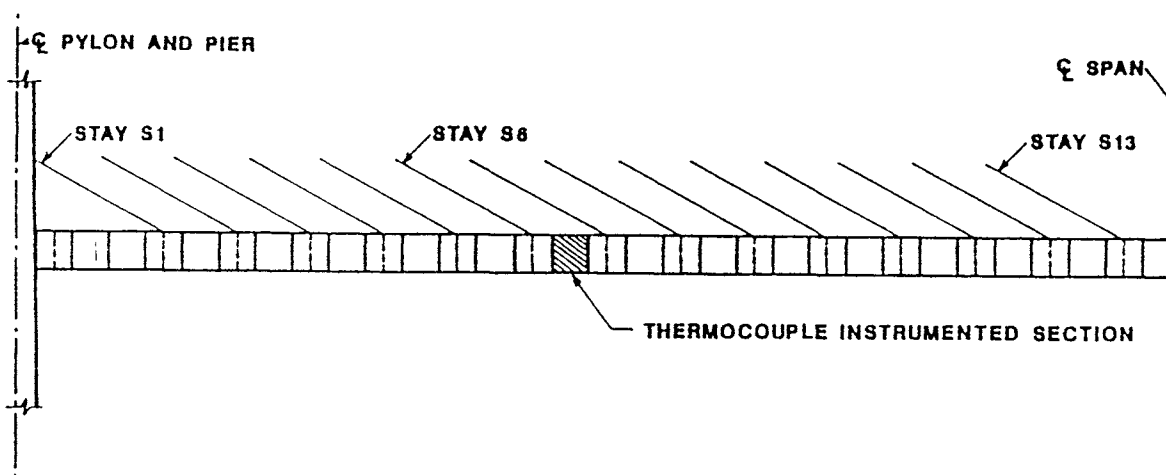


Figure 13. Location of Box Girder Segment Instrumented with Thermocouples.

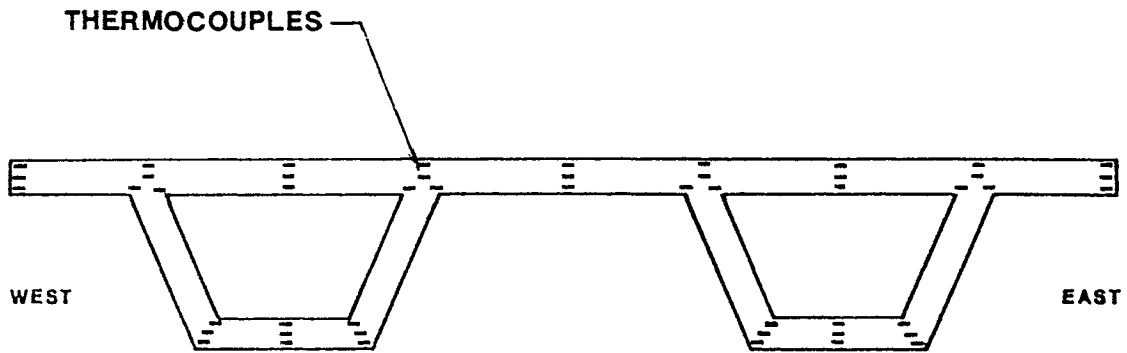


Figure 14. Location of Thermocouples in Instrumented Box Girder Segment.

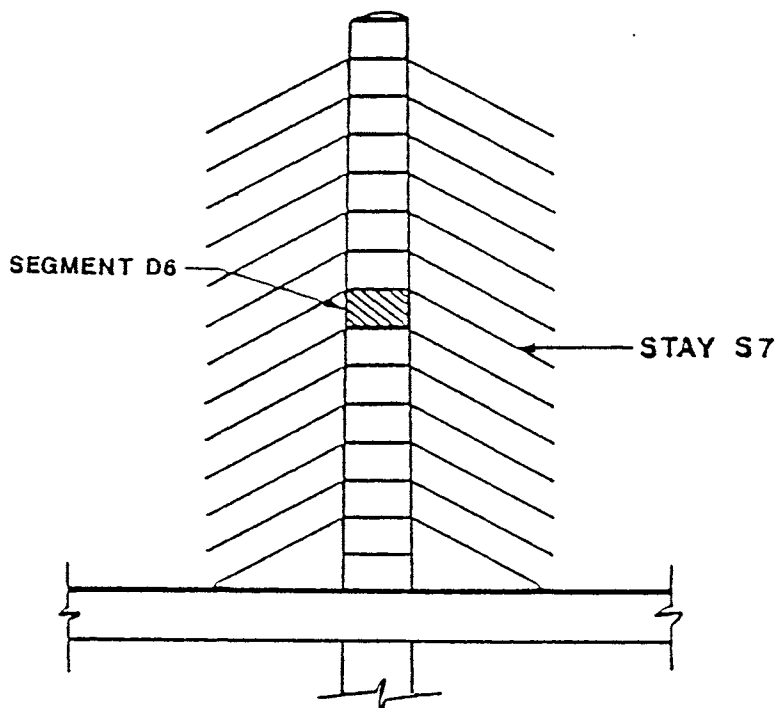


Figure 15. Location of Pylon Segment Instrumented with Thermocouples.

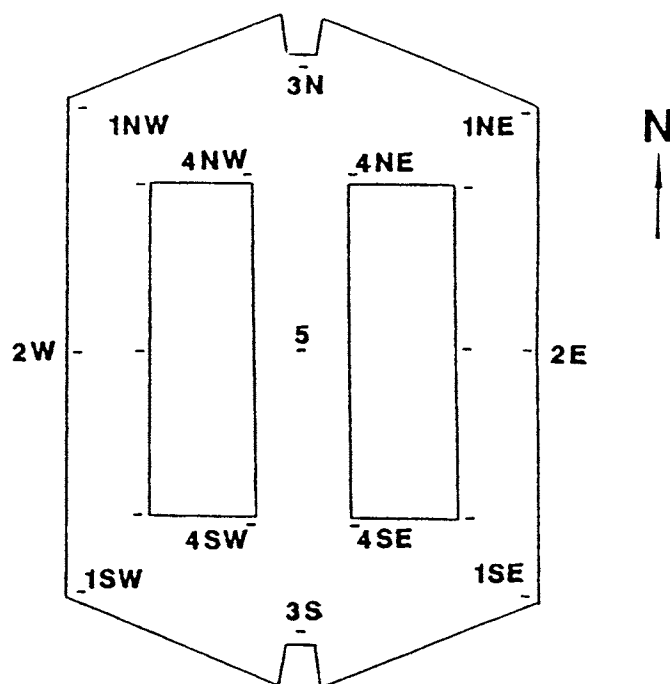


Figure 16. Location of Thermocouples in Instrumented Pylon Segment.

the thermocouples within the cross section. Considerable care was taken in locating the thermocouples within the box girder and pylon cross sections to ensure the accuracy of the measured temperature distributions. Thermocouple wires were attached to the reinforcing cages of the segments and then connected to the data acquisition system after the segments were cast and lifted into place.

### Data Acquisition System

A distributed data acquisition system manufactured by the John Fluke Company was used to obtain the data. The system uses a Helios main controller to communicate with the remote scanning units located in the instrumented bridge segments. The strain gages and thermocouples located in each instrumented section of the bridge were connected to individual scanning units, which in turn were connected to the Helios controller via data lines. The scanning units can read thermocouples and electrical resistance strain gages in various configurations, each requiring a single data acquisition channel. The data were stored on a Compaq portable computer in Lotus 1-2-3 format by means of Helios Toolbox data acquisition software, a QuickBasic program. The system uses 110-volt line power via an uninterruptible power supply (UPS), which provides surge protection and a backup power source. The main controller unit, data logging computer, and UPS are protected in an enclosure cabinet with heating and air conditioner units to maintain operational temperature and humidity limits. Further details of the data acquisition system and instrumentation are provided by Baber and Hilton (1988) and Hayes (1988).

### Model for Prediction of Thermal Strains

The longitudinal stresses induced by nonlinear temperature distributions are of primary interest in this study. Previous field studies have indicated that these stresses are often significant. Transverse stresses resulting from thermal gradients through the thickness of the walls of the box girder cross section, though possibly high, are beyond the scope of this study. Additional field instrumentation, such as strain gages oriented perpendicular to the long axis of the bridge, as well as additional thermocouples located through the thickness of the flanges and webs, would be necessary to predict and measure transverse thermal stresses.

Stresses resulting from thermal gradients can be calculated if one knows the temperature distribution through the depth of a beam. The following procedure is based on the approach presented by Elbadry and Ghali (1986). The simply supported beam in Figure 6(a) is subjected to a vertical gradient of temperature change  $T(y)$ , shown in Figure 6(b), where  $y$  is measured from the centroid of the section. If the section is unrestrained through its depth, the free strain profile is given by

$$\epsilon_f = \alpha_t T(y) \quad [2]$$

where  $\alpha_t$  is the coefficient of thermal expansion. The stress required to restrain this free strain artificially would be

$$\sigma_r = -E\alpha_t T(y) \quad [3]$$

where  $E$  is the modulus of elasticity of the material. The force resultants of this stress over the cross section are

$$N = \int \sigma_r dA \quad [4]$$

and

$$M = \int \sigma_r y dA \quad [5]$$

Assuming that plane sections remain plane in bending, the strain at any fiber is

$$\epsilon = \epsilon_0 + \psi y \quad [6]$$

where  $\epsilon_0$  and  $\psi$  are the axial strain at the centroid and the curvature, respectively. These are given by

$$\epsilon_0 = -\frac{N}{EA} \quad [7]$$

$$\psi = -\frac{M}{EI} \quad [8]$$

where  $A$  and  $I$  are the area and moment of inertia about the centroid. Substituting equations 3 through 5 into 7 and 8 gives the axial strain and curvature of a statically determinate member as a function of temperature change over its depth:

$$\epsilon_0 = \frac{\alpha_t}{A} \int T(y)b dy \quad [9]$$

$$\psi = \frac{\alpha_t}{I} \int T(y)by dy \quad [10]$$

where  $b$  is the width of the section at a depth  $y$ . The relationship between the free strain, axial strain, and curvature are shown in Figure 6(c). The difference between actual strain and the free thermal strain represents the restrained nonlinear strain component of the free strain given by

$$\epsilon_{nl} = \epsilon_0 + \psi y - \alpha_t T(y) \quad [11]$$

and the resulting nonlinear stress distribution, assuming full restraint through the section, is

$$\sigma(y) = E[\epsilon_0 + \psi y - \alpha_t T(y)] \quad [12]$$

These stresses, shown in Figure 6(d), are self-equilibrating; i.e., the net stress resultant is zero.

If the girder shown in Figure 6(a) were continuous over multiple spans, the axial strain and curvature would be restrained and statically indeterminate reactions and moments would result in continuity stresses. The upward displacement of each span resulting from a positive unrestrained curvature  $\psi$  is resisted by the

moment  $M = EI\psi$  in the continuous spans. The statically indeterminate reactions and bending moments caused by the calculated axial strain and curvature can be determined using displacement methods of analysis. The total stress, as a function of depth, at any location along the bridge is then

$$\sigma_t = E[\epsilon_0 + \psi y - \alpha_t T(y)] + \frac{M'y}{I} + \frac{P'}{A} \quad [13]$$

where  $M'$  and  $P'$  are the calculated indeterminate moment and axial force at the section of interest. An examination of equation 13 shows that the longitudinal stresses attributable to a thermal gradient can be calculated at any point within the beam if one knows the temperature distribution, and hence the distribution of temperature change, through the depth of the section.

In this study, the temperature distributions within the box girder and pylon sections were measured with thermocouples. Previous research has shown that little variation in temperature occurs along the length of box girder bridges, so the thermocouple data obtained from segment 46 were considered to be representative of the temperatures at each of the instrumented box girder segments. Likewise, thermocouple data from precast pylon segment D6 were considered representative of the temperatures over the height of the pylon. Since the cable stays were not instrumented with thermocouples, the temperature response of these elements was approximated using thermocouple data measured in the pylon section.

Approximate cross sections were developed to simplify the calculations in equations 9 and 10 and to make the most use of the available thermocouple data. The geometry of the approximate sections was based on the location of the thermocouples and the actual shape of the box girder and pylon cross sections. The dimensions of the approximate sections were calculated such that overall dimensions, area, and section properties of the true cross section were not significantly altered. The approximate box girder cross section is shown in Figure 17. For this section, the tapered webs of the box girder were replaced with webs of constant thickness and the top flange was divided into regions of uniform depth. The approximate pylon cross section is shown in Figure 18. Here, the dimensions of the individual rectangular regions were chosen to correspond with the locations of thermocouples within the section.

The continuity stresses resulting from restraint of the axial strain and curvature were determined using the beam element model developed for the live load study (Duemmel et al., 1992). Forces and moments attributable to respective axial strains and curvatures within the pylon and box girder were applied to the model as end forces, and temperature effects were applied to the cable stays in the form of initial strains. Analysis of the bridge model subject to these forces yielded the indeterminate forces  $P_4$  and  $M_4$  at locations along the box girder and pylon. The internal resultants of interest were found from the end forces of the beam elements corresponding to the instrumented box girder segments. Once the internal forces were

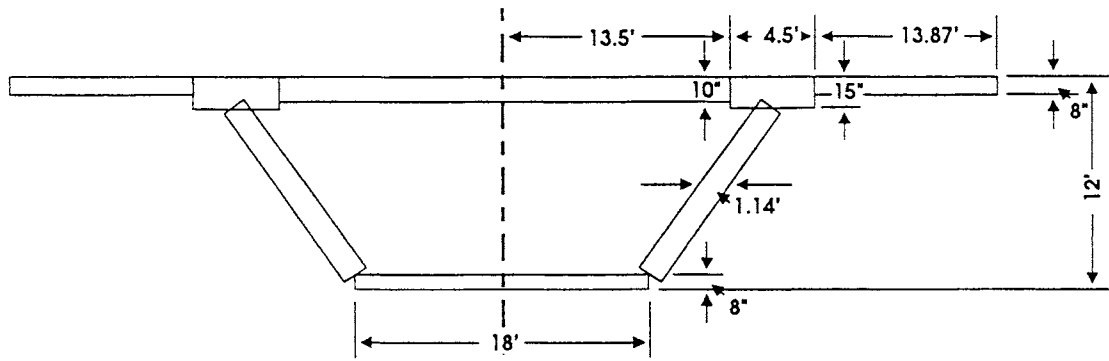


Figure 17. Approximate Box Girder Cross Section.

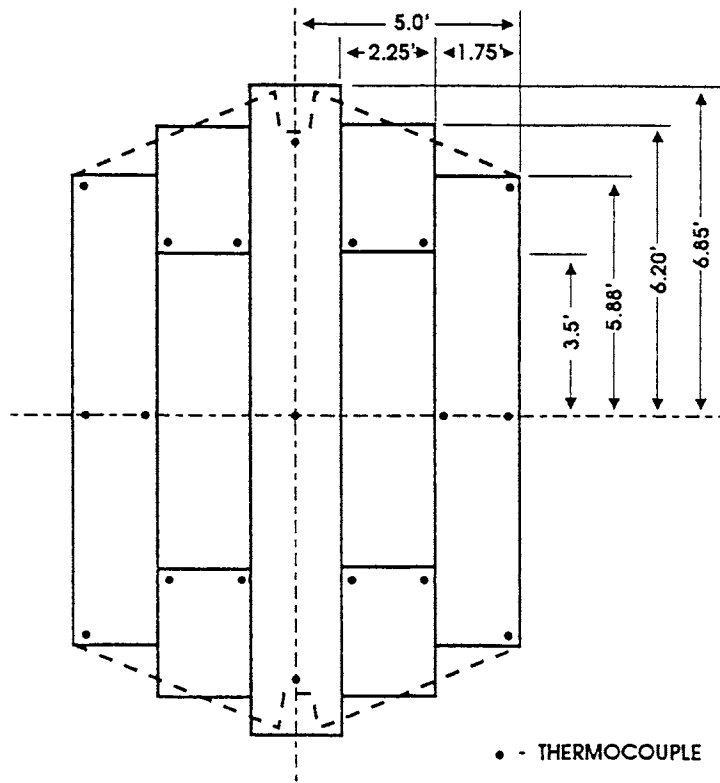


Figure 18. Approximate Pylon Cross Section.

known, the stresses at the levels of the top and bottom strain gages were calculated for each instrumented segment using equation 13.

## RESULTS

### Box Girder Segments

#### Measured Temperature Variations with Time

Temperature data recorded by the thermocouples in segment 46 are presented in Figures 19 through 22. These plots represent temperatures measured in the top and bottom flanges of the box girder over the 3-day period beginning at midnight, November 17. Figure 19 presents temperatures recorded by thermocouples in the vicinity of gages 2 and 7 located near the outer web of the box girder carrying the southbound lanes (see Figure 14). Figure 20 shows data recorded at thermocouples near gages 4 and 6, located at the inner web of the southbound box girder. Similarly, Figures 21 and 22 present temperature variations recorded by thermocouples near the outer and inner webs, respectively, of the northbound box girder.

It is observed from these figures that daily temperature variations on the order of 4 to 8 degrees Celsius occurred within the box girder and an overall cooling

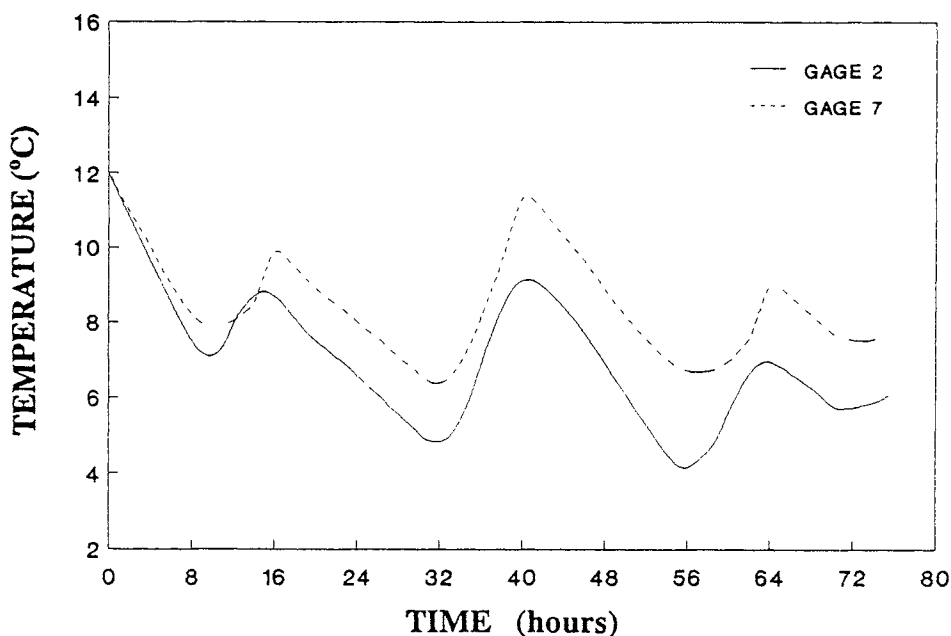


Figure 19. Measured Temperature Variations, Box Girder Segment 46, Southbound Outside Web.

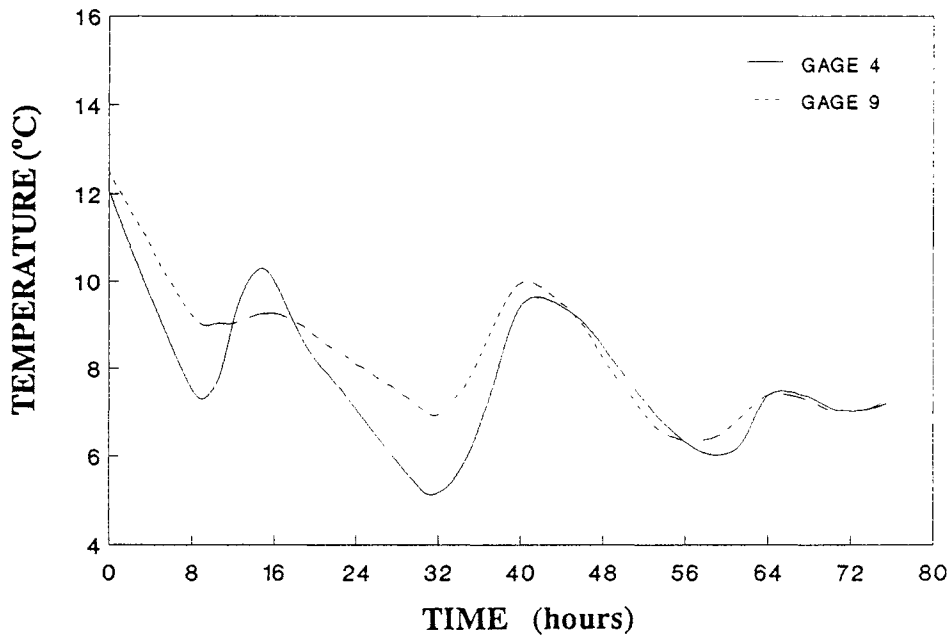


Figure 20. Measured Temperature Variations, Box Girder Segment 46, Southbound Inside Web.

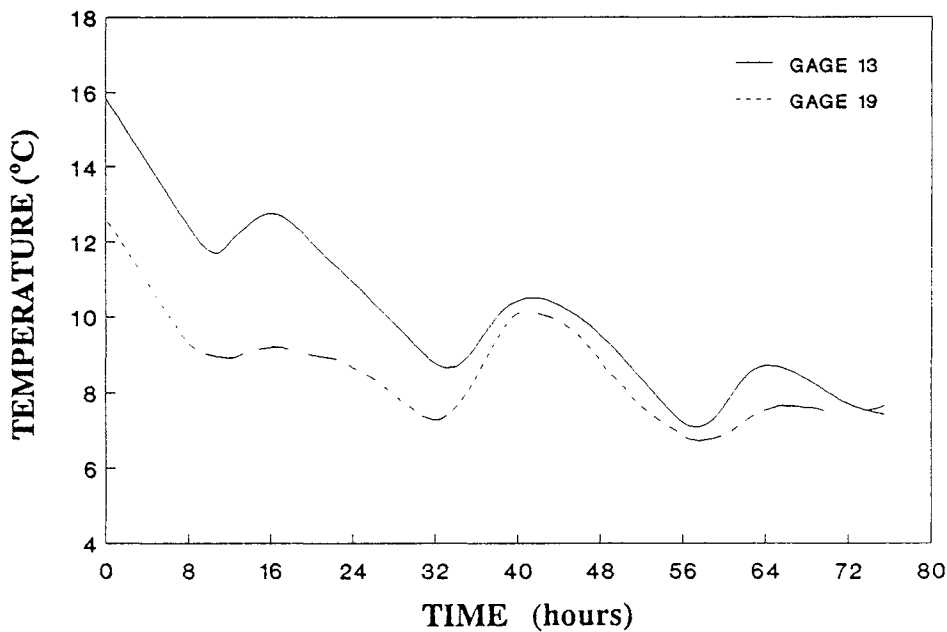


Figure 21. Measured Temperature Variations, Box Girder Segment 46, Northbound Outside Web.

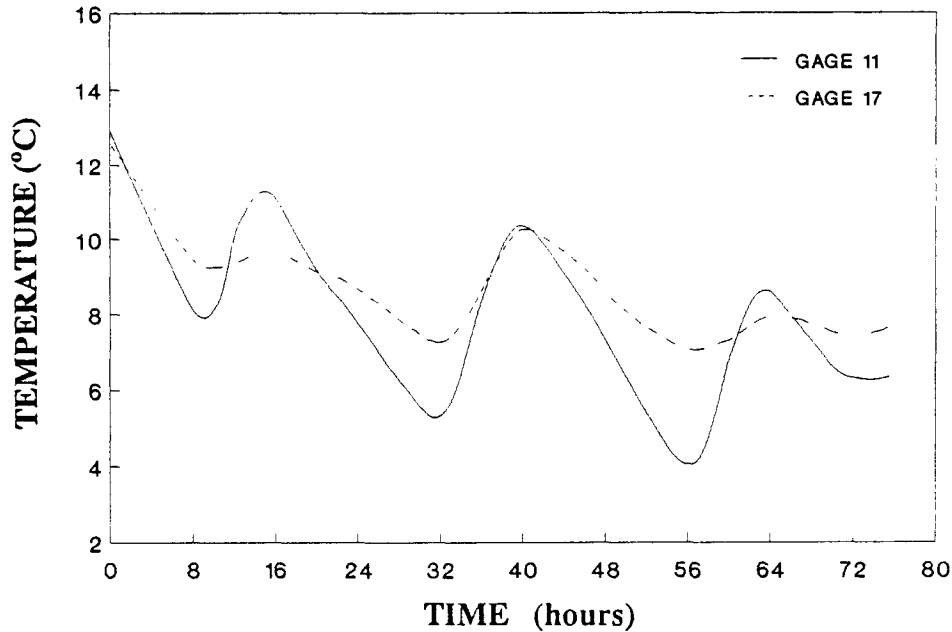


Figure 22. Measured Temperature Variations, Box Girder Segment 46, Northbound Inside Web.

trend took place over the period. The largest changes in temperature occurred in the top flange, or deck region, which was exposed to direct solar radiation. The daily minimum and maximum temperatures occurred at approximately 9 A.M. and 2 P.M., respectively, and the extreme temperatures in the webs and bottom flanges lagged behind those of the top flange by 1 to 2 hr. Figures 20 and 22 indicate that similar temperatures were recorded at the inner webs of the two girders. Further examination of these figures shows that, although the top flange underwent larger changes in temperature, the bottom flanges were often warmer during the nighttime hours. A comparison of Figures 19 and 21 illustrates the difference in thermal response between locations having eastern versus western exposure. Figure 21 shows that, at the eastern side of the bridge, temperatures recorded in the top flange, at gage 13, were consistently higher than those at gage 19, in the bottom flange. On the western side of the bridge, the opposite was true, as shown in Figure 19, where higher temperatures were recorded at gage 9 in the bottom flange than at gage 2 in the top flange.

### Measured Temperature Distributions Across the Girder

To allow for more insight into the distribution of temperature at a given time, thermal data from the I-295 bridge were plotted into color contours at several time steps. Two of the measured temperature distributions are shown as contour plots over the box girder cross section in Figures 23 and 24. These plots represent snapshots of the temperature distribution within the box girder, taken at times at which extreme temperatures occurred in the top flanges. Figure 23 shows the box girder

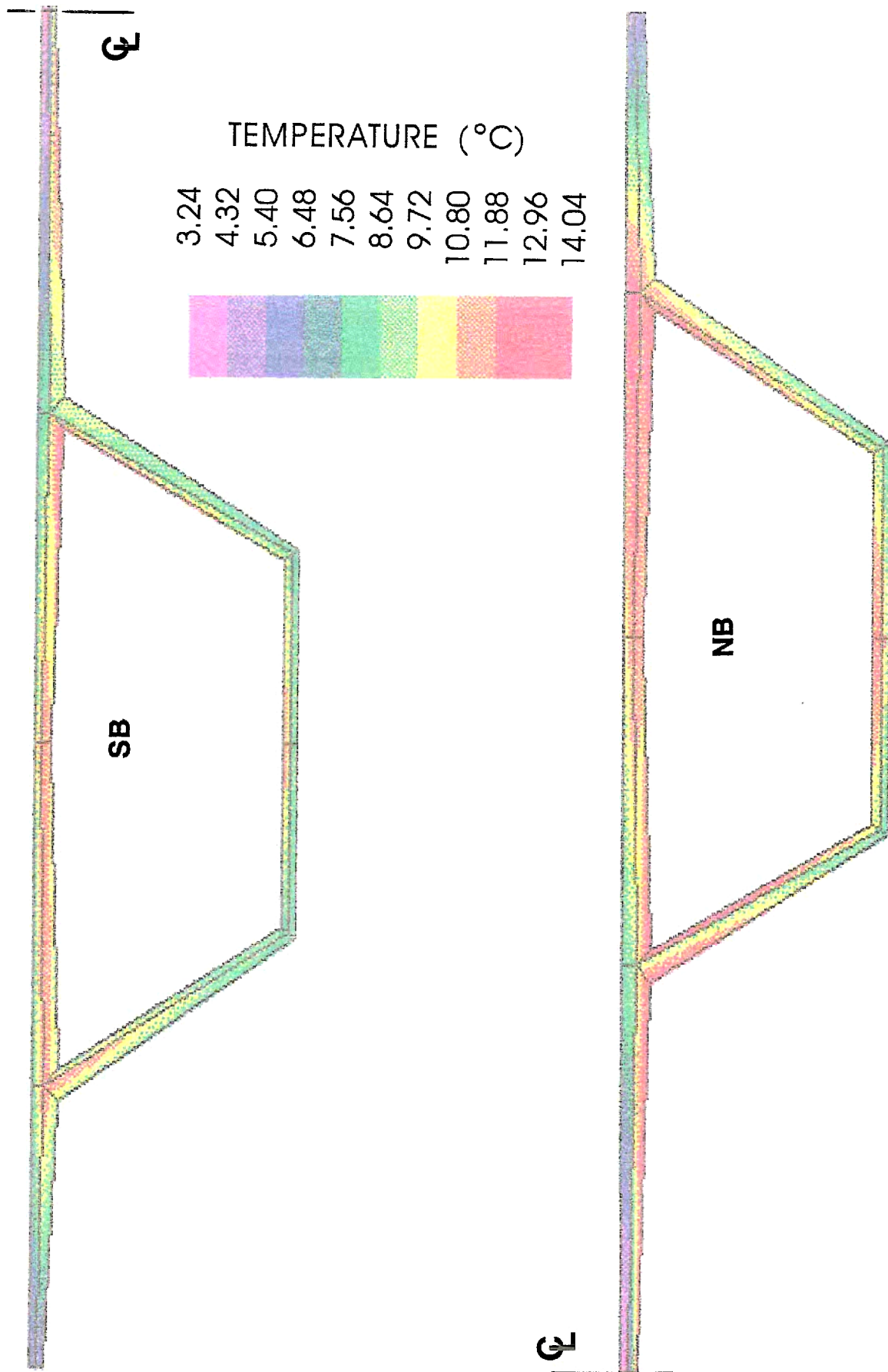


Figure 23. Measured Box Girder Temperature Distribution, 11/17/89, 9:00 A.M.

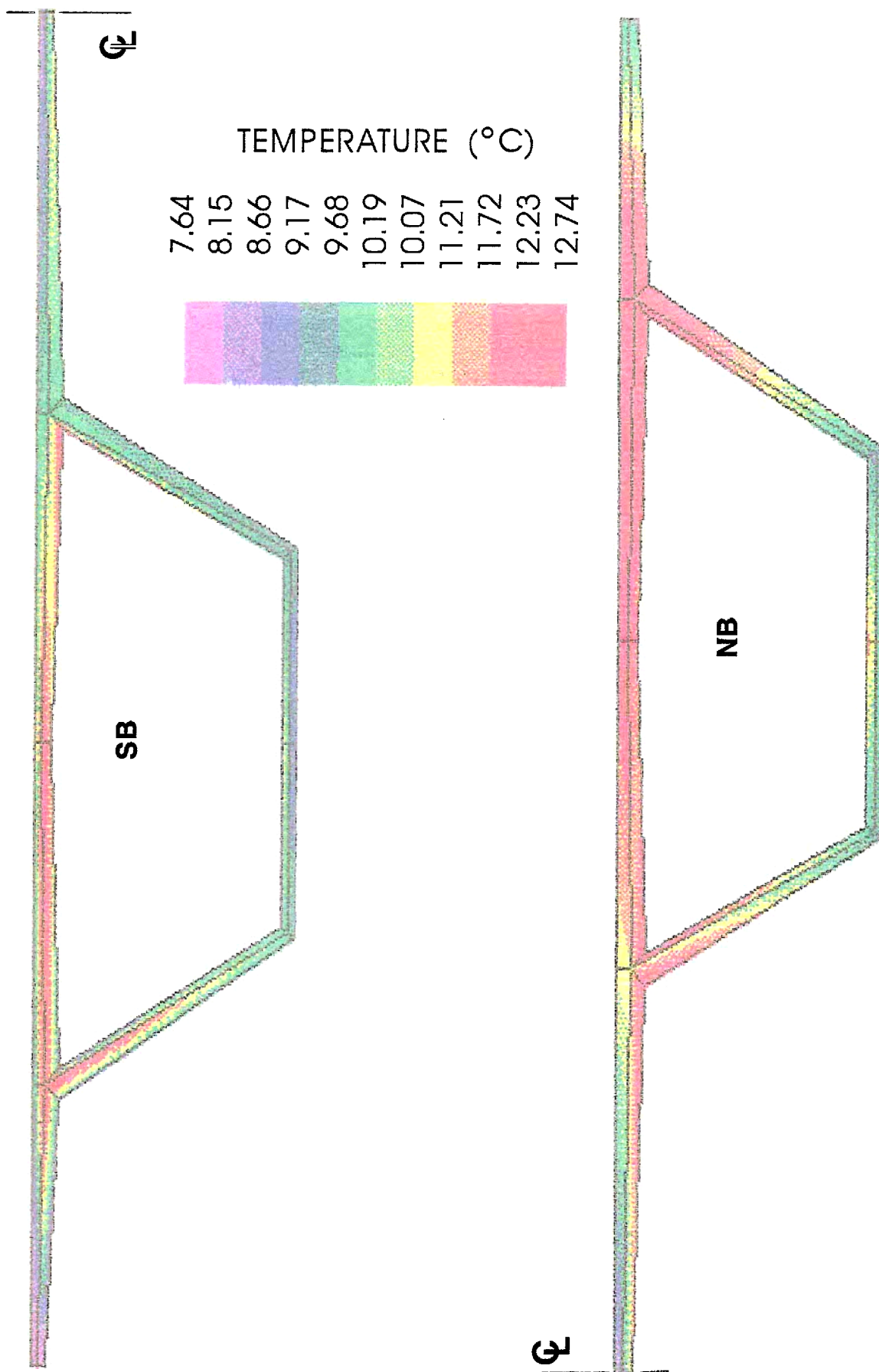


Figure 24. Measured Box Girder Temperature Distribution, 11/17/89, 2:00 P.M.

temperature distribution recorded at 9 A.M. on November 17, and Figure 24 shows the distribution at 2 P.M. the same day. Temperature contours were obtained by applying measured temperature data as nodal values in a finite element model in which the nodes corresponded to the locations of the thermocouples in segment 46. For clarity, the northbound and southbound portions of the twin box girder are plotted individually in each figure. The following discussion is limited to the temperature data recorded on November 17, which were representative of the data recorded on the following days of the study.

An examination of Figure 21 shows that the lowest temperatures in the box girder were recorded 9 A.M. at the closure pour between the girders and at the extreme ends of the top flange. Temperatures of approximately 3 to 4 degrees C were recorded at the ends of the flange, and temperatures on the order of 10 to 12 degrees C were measured at locations in the top flange, near the interior of the box sections. The large difference in temperatures observed between these points illustrates the insulating effect of the dead air space within the box girders. Temperatures of approximately 8 to 9 degrees C were recorded in the bottom flanges.

Figure 24 shows that significant warming occurred in the top flange between 9 A.M. and 2 P.M. Temperatures of approximately 14 to 16 degrees C were recorded in the top flange in the vicinity of the outer web of the northbound box girder. Again, the lowest temperatures (approximately 7 degrees C) were measured at the western end of the top flange and between the girders, at the closure pour. Temperatures of approximately 10 degrees C were recorded in the bottom flanges, and the variations in temperature through the webs are clearly shown. As shown in Figures 23 and 24, the highest temperatures in the girders were recorded in the top flange, above the outside web of the northbound girder. One explanation for this could be that the location was more protected from wind than other locations across the box girder, such as the ends of the flanges, which are exposed to winds from both above and below. In both figures, closely spaced contours through the top deck and webs depict the thermal gradient over the depth of the girders. The measured temperature distributions presented in Figures 23 and 24 clearly show the complex, two-dimensional thermal state of the twin box girder at a section.

### Measured Thermal Strains

Evaluation of the strain data indicated that a significant amount of measured data were unreliable. Potentially defective components of the data acquisition system were identified and replaced, but unfortunately, only about the same number of strain gages were operational after the repair efforts were made. This seemed to indicate that the problems with the data acquisition system were more complex than originally thought and that repairs may have been beyond the expertise of the researchers. Consultations with manufacturer's representatives also failed to lead to a solution.

All of the strain gages located in the bottom flange and webs of the northbound portion of segment 33 recorded unreliable data. Later troubleshooting indicated that these gages were apparently controlled by a defective excitation card

within the data acquisition system. A similar problem was also identified for the gages located in the bottom flange of the northbound portion of segment 48. The defective modules were replaced, but the results were inconsistent in that malfunctions continued to occur for some groups of gages and not others. This would suggest that the problems with the system may have been compounded by malfunctions within the back-planes of the remote scanning chasses. Strain data recorded by all gages in midspan segment 62 underwent seemingly random oscillations on the order of 5 to 20 microstrains, which again suggested a malfunction in the data acquisition hardware. A few of the gages in segments 33 and 48 did not record data at all, caused by damage to the gage and/or lead wires. In the following discussion, only the strain data from the reliable gages in segments 33 and 48 are presented.

As discussed previously, it was necessary to correct the raw strain data to account for temperature effects introduced by mounting the transverse gage of the 90-degree strain rosette on the curved surface of a reinforcing bar. To make this correction, the temperature at each strain gage in the instrumented box girder segments was estimated using the thermocouple data from segment 46. Evaluation of equation 1 with the specific parameters of the strain gages, adhesive, and reinforcing bar used for the instrumentation yielded a correction of approximately 0.659 microstrains per degree Celsius of temperature change. The largest daily temperature variations in the box girder were shown to be on the order of 10 degrees C in Figures 19 through 22, and the resulting maximum values of temperature correction were approximately 7.0 microstrains.

In addition to the temperature correction for strain gages mounted on a curved surface, further corrections were necessary to account for the differences in the coefficients of thermal expansion between the concrete and reinforcing steel. Though nominally considered equal, a laboratory test of concrete and reinforcing steel specimens taken from the James River Bridge indicated that there was a significant difference in the coefficients of thermal expansion between the two materials. Strains resulting from changes in temperature were measured in the specimens using a mechanical strain gage and are shown in Figure 25. In the figure, the slope of the lines corresponds to the coefficient of thermal expansion for the particular material. The coefficients of thermal expansion for the concrete and reinforcing steel were measured to be  $4.8 \times 10^{-6}/\text{degree F}$  and  $6.2 \times 10^{-6}/\text{degree F}$ , respectively. This corresponds to a difference of approximately 1.4 microstrains per degree Fahrenheit of temperature change (or 2.5 microstrains/degree C), in which a temperature increase would place the strain-gaged rebar into compression. Based on the variations of temperature observed during the period of the study, corrections for differences between coefficients of thermal expansion were found to be on the order of 10 to 25 microstrains.

Strain data recorded by the gages located in segments 33 and 48 are presented in Figures 26 through 37. The corrected temperature-induced mechanical strains, measured at the various gages, are shown plotted as changes in strain relative to reference strains for each of the 3 days under consideration. In order to investigate the magnitude of the diurnal strain variations induced by changes in temperature, the reference strains were selected roughly at the times during the

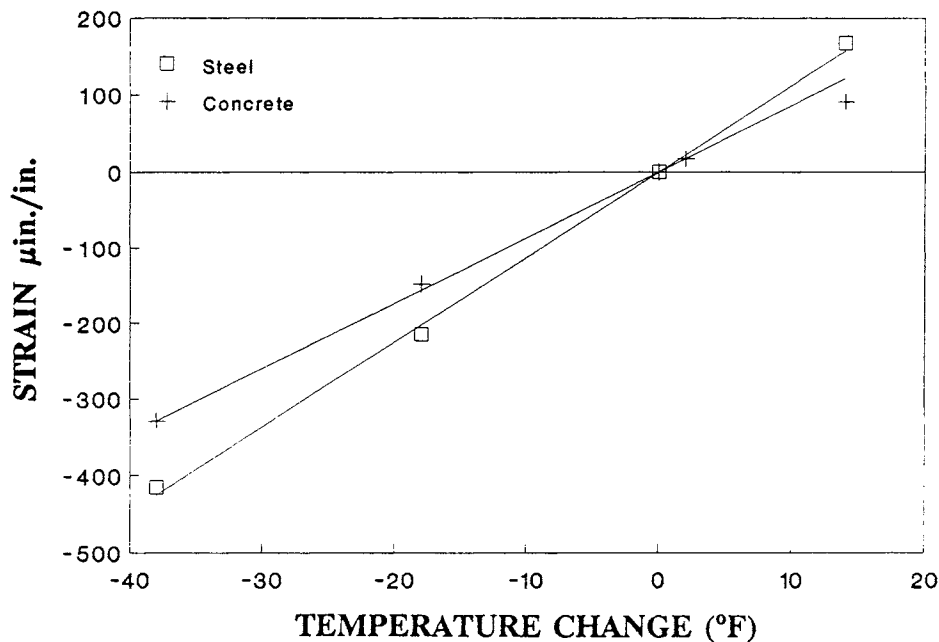


Figure 25. Comparison of Measured Coefficients of Thermal Expansion.

morning hours at which the temperatures in the box girder were at a minimum. Thus, the strain response data recorded on November 17 are plotted as changes in strain relative to strains measured at 9:20 A.M. that day. Likewise, the strain data taken on November 18 and 19 are presented as changes in strain relative to the strains recorded at 8 A.M. of each day.

The strain response data measured at segment 33, located near the south pier, are shown in Figures 26 through 31. Figure 26 presents the thermal strain data recorded on November 17 at top flange gages 1 through 4, 10, and 12. Referring to Figure 10, it may be seen that a majority of these gages are located within the southbound portion of the twin box girder. Figure 27 shows the strain data recorded on November 17 at gages 8 and 9, located in the bottom flange of the southbound portion of the girder. Figures 28 and 29 present strain data recorded on November 18 at the respective top and bottom flange gages, and Figures 30 and 31 show similar strain gage data recorded on November 19.

An examination of Figure 26 indicates that strain variations on the order of 60 to 80 microstrains were recorded on November 17 in the top flange of the box girder. Significant jumps in the measured strains were observed at all gages during the morning hours, probably resulting from bridge traffic or cable-stay retensioning that took place during that time. The measured data also show a 2-hr gap around 12:00 hr during which strain measurements were temporarily halted so that previously stored data could be retrieved. Although similar magnitudes of strain variations were recorded over the course of the day, independent behavior was observed

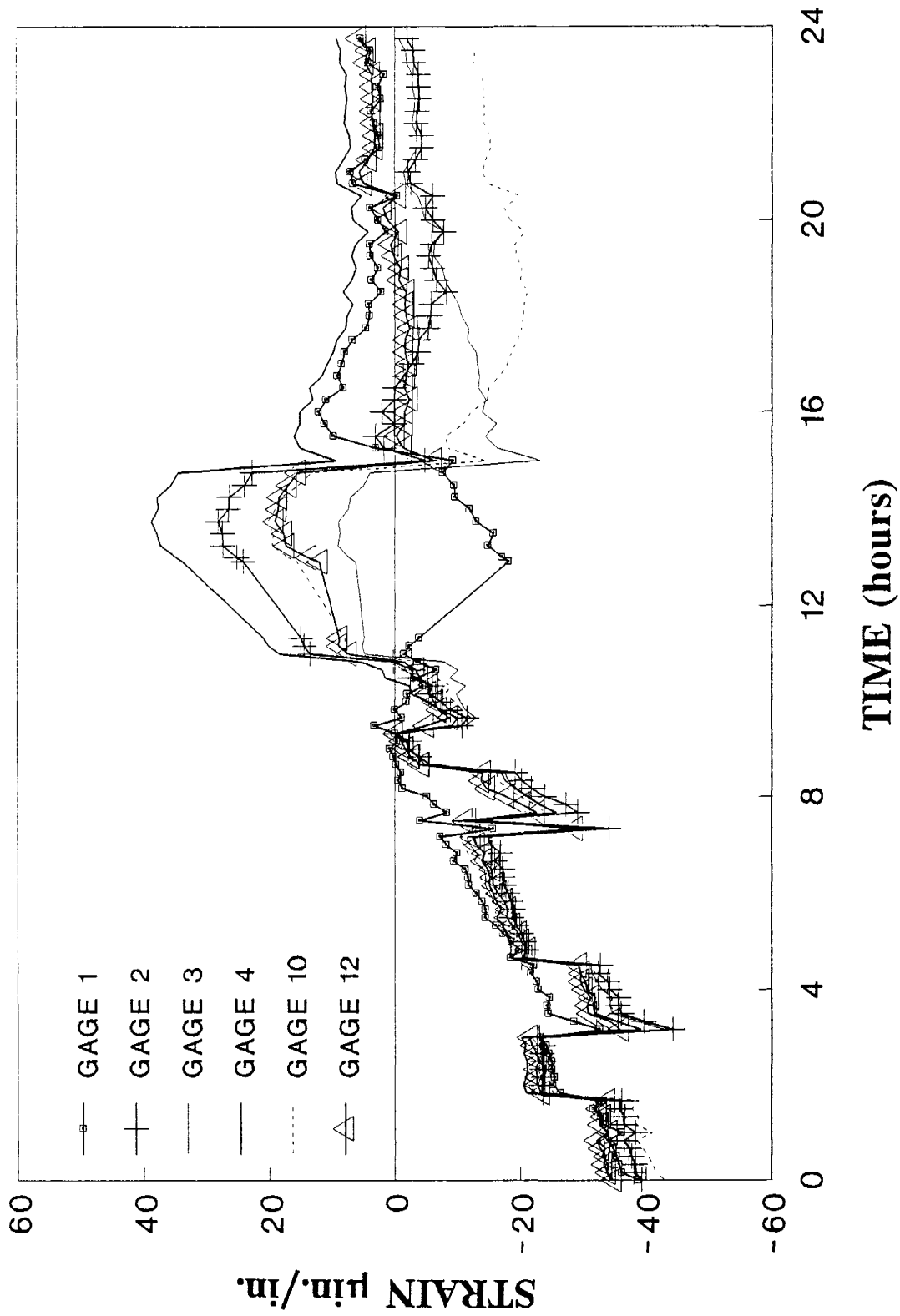


Figure 26. Measured Strain Variations, Segment 33, Top Flange Gages, 11/17/89.

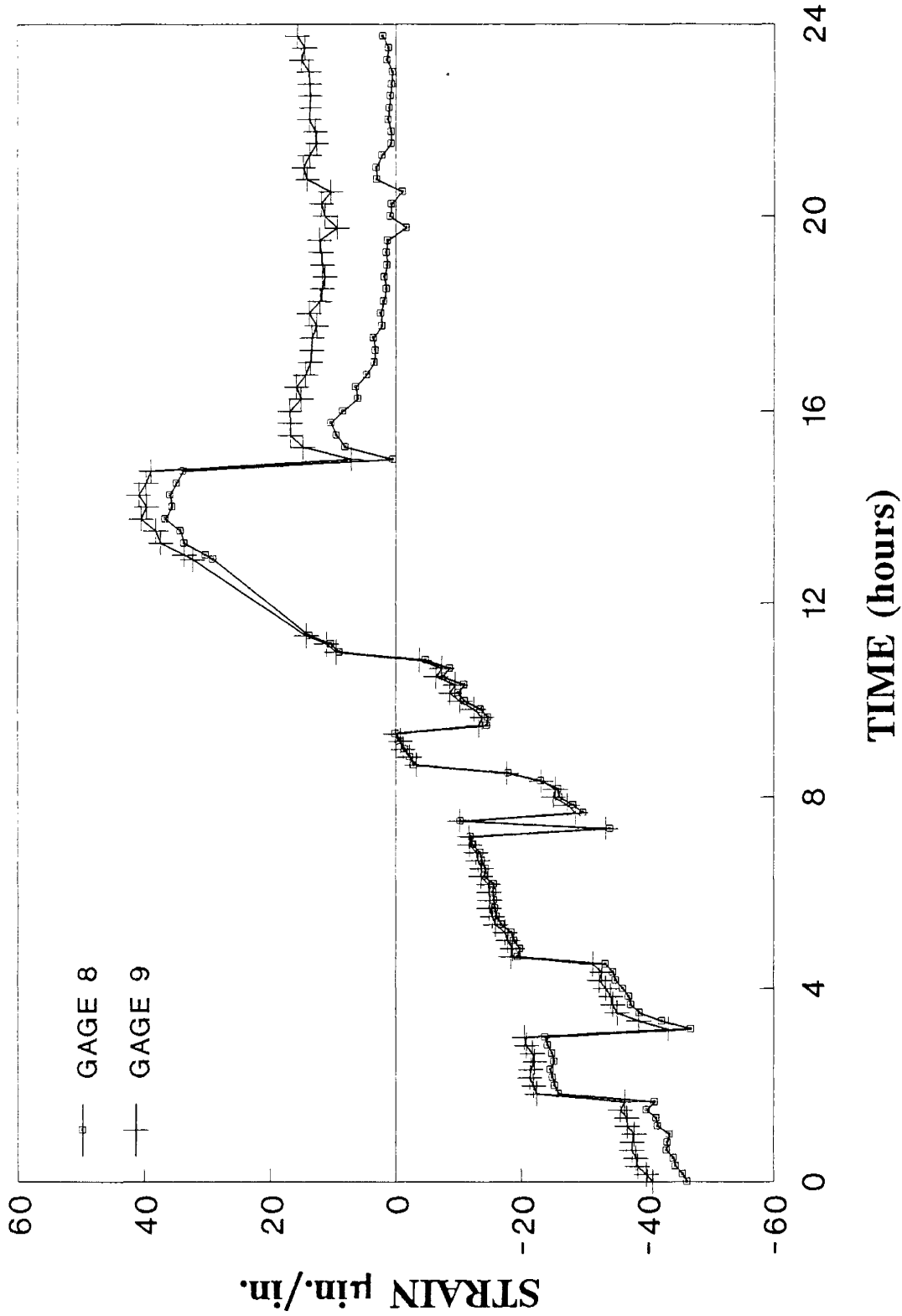


Figure 27. Measured Strain Variations, Segment 33, Bottom Flange Gages, 11/17/89.

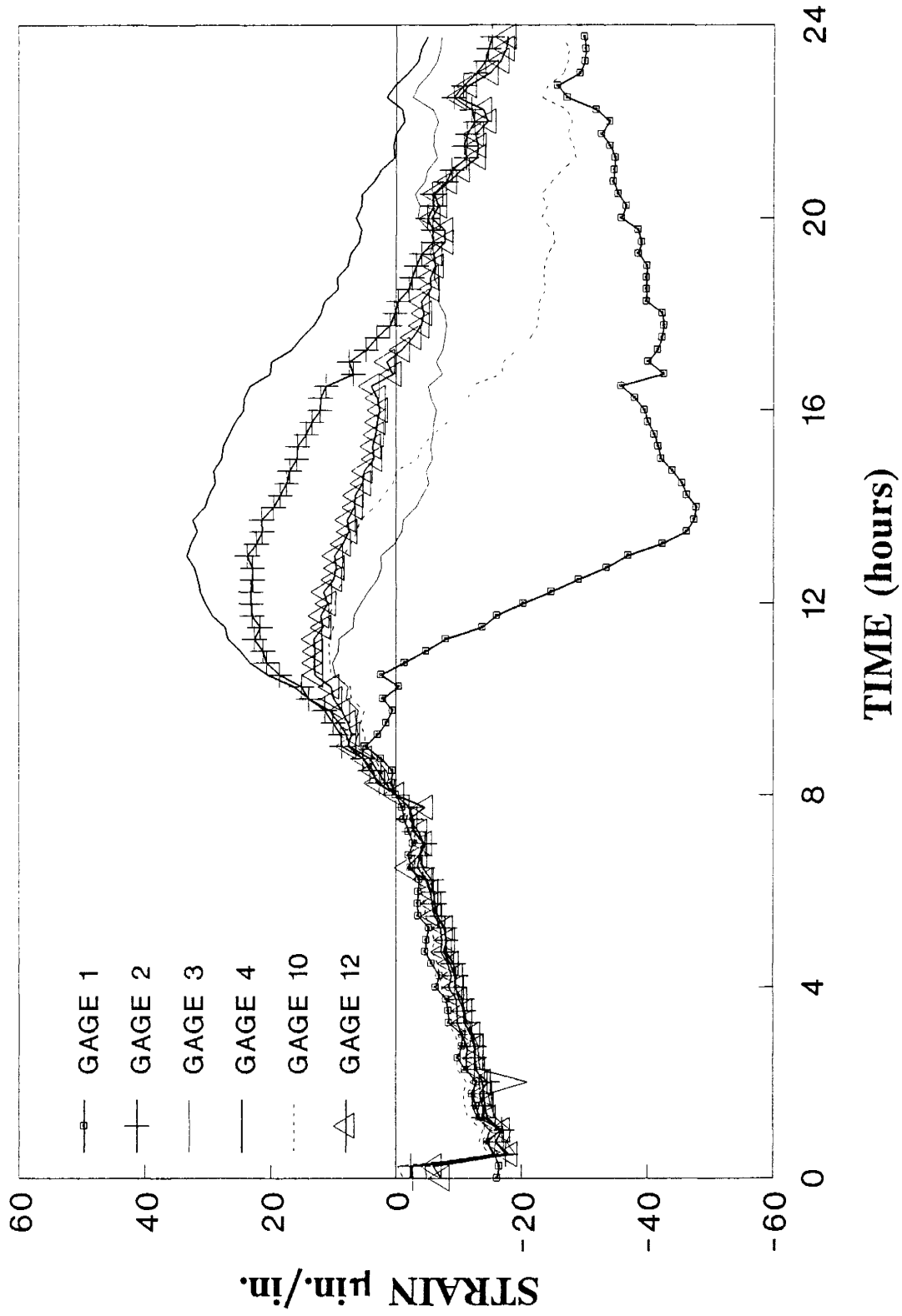


Figure 28. Measured Strain Variations, Segment 33, Top Flange Gages, 11/18/89.

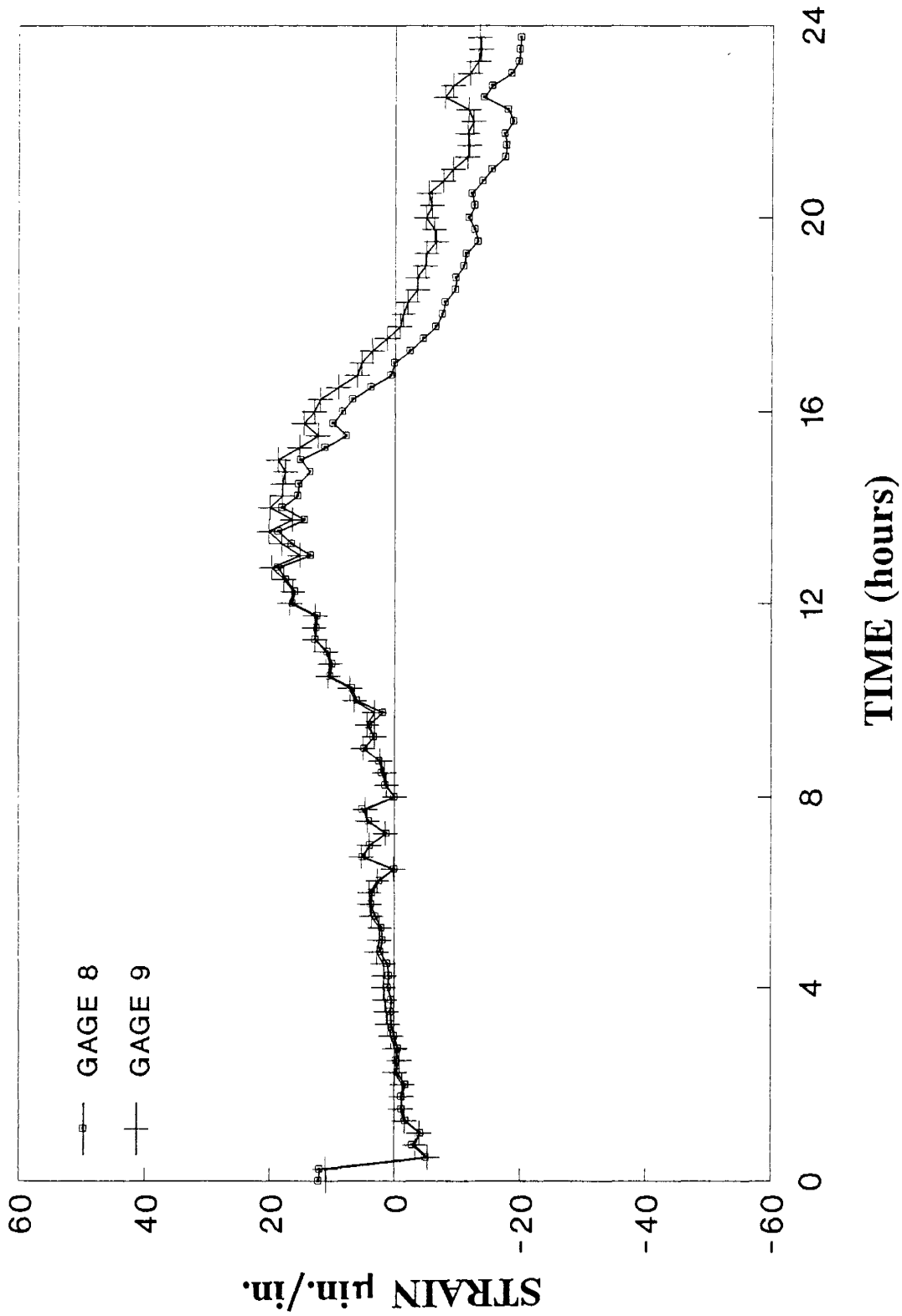


Figure 29. Measured Strain Variations, Segment 33, Bottom Flange Gages, 11/18/89.

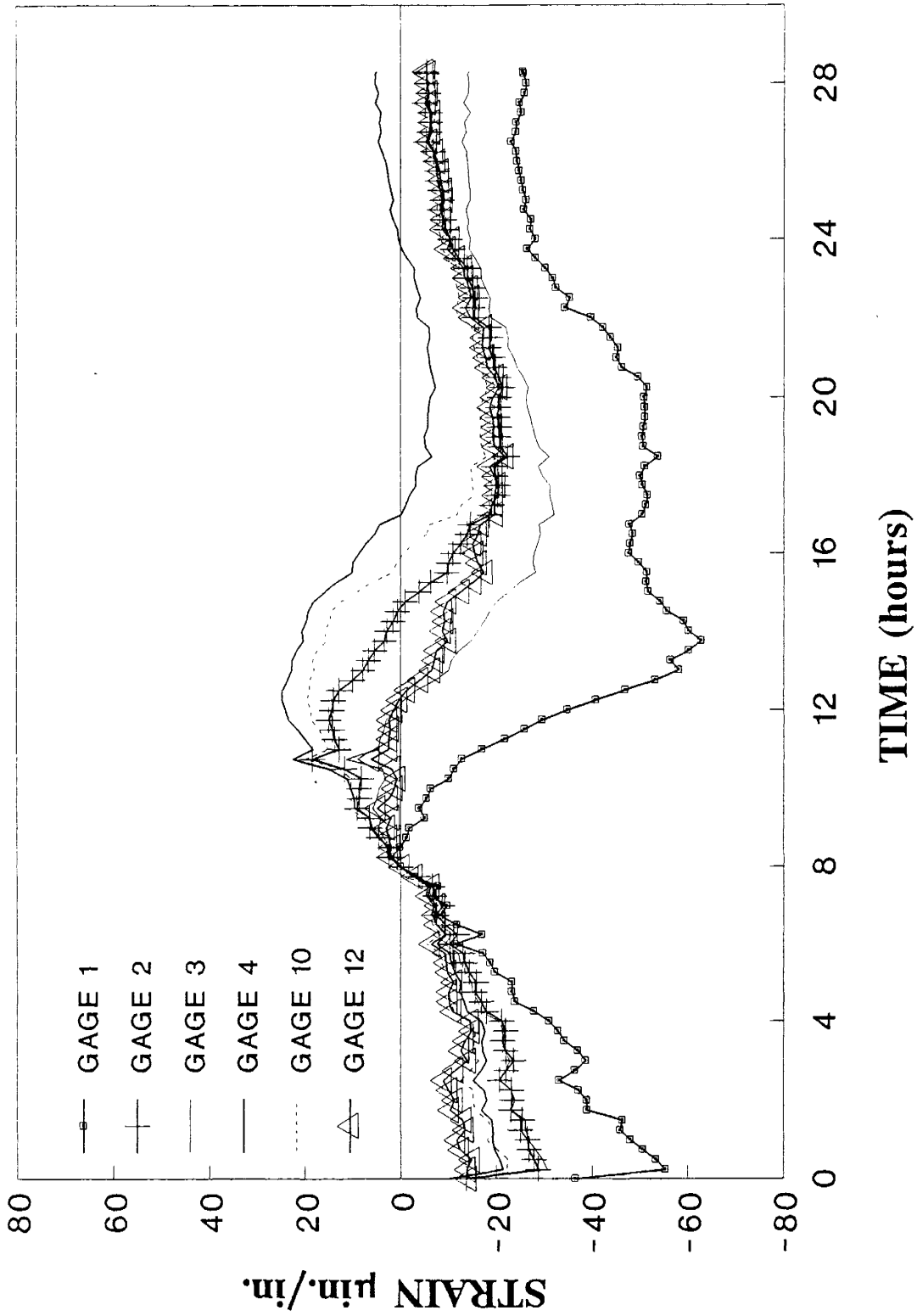


Figure 30. Measured Strain Variations, Segment 33, Top Flange Gages, 11/19/98.

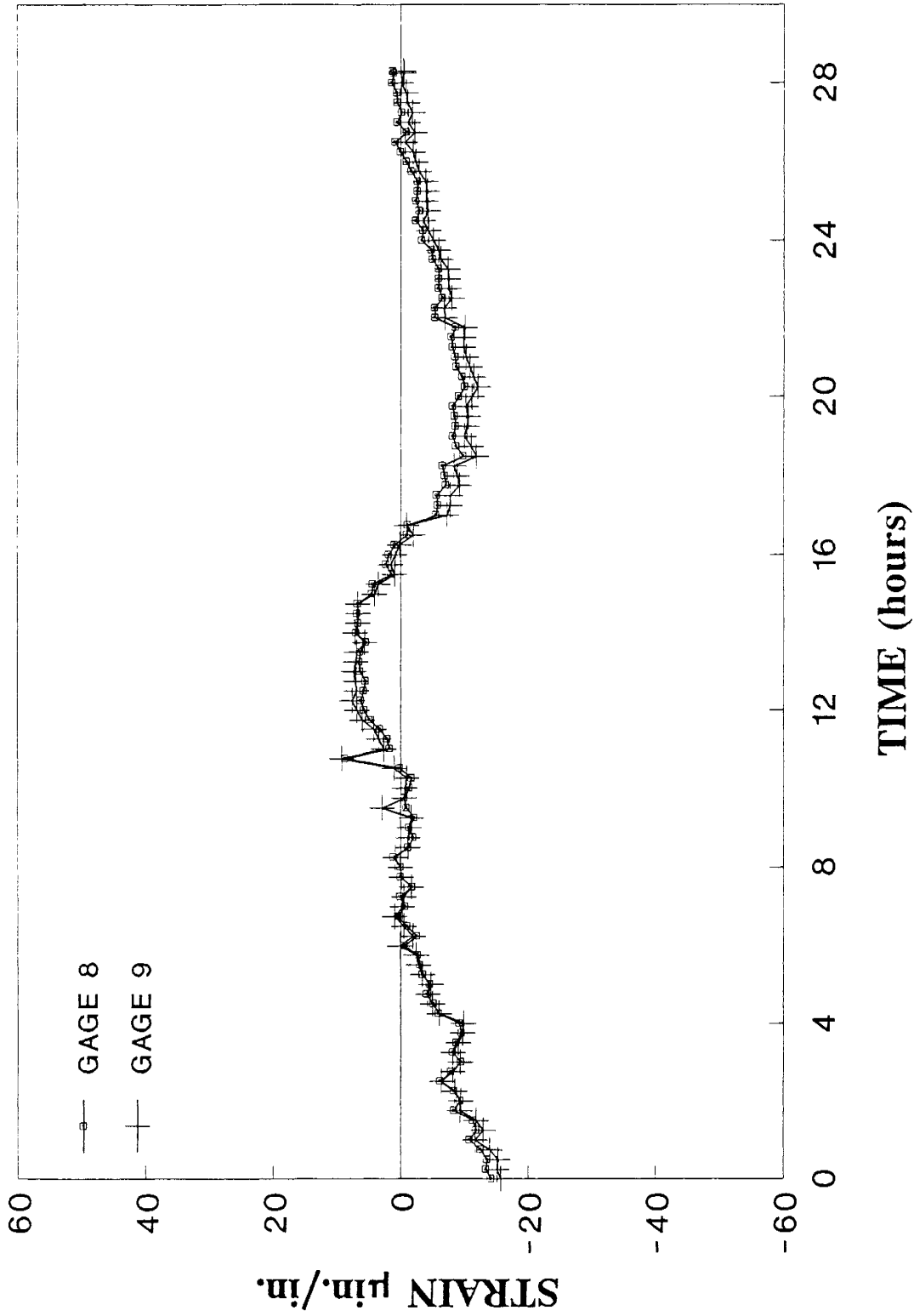


Figure 31. Measured Strain Variations, Segment 33, Bottom Flange Gages, 11/19/89.

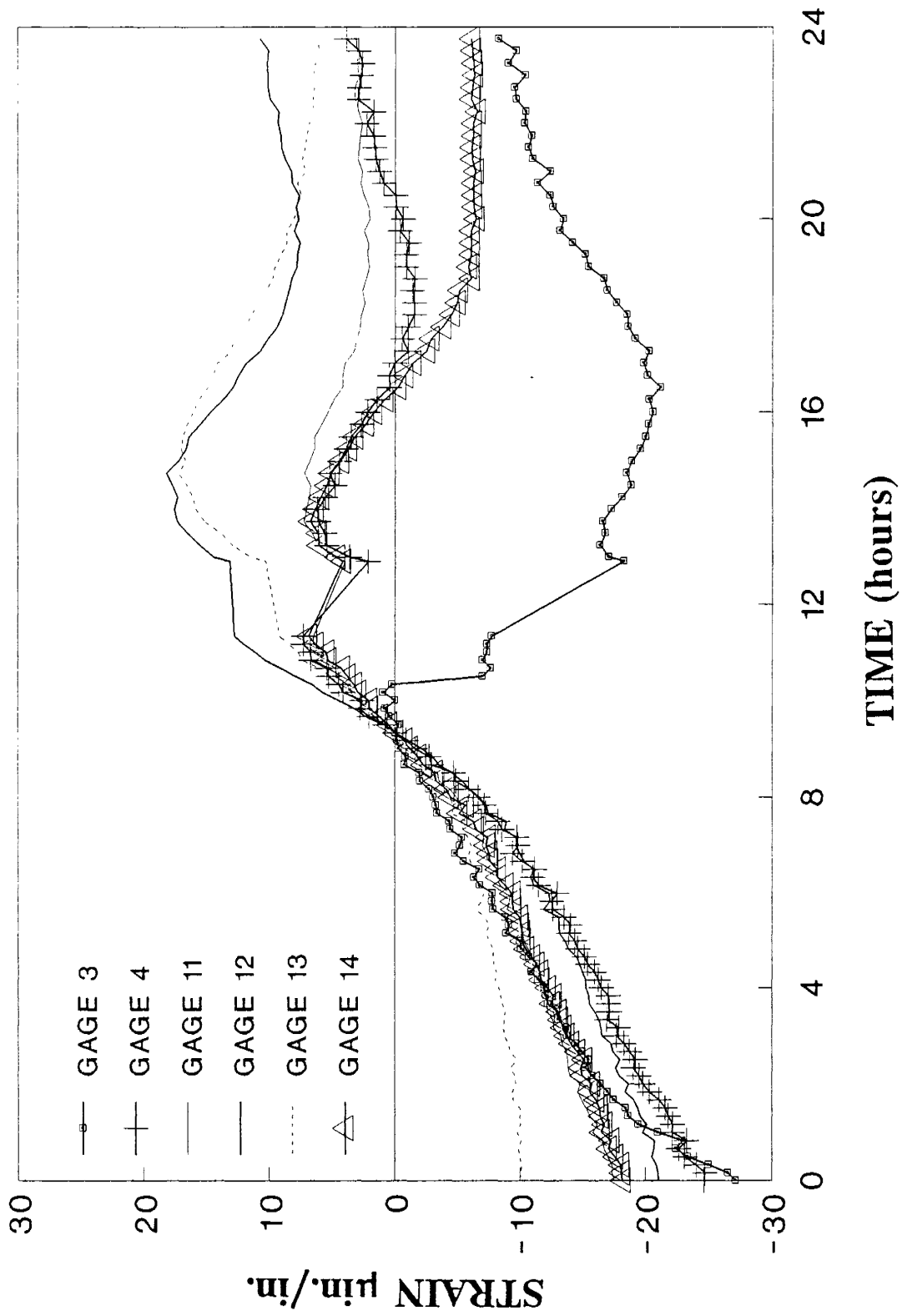


Figure 32. Measured Strain Variations, Segment 48, Top Flange Gages, 11/17/89.

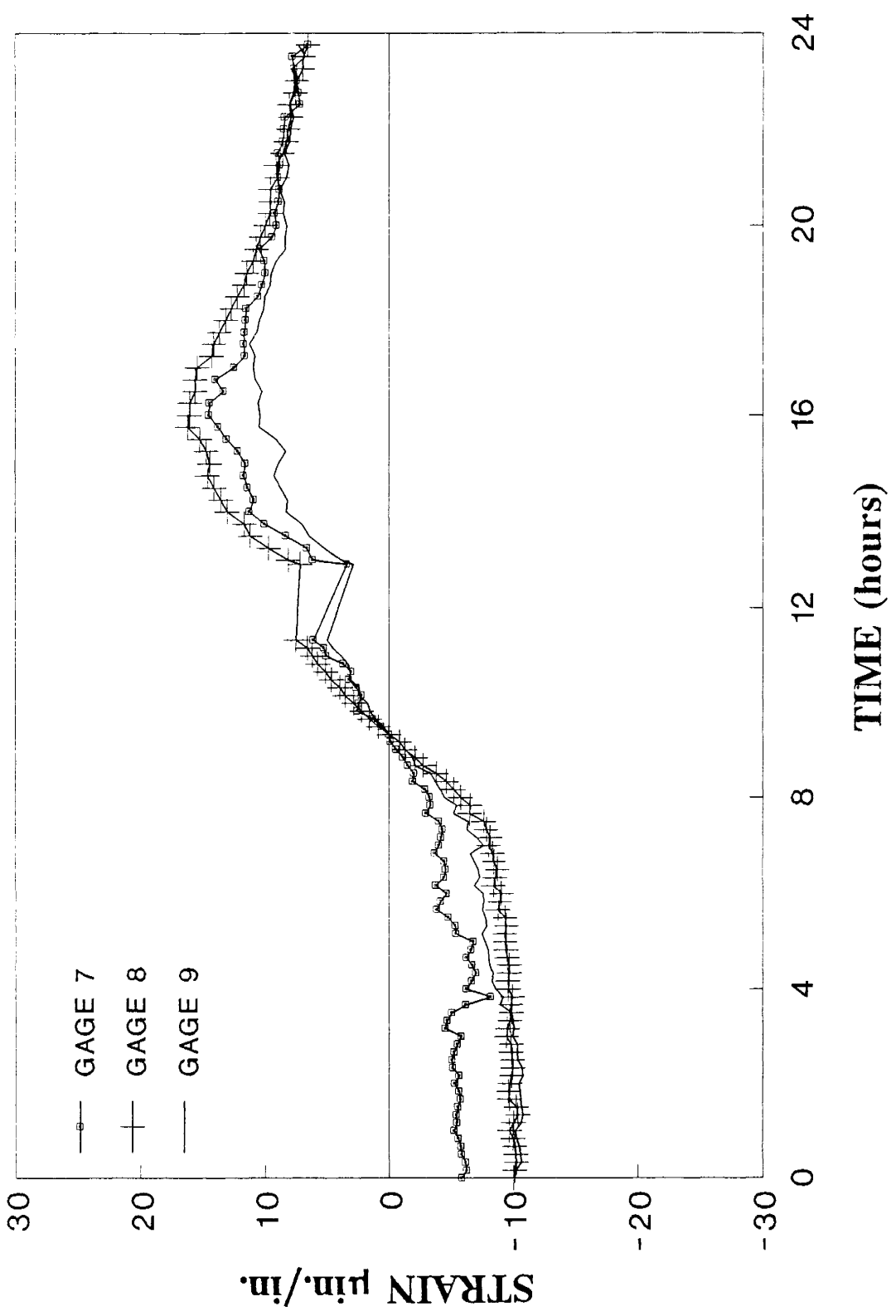


Figure 33. Measured Strain Variations, Segment 48, Bottom Flange Gages, 11/17/89.

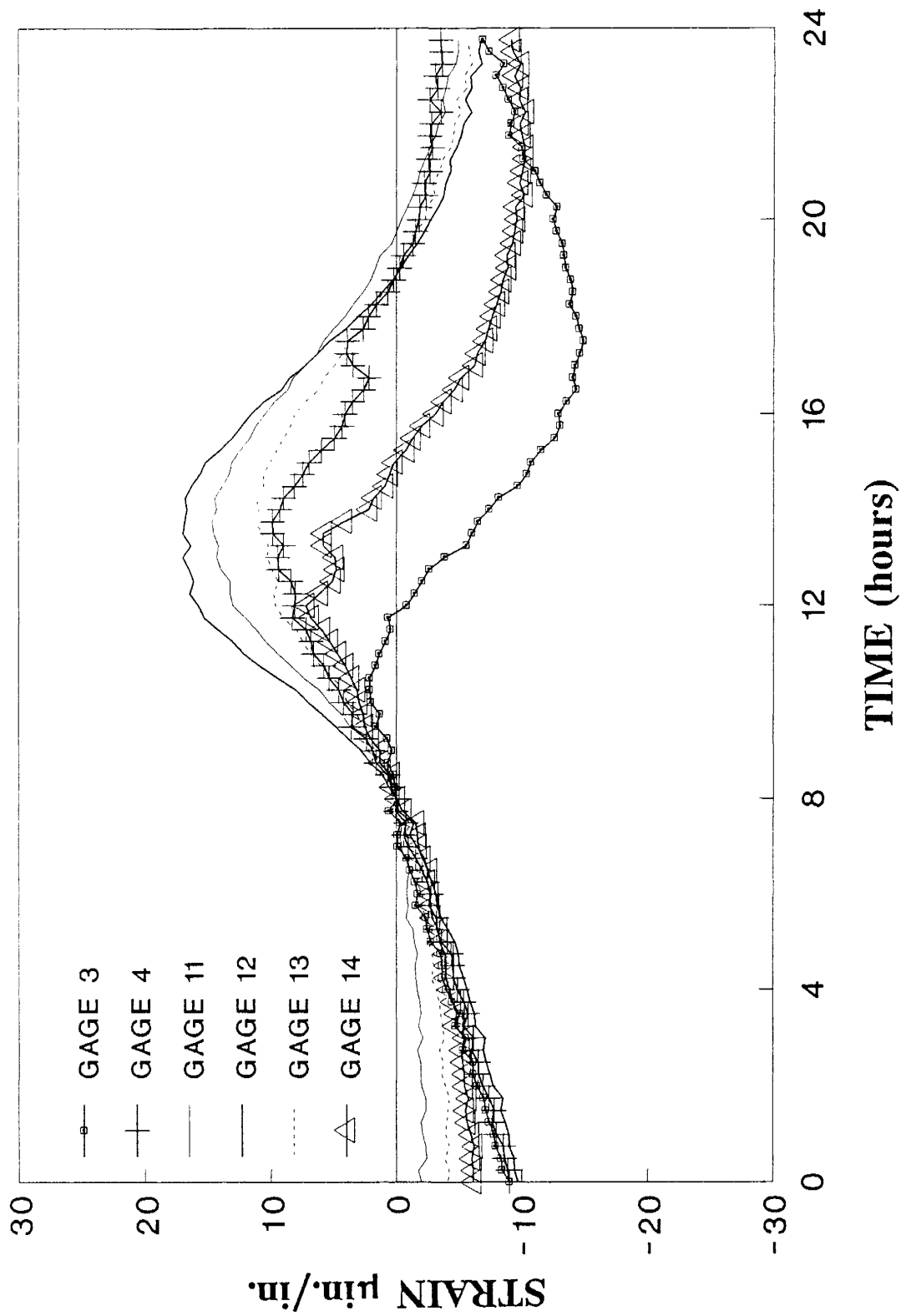


Figure 34. Measured Strain Variations, Segment 48, Top Flange Gages, 11/18/89.

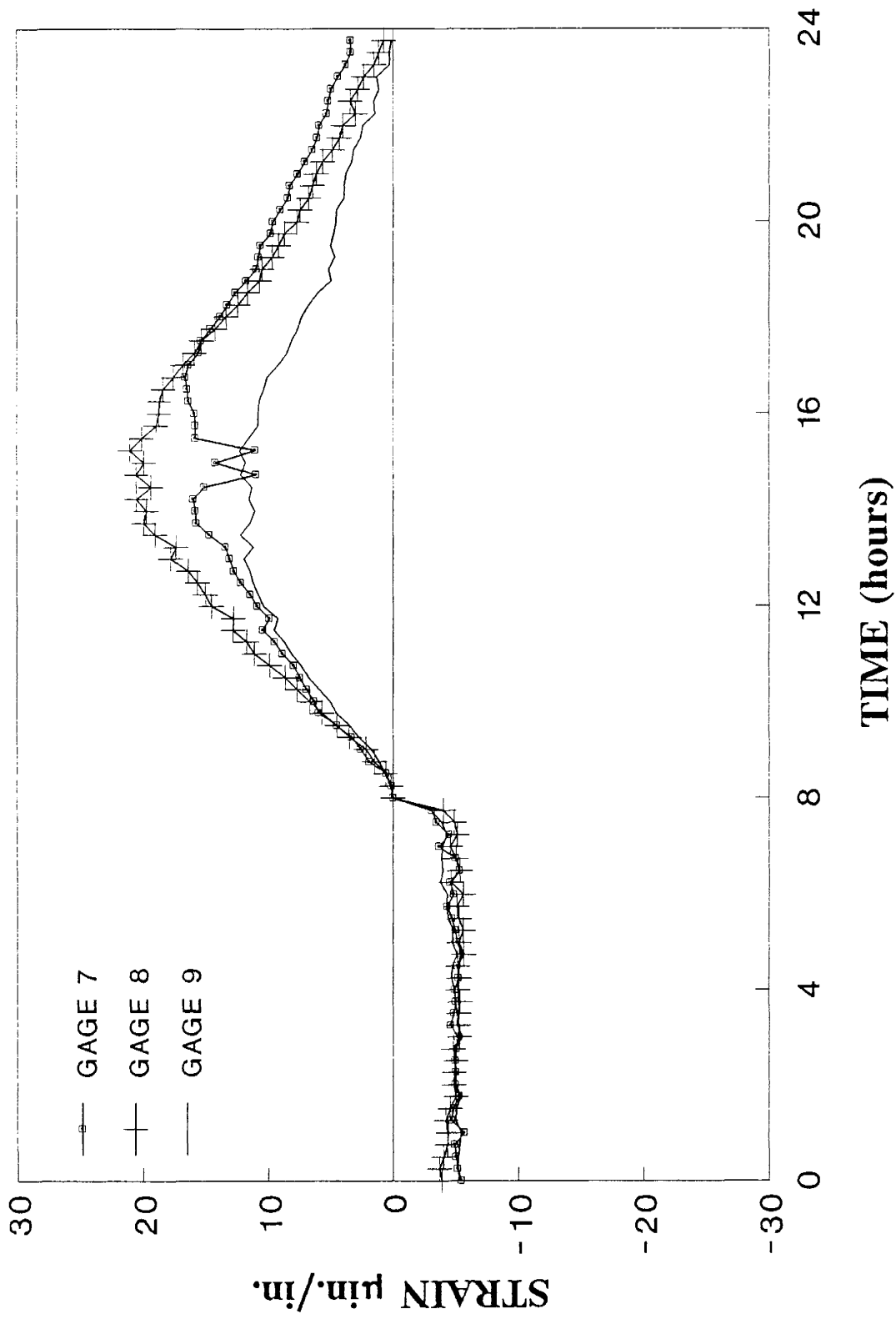


Figure 35. Measured Strain Variations, Segment 48, Bottom Flange Gages, 11/18/89.

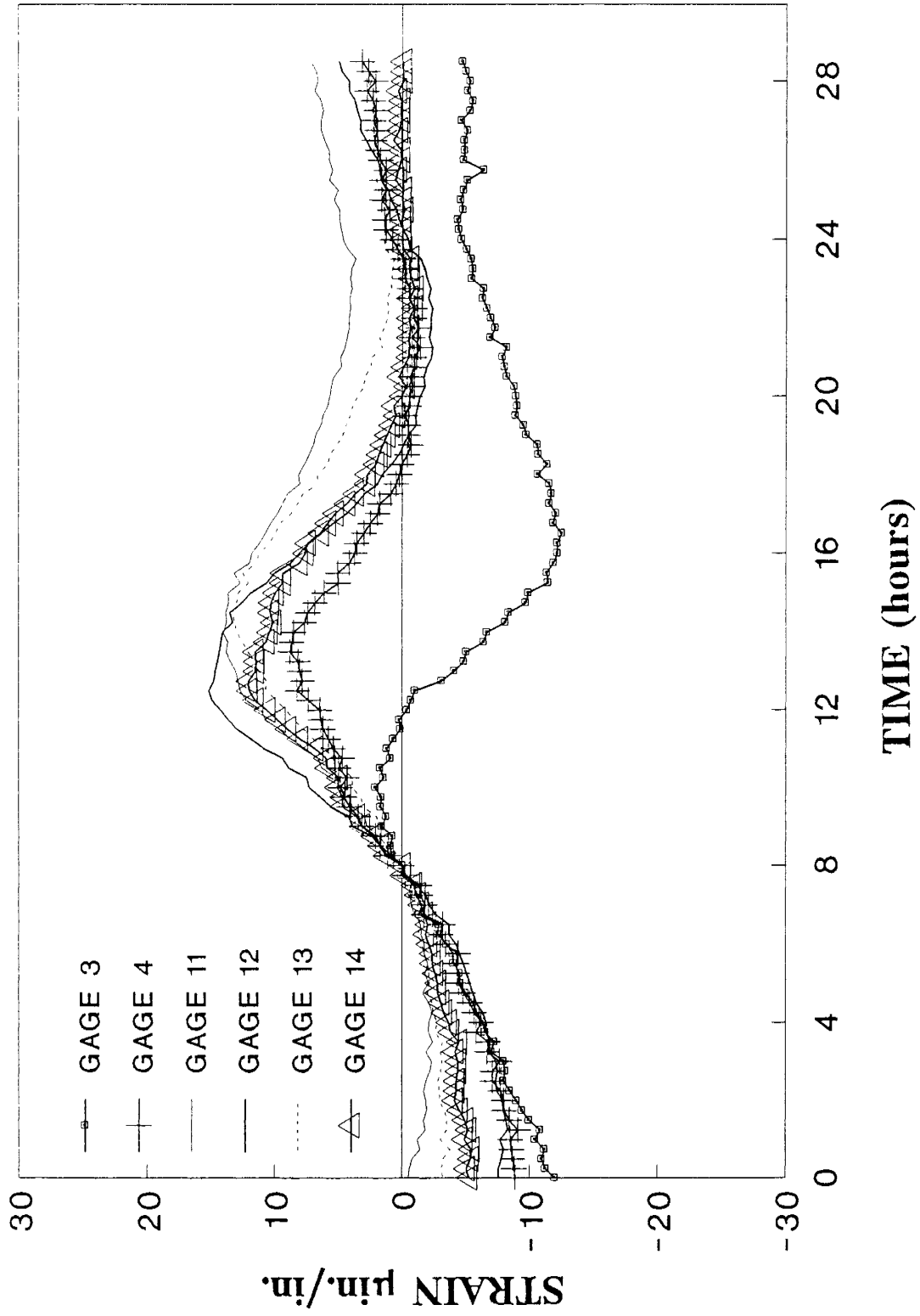


Figure 36. Measured Strain Variations, Segment 48, Top Flange Gages, 11/19/89.

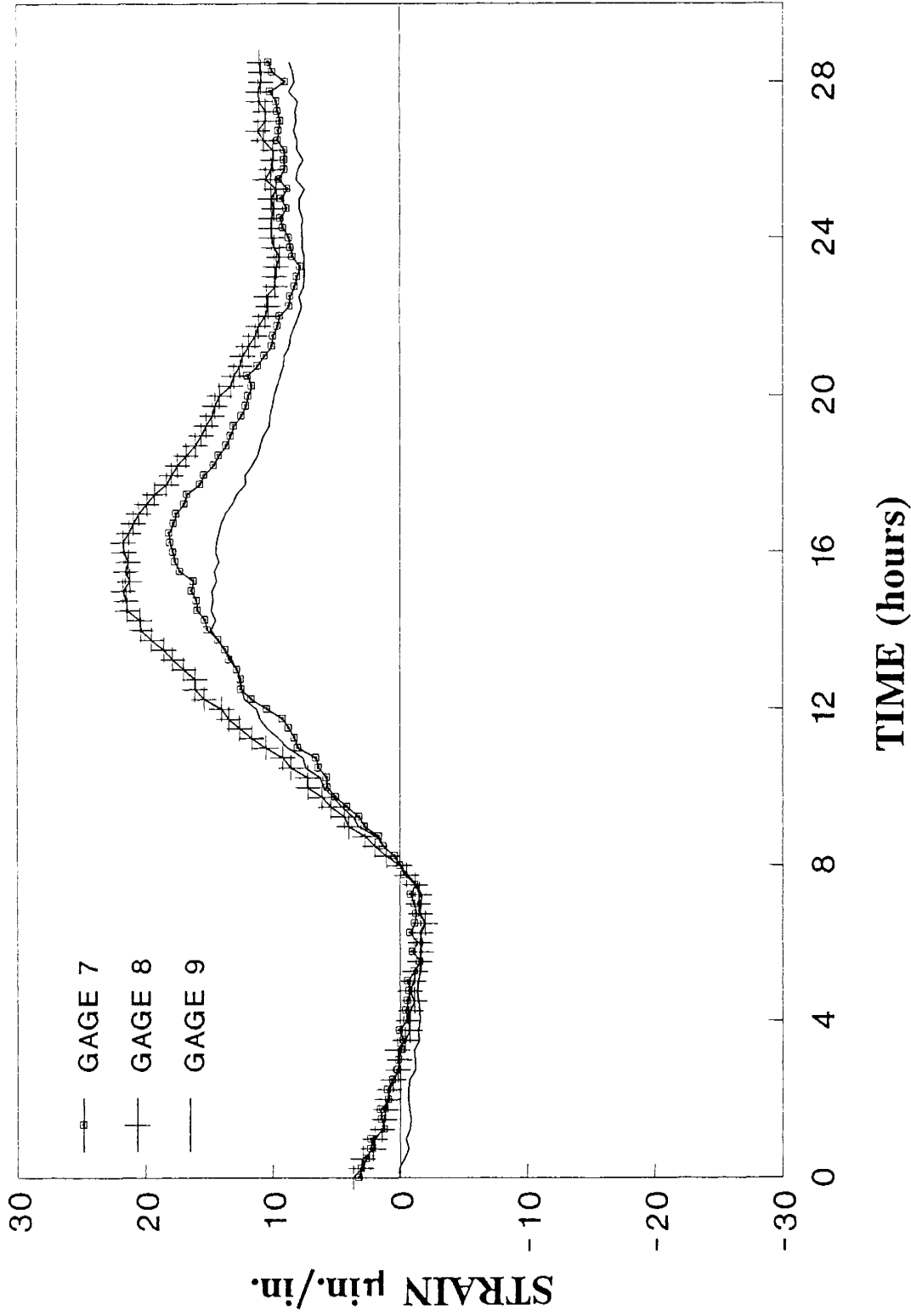


Figure 37. Measured Strain Variations, Segment 48, Bottom Flange Gages, 11/19/89.

between gages across the flange during the afternoon hours. In particular, gages 2 and 4, located over the webs of the southbound girder, displayed larger relative tensile strains between 12:00 and 16:00 hr than did gages 3, 12, and 10, which were located between webs and at the closure pour. In contrast, gage 1, located at the extreme western edge of the top flange, exhibited relative compressive strains on the order of 20 microstrains between the same hours, after which tensile strains were recorded over the remainder of the day.

Figure 27 shows that similar strain behavior occurred in the bottom flange of segment 33. The strain response recorded at the bottom flange of the southbound girder was nearly identical with that measured in the top flange. Again, large jumps in the data were observed during the morning hours. Both gages 8 and 9 recorded similar strains during the morning, but after 12:00 hr, the measured strains diverged and a difference of approximately 10 microstrains was reflected between the two gages. Gage 9, located near the inside web of the southbound girder, underwent larger relative tensile strains than gage 8, which was located between webs.

Strains measured in the top flange on November 18 are presented in Figure 28. As expected, the trends in overall thermal strain response were similar to those recorded on the previous day. The top flange gages reflected relative compressive strains during the morning hours, the largest of which was approximately 20 microstrains. Again, significant variations in strain readings were observed at locations across the flange during the afternoon. Web gages 2 and 4 recorded tensile strain variations of up to 25 and 35 microstrains, respectively. Strains measured at gage 1, on the other hand, reflected relative compressive strains that varied from approximately 50 to 35 microstrains between 14:00 and 24:00 hr. Little difference in strain response was observed between gages 3 and 12, and gage 10, located at the closure pour, recorded relative compressive strains during the latter part of the day.

Strains measured at the bottom flange on November 18 are presented in Figure 29. It is seen from this figure that the strain variations measured in the top and bottom flange were again similar and reflected the ambient temperature changes that occurred during the day. Though the magnitudes of the relative strains recorded by gages 8 and 9 were smaller than those recorded on the previous day, the overall trends in strain response were largely similar. During the morning hours, nearly identical strains were measured at the two gages; during the afternoon, noticeable differences were observed. As was noted for the November 17 data, gage 9, nearest the web, exhibited larger relative tensile strains. In this case, however, the magnitude of the difference between gages was, at most, 5.0 microstrains.

Figure 30 shows the top flange strain data recorded on November 19. Examination of this figure indicates that the trends in measured strain response closely match those recorded on the previous day and significant variations were observed between gages. For example, differences in relative compressive strains on the order of 10 to 20 microstrains were noted between adjacent gages 1 and 2 during the morning hours. As was shown in Figures 26 and 28, strains recorded at gage 1 exhibited somewhat independent behavior relative to the other top flange gages. At

this location, relative compressive strains up to approximately 60 microstrains were recorded during the afternoon hours. Again, it may be seen that only small differences in strain response were measured on successive days between web gages 2 and 4 and between gages 3 and 12.

Strains measured in the bottom flange on November 19 are presented in Figure 31. The variations in strains recorded at gages 8 and 9 were again similar to those recorded on the preceding days. In contrast to the data presented before, there was little difference in measured strain response between gages during the afternoon hours. In fact, slightly larger compressive strains were recorded at the gage near the web. Relative to 8 A.M., compressive strains of approximately 18 microstrains were measured during early morning hours and tensile strains of up to 10 microstrains were observed during the afternoon.

The strain data recorded at quarter-span segment 48 are presented in Figures 32 through 37. Figure 32 shows the strain response data recorded on November 17, at top flange gages 3, 4, and 11 through 14, most of which are located in the northbound portion of the segment. Figure 33 presents the strain data recorded on November 17, at bottom flange gages 7, 8, and 9, located in the southbound portion of the segment. Strain data recorded on November 18 are plotted for the top and bottom flange gages in Figures 34 and 35, respectively. Similarly, Figures 36 and 37 present the top and bottom flange strains recorded on November 19.

An examination of Figure 32 indicates that strain variations measured in the top flange of segment 48 were similar to those observed at segment 33. It may also be seen that these data did not exhibit the large jumps that were observed at segment 33. This would seem to indicate that the stay tensioning or traffic that caused these anomalies occurred near the pier segment and had little effect on the rest of the structure. Relative compressive strain variations were recorded during the morning hours. During the afternoon, a dissimilar strain response was recorded between gages across the top flange. Gage 12, located between webs in the northbound girder, and gage 13, located above the outer web of the girder, recorded similar magnitudes of relative tensile strain between 12:00 and 20:00 hr. Gages 4 and 11, located above the interior webs of the two girders, showed similar variations in strain, which ranged up to approximately 10 microstrains. Gage 3, located above the outer web of the southbound girder, recorded relative compressive strains ranging up to approximately 20 microstrains during the latter half of the day. Slightly smaller compressive strains were measured at gage 14, located at the extreme eastern edge of the top flange.

Strain data recorded in the bottom flange of segment 48 are shown in Figure 33. A comparison with Figure 32 shows that similar strain response was measured between the top and bottom flanges of the segment. Relative compressive strains ranging up to 10 microstrains were recorded at gages 7, 8, and 9 during the morning hours, and slightly larger relative tensile strains were observed during the afternoon. Data from gages 8 and 9 reflected a similar measured response during the morning hours, and gage 7, located near the outer web of the southbound box girder, recorded slightly smaller compressive strains. The measured strain response

showed dissimilarities between gages, but the magnitudes of these differences were somewhat smaller than those observed between gages in the top flange.

Figure 34 presents the strains measured in the top flange of segment 48 on November 18. Although the overall trends of the strain variations were similar to those recorded on the previous day, the magnitudes of the relative compressive and tensile strains were somewhat smaller. A dissimilar strain response between gages was again observed during the afternoon hours. The strain response recorded at a majority of the gages reflected relative tensile strains between 8:00 and 20:00 hr. During this period, strains on the order of 10 to 15 microstrains were measured at gages 11 and 12. Web gages 4 and 13 showed similar trends in measured strain response, but the magnitudes of relative tensile strain were slightly smaller than at the gages between webs. Again, after 8 A.M., gage 3 recorded noticeably larger compressive strains than the other gages.

Figure 35 presents the strains measured in the bottom flange of segment 48 for November 18. An examination of this figure along with Figure 34 illustrates that a similar strain response was again measured in both the top and bottom flanges. It may also be seen that little change in relative strains was observed between 0:00 and 8:00 hr. There appeared to be smaller differences in strain response between gages during the morning hours, whereas more noticeable dissimilarities occurred during the afternoon. At 15:00 hr, relative tensile strains of approximately 20 and 10 microstrains were recorded at gages 8 and 9, respectively.

Figures 36 and 37 present the measured strain response from the top and bottom flanges of segment 48 recorded on November 19. These figures show that similar strain variations were recorded by the individual gages on each day of the study. As shown in Figure 37, gage 3 again recorded noticeably different strain variations during the latter half of the day. Similar trends in strain variation were measured at gage 4 and gages 11 through 14. At the bottom flange, gages 7, 8, and 9 recorded tensile strain variations on the order of 10 to 20 microstrains for most of the day. As depicted in Figure 37, differences of approximately 5 to 10 microstrains were observed between gages during the afternoon hours.

The measured strain data presented in Figures 26 through 37 reflected the changes caused by the ambient diurnal temperature variations that occurred during the study. Examination of the relative strain variations demonstrated consistencies that served to confirm the validity of the measured data. Apart from the anomalies observed at segment 33, consistent strain data were recorded at the two instrumented segments and both portions of the twin box girder showed similar strain behavior. Individual strain gages recorded comparable strain variations on each of the 3 days, and similarities in measured response were observed between gages at corresponding locations within the cross section. Strains measured at gages located above the webs in segment 33, for instance, were similar on each of the 3 days. During the morning hours, there was little variation between gages at either segment. The dissimilarities between gages observed during the afternoon suggested the presence of differential heating. As would be expected, the differ-

ences in measured response between gages were greater in the top flanges of the girders.

### Comparison of Computed and Measured Thermal Strains

Temperature-induced stresses were calculated for the study period, and the corresponding thermal strains are shown in Figures 38 through 43. The calculated strain values are plotted as daily relative changes in strain, similar to the measured strain data. Figure 38 shows the predicted strain variations for the top and bottom flanges of segment 33 calculated for November 17. Figure 39 presents the strain variations calculated on the same day for the top and bottom flanges of segment 48. Calculated strain variations for November 18 are shown for segments 33 and 48 in Figures 40 and 41, respectively. Similarly, the strain variations predicted for the two segments on November 19 are shown in Figures 42 and 43.

Examination of the calculated strains presented in Figure 38 indicates that significantly different strain variations were predicted for the top and bottom flanges of the box girder. Relative compressive strains in the top flange were shown to decrease between midnight and 9:20 A.M. This was followed by an increase in relative compressive strain during the afternoon, which peaked at 16:00 hr. The opposite was true for the bottom flange, where relative tensile strains were shown to decrease during the morning then increase during the afternoon, peaking at 16:00 hr. Relative compressive strains on the order of 10 to 18 microstrains were predicted for the top flange, and tensile strains of approximately 22 and 18

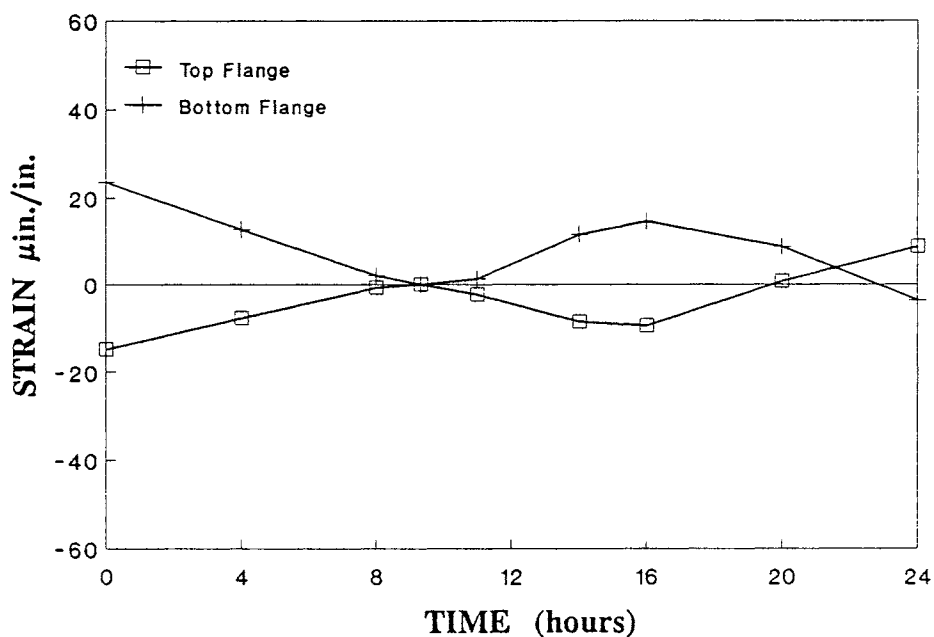


Figure 38. Predicted Strain Variations, Beam Element Model, Segment 33, 11/17/89.

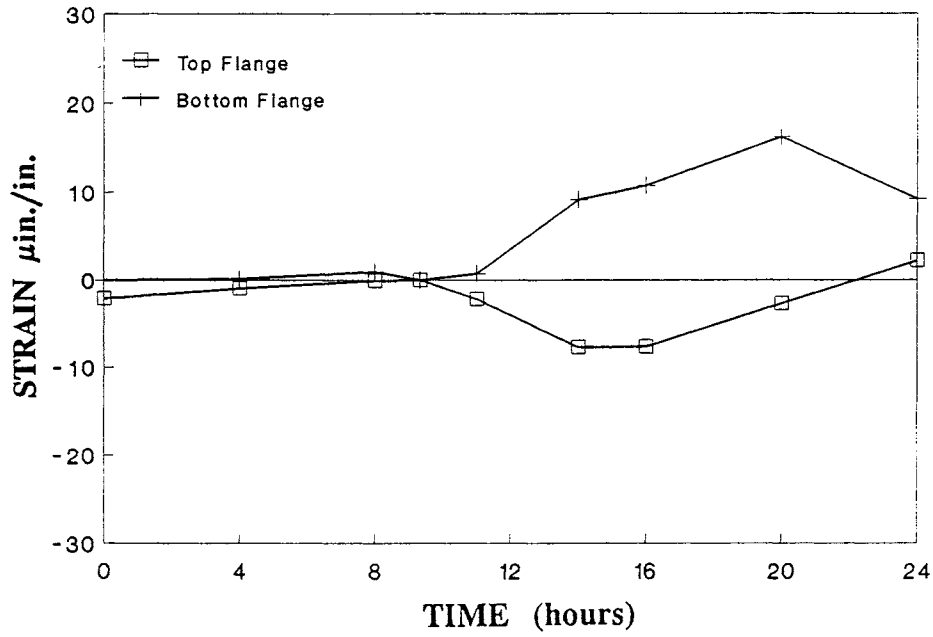


Figure 39. Predicted Strain Variations, Beam Element Model, Segment 48, 11/17/89.

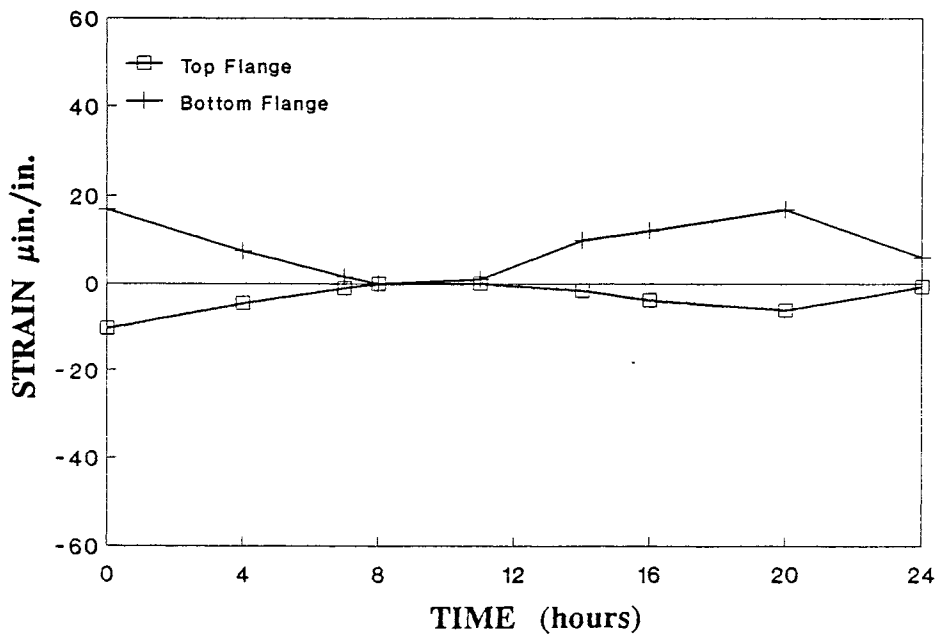


Figure 40. Predicted Strain Variations, Beam Element Model, Segment 33, 11/18/89.

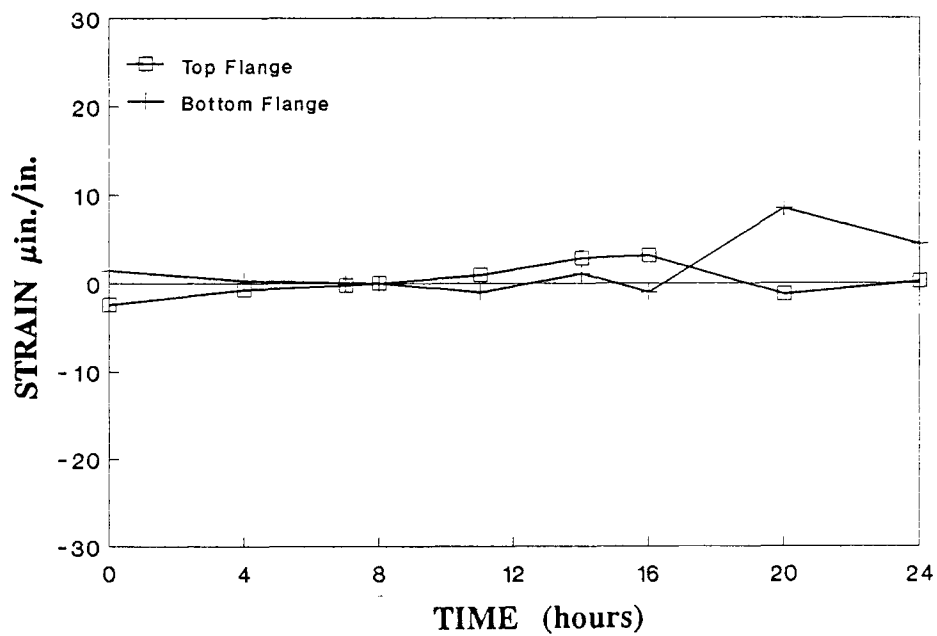


Figure 41. Predicted Strain Variations, Beam Element Model, Segment 48, 11/18/89.

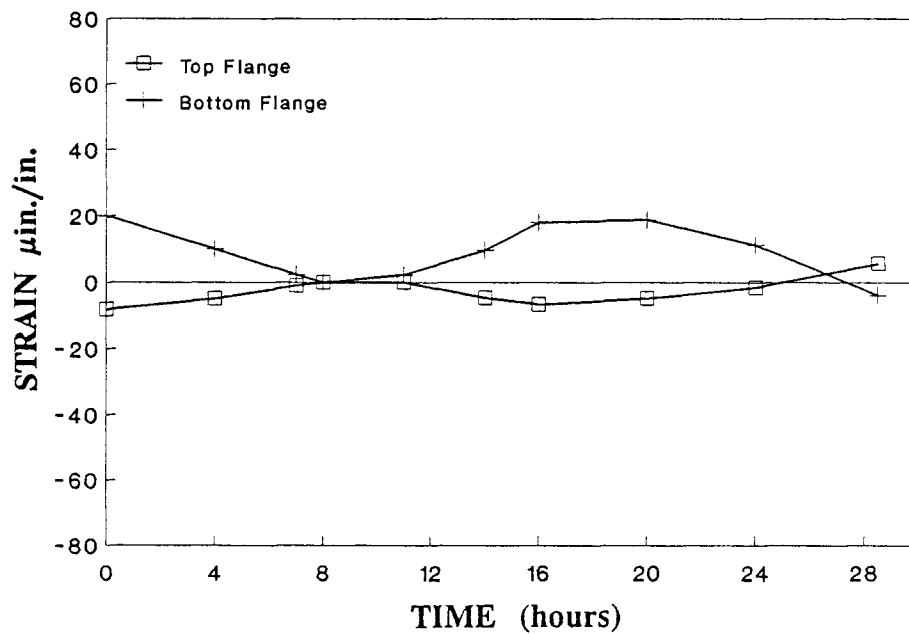


Figure 42. Predicted Strain Variations, Beam Element Model, Segment 33, 11/19/89.

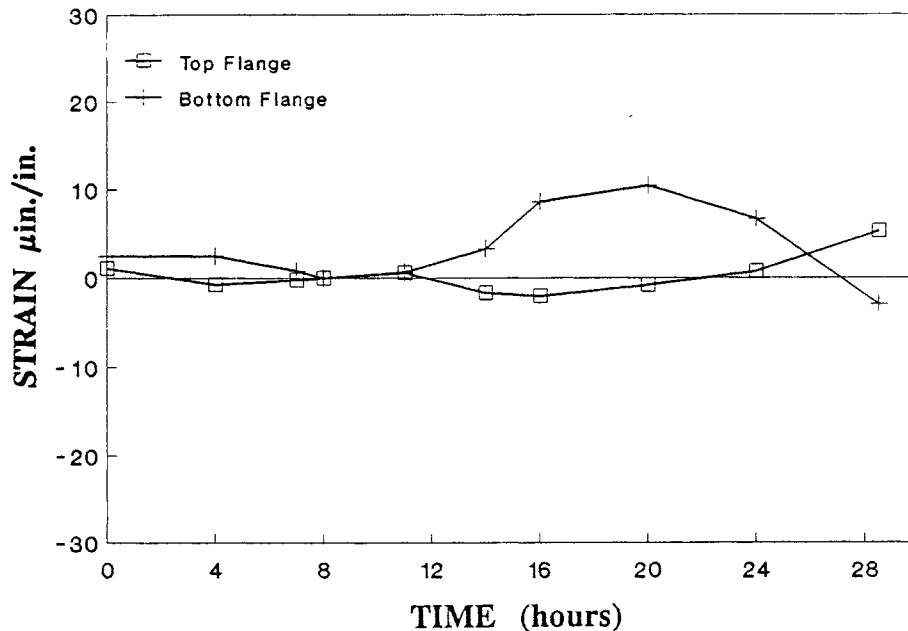


Figure 43. Predicted Strain Variations, Beam Element Model, Segment 48, 11/19/89.

microstrains were calculated at the bottom flange. As indicated in the figure, the predicted variations in the two flanges are of the same magnitude but opposite in sign, which suggests the presence of bending behavior.

The measured data for the top flange, presented in Figure 26, showed only limited correlation with the calculated values. The trends in strain variation were similar for the morning hours, but the magnitudes of the measured compressive strains were almost twice as large as those predicted by the computer model. The predicted strain response did not reflect the tensile strains measured during the afternoon. A comparison of the strains calculated for the bottom flange with the measured data shown in Figure 27 shows that, although little correlation was observed prior to 9:20 A.M., some similarities were observed during the afternoon hours. Compressive, rather than tensile, strain variations were measured at the three gages in the bottom flange between 0:00 and 9:00 hr. During the afternoon, however, the calculated tensile strains were of approximately the same magnitude as the measured data.

Figure 39 shows the calculated strains in the top and bottom flanges of segment 48 for November 17. As was shown for segment 33, a dissimilar strain response was predicted for the top and bottom flanges. Small strains were calculated at both locations during the early morning hours. Between 12:00 and 20:00 hr, compressive strain variations up to approximately 10 microstrains were calculated at the top flange and tensile strains of approximately 10 to 15 microstrains were calculated for the bottom flange. A comparison with Figure 32 shows little correla-

tion between measured and predicted strain variations for the top flange. The calculated relative compressive strains did not reflect the relative tensile strains measured by a majority of the top flange gages during the afternoon. The strains predicted at the bottom flange showed reasonable correlation with the measured data from Figure 33, but the calculated strain values are noticeably smaller between midnight and 11 A.M.

The strain variations calculated at segment 33 for November 18 and 19 are presented in Figures 40 and 42. It may be seen from these figures that the predicted strain variations were similar to those calculated on the preceding day. The strain variations at the top and bottom flanges were again similar in magnitude but opposite in sign. Relative compressive strain values of less than 10 microstrains were calculated for the top flange, and relative tensile variations up to approximately 15 microstrains were determined for the bottom flange. The analytical values again show only limited correlation with the measured strain data, presented in Figures 28 through 31. For the top flange, a reasonable correlation was observed between the strain variation trends during the early morning hours, but again, the calculated strains did not reflect the relative tensile variations measured during the afternoon. The strain variations calculated for the bottom flange showed limited agreement with the measured data during the afternoon, but the overall correlation was poor.

Figures 41 and 42 present the strain responses calculated at segment 48 for November 18 and 19. An examination of Figure 41 indicates that very small variations of strain were predicted at the top and bottom flanges of the segment on November 18. The strain variations calculated for November 19, shown in Figure 42, were similar to those calculated for November 17, where relative strains of less than 10 microstrains were predicted for the top and bottom flanges. Correlation between the measured data and predicted strain values was also limited on these days. The strain response calculated for the top flange again did not agree with the relative tensile strains measured by a majority of the gages. The relative tensile strains predicted at the bottom flange showed better comparison with the measured data on both days.

As previously indicated, the thermal strains in the cable stays were approximated based on temperature data measured by pylon thermocouples. For the calculated strain data presented in Figures 38 through 43, it was assumed that the cable-stay strands, which are encased in 1-in-thick grouted polyethylene pipe, did not undergo large daily temperature variations. The temperature variations recorded by thermocouples located at the interior of pylon segment D6 were assumed to be representative of those that may have occurred in the cable stays. In order to assess the possible implications of this assumption, the response of the box girder segments was calculated considering larger variations in cable-stay strain based on the temperature variations recorded at the southwest corner of the pylon. The assumed cable-stay strains used in calculating the box girder thermal response are shown in Figure 44 for November 17. Gages 4S and 1SW denote the number and location of the pylon thermocouples from which the assumed temperature variations were taken.

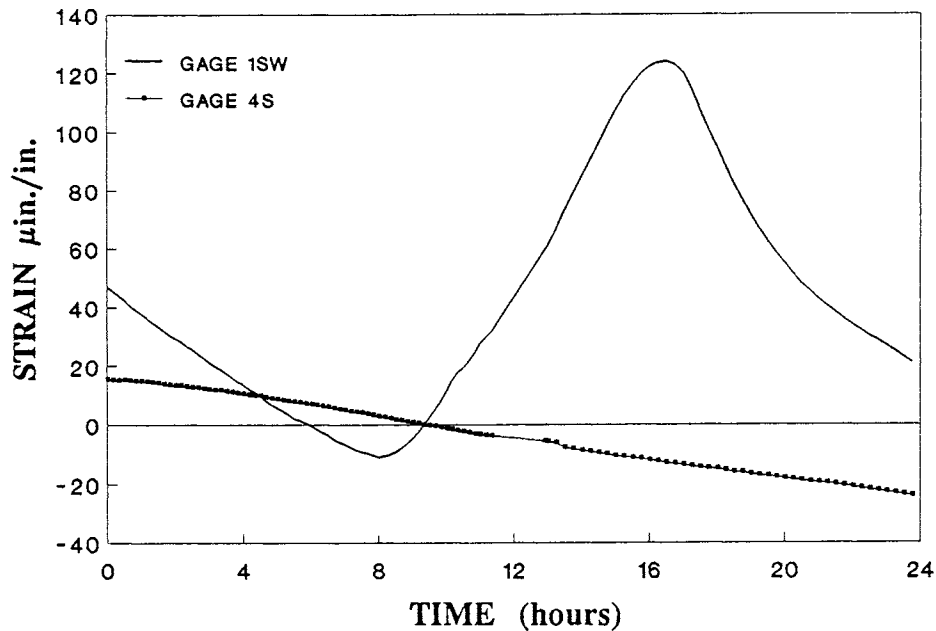


Figure 44. Assumed Cable-Stay Strain Variations, 11/17/89.

The box girder strain responses calculated using the two sets of assumed cable-stay strains are compared in Figures 45 and 46. It is seen from Figure 45 that the assumed thermal strains in the cable stays have a considerable effect on the calculated strain values at segment 33. It is also seen that the overall trends were similar for the two sets of data, but the larger cable-stay strains resulted in significantly larger magnitudes of relative strain in the box girder. At 16:00 hr, compressive strains of approximately 30 and 50 microstrains were calculated for the top and bottom flanges, respectively, using the assumed stay strains from pylon thermocouple 1SW. The larger cable-stay strains did not improve the correlation between measured and predicted response since the overall trends of the predicted strain variations remained unchanged.

Similar comparisons are made in Figure 46 for the strain response calculated at segment 48. Again, the assumed cable-stay strains resulted in significant differences at both the top and bottom flanges. For this segment, the larger cable-stay strains led to a decrease in the predicted strain values, particularly during the latter half of the day. In fact, the bottom flange strains calculated using the strains corresponding to thermocouple 1SW reflected a relative compression on the order of 5 to 10 microstrains, whereas those calculated using cable-stay strains from thermocouple 4S yielded tensile strains ranging between 5 and 15 microstrains. Although the assumed cable-stay strains resulted in large differences between predicted strain response, the strain variations determined using the larger stay strains did not accurately reflect the measured behavior.

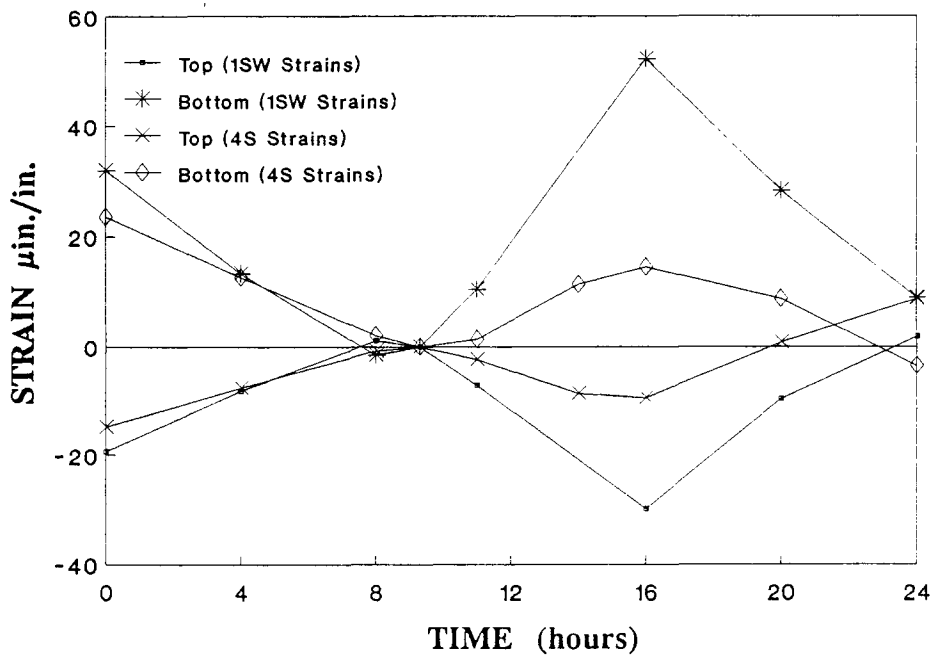


Figure 45. Comparison of Predicted Strain Variations Based on Assumed Cable-Stay Strains, Segment 33, 11/17/89.

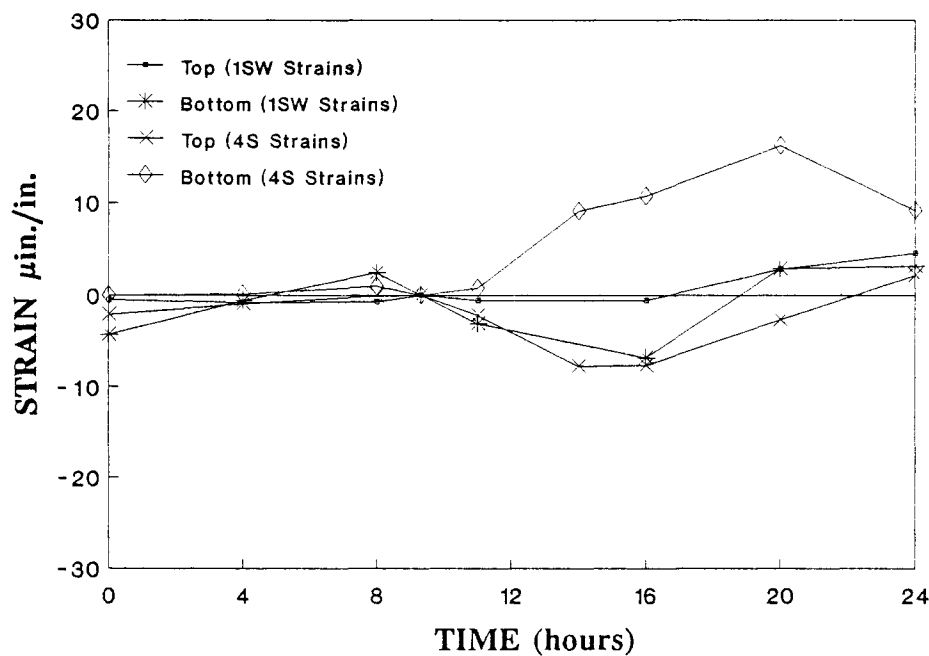


Figure 46. Comparison of Predicted Strain Variations Based on Assumed Cable-Stay Strains, Segment 48, 11/17/89.

A more detailed finite element model was used in order to verify the response predicted by the beam element model and account for local behavior within the box girder. This model, shown in Figure 47, was developed by Yen (1992) for dynamic analysis of the James River Bridge. The box girder cross section was modeled with plate elements of varying thickness, and the pylon and cable-stay members were represented as beam elements. Because of size restrictions, only one quarter of the bridge was modeled, so appropriate boundary conditions were applied along lines of symmetry. Changes in temperature, obtained from measured thermocouple data, were applied to the plate elements, and the resulting element stresses were calculated at locations corresponding to box girder segments 33 and 48.

Figure 48 shows the locations of the nodes corresponding to points on the cross section of box girder segments 33 and 48. As shown in Figure 48(a), nodes 260, 190, 155, 120, 85, and 15 represent locations in the top flange of segment 33, moving in the direction from the center line of the structure, at the cable stays, toward the outer flange. Similarly, nodes 435, 400, and 365 represent locations in the bottom flange of this segment. In Figure 48(b), nodes in the top flange of segment 48 are designated as numbers 252, 182, 147, 112, 77, and 7, in sequential order from the center line of the structure toward the outer flange. Likewise, nodes 427, 392, and 357 represent locations in the bottom flange of segment 48.

Figure 49 presents the strain variations obtained from the plate element model at the various nodes within the top flange of segment 33 for November 17. It is clear that significant differences in strains were predicted at locations across the deck. The overall trends in response were similar to those calculated using the simpler beam element model, however. Decreasing relative compressive strains were predicted during the morning hours, followed by an increase in compressive strains during the afternoon. It may also be noted that the largest strains were calculated at the nodes nearest the cable stays. The corresponding strain variations calculated at the bottom flange nodes are shown Figure 50. Once again, the strain variations predicted by the plate element model closely resemble those predicted by the simpler beam element model. Differences in relative strains of up to 20 microstrains were observed between nodes, where the largest strain magnitudes were also calculated at nodes nearest the cable stays.

Similar plate element model results are shown for the top and bottom flanges of segment 48 in Figures 51 and 52, respectively. As was shown for segment 33, significant differences between strain variations were observed at the various locations across the flanges. The largest strain magnitudes were predicted during the afternoon hours at the nodes nearest the cable stays. The calculated strain variations for the top and bottom flanges of this segment were also similar to those predicted using the beam element model.

Strains calculated using the plate and beam element models are compared in Figures 53 and 54. Figure 53 compares the strains calculated for the top and bottom flanges of segment 33, in which the plate element model results were averaged over the nodes in the respective flanges. Figure 54 shows a similar comparison of average strain variations calculated for segment 48. Although differences in

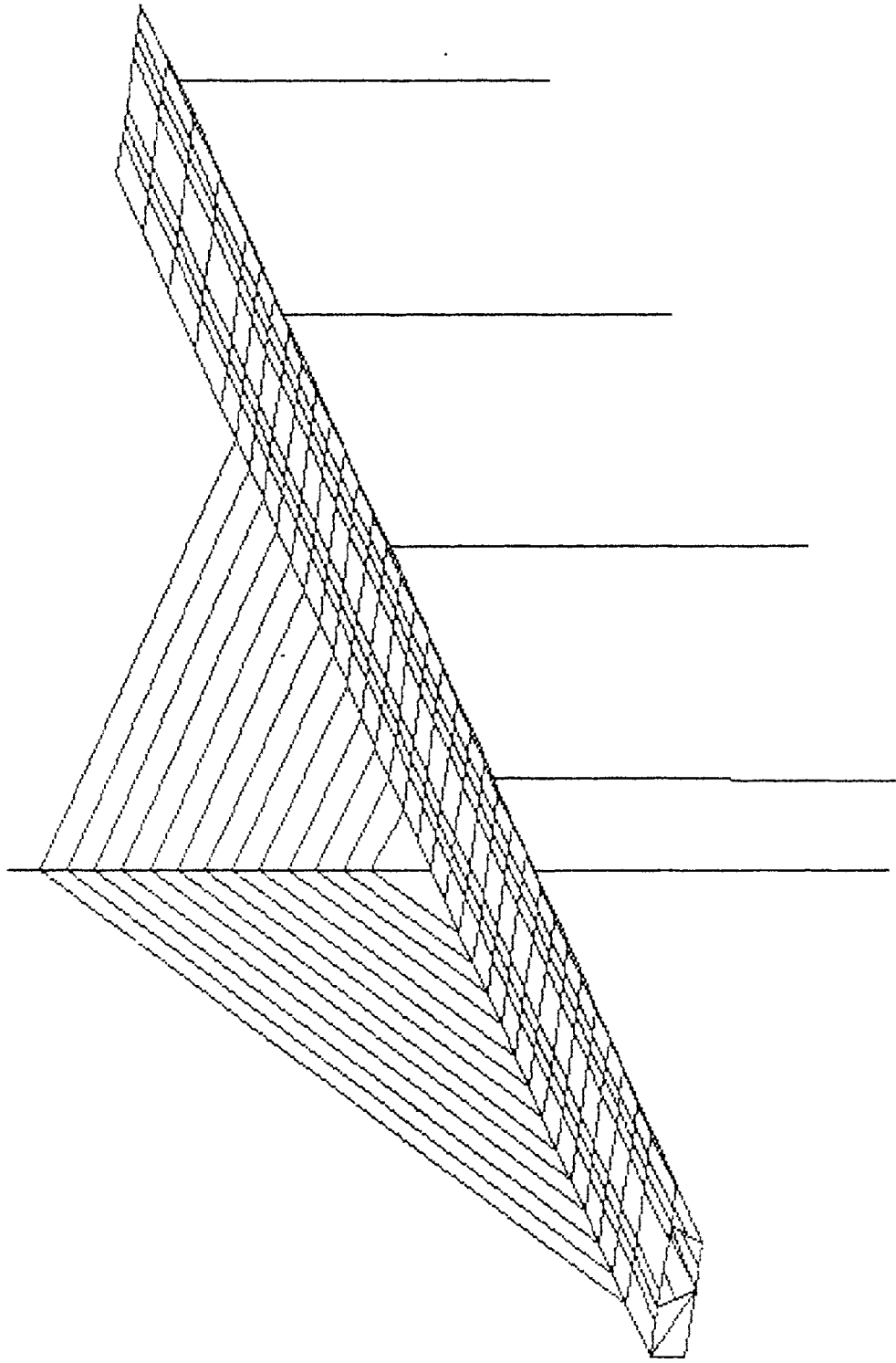
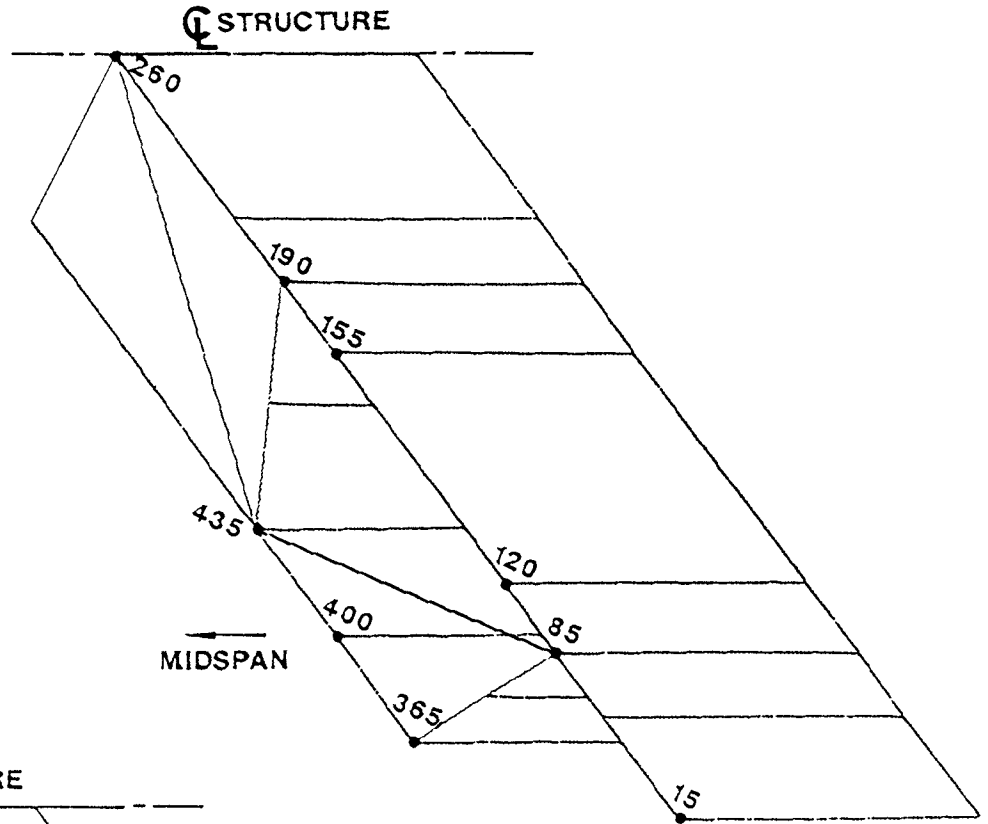
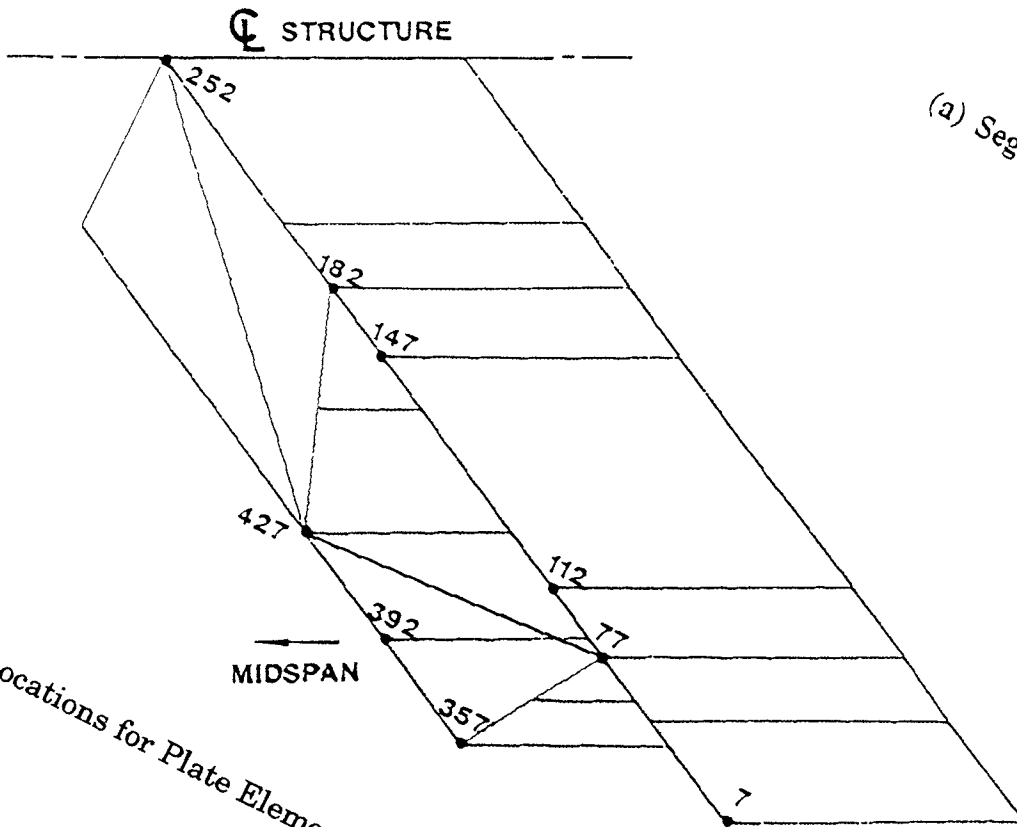


Figure 47. Quarter-Bridge Plate Element Model.



(a) Segment 33



(b) Segment 48

3. Node Locations for Plate Element Model.

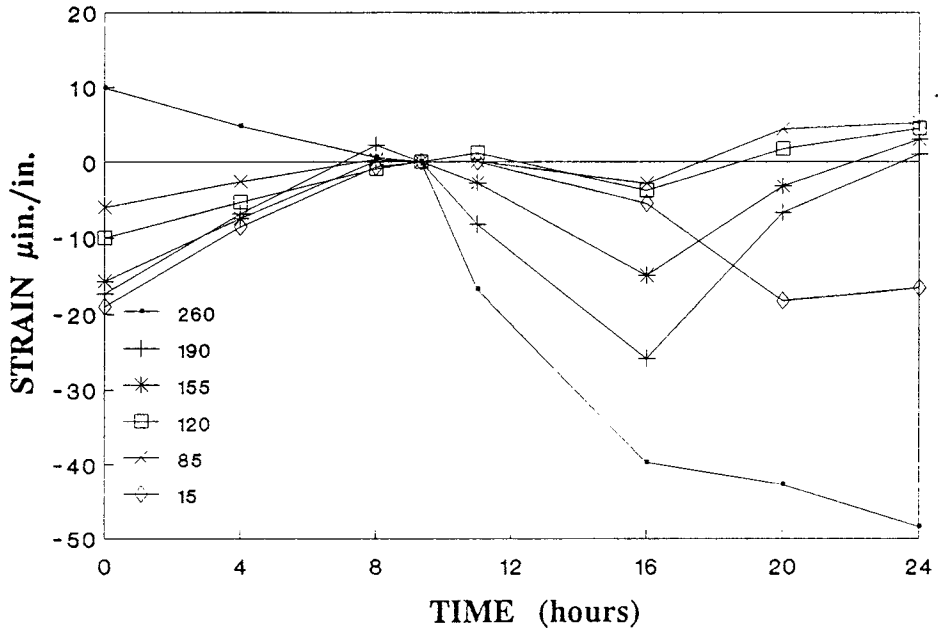


Figure 49. Predicted Strain Variations, Plate Element Model, Segment 33, Top Flange Nodes, 11/17/89.

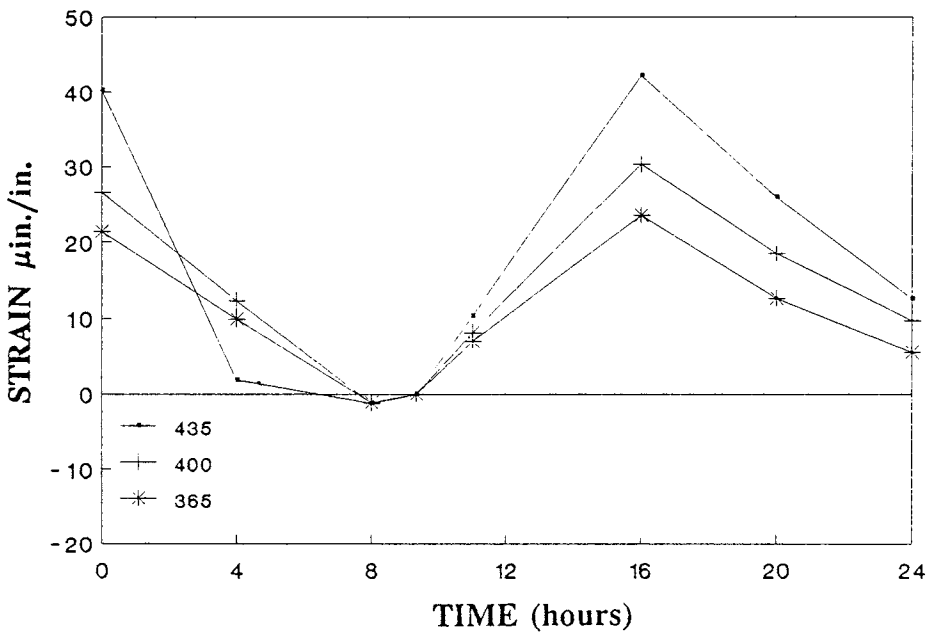


Figure 50. Predicted Strain Variations, Plate Element Model, Segment 33, Bottom Flange Nodes, 11/17/89.

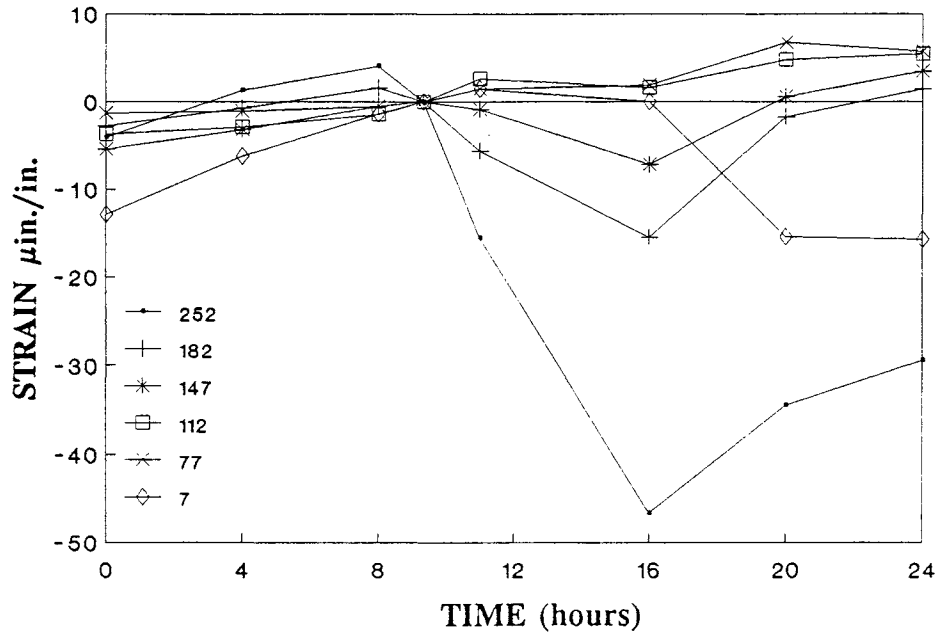


Figure 51. Predicted Strain Variations, Plate Element Model, Segment 48, Top Flange Nodes, 11/17/89.

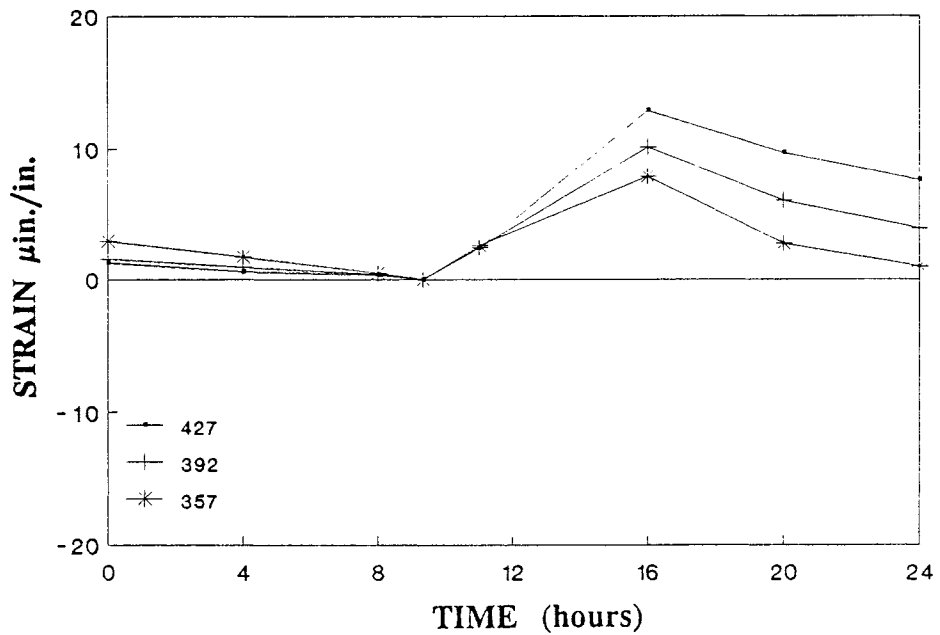


Figure 52. Predicted Strain Variations, Plate Element Model, Segment 48, Bottom Flange Nodes, 11/17/89.

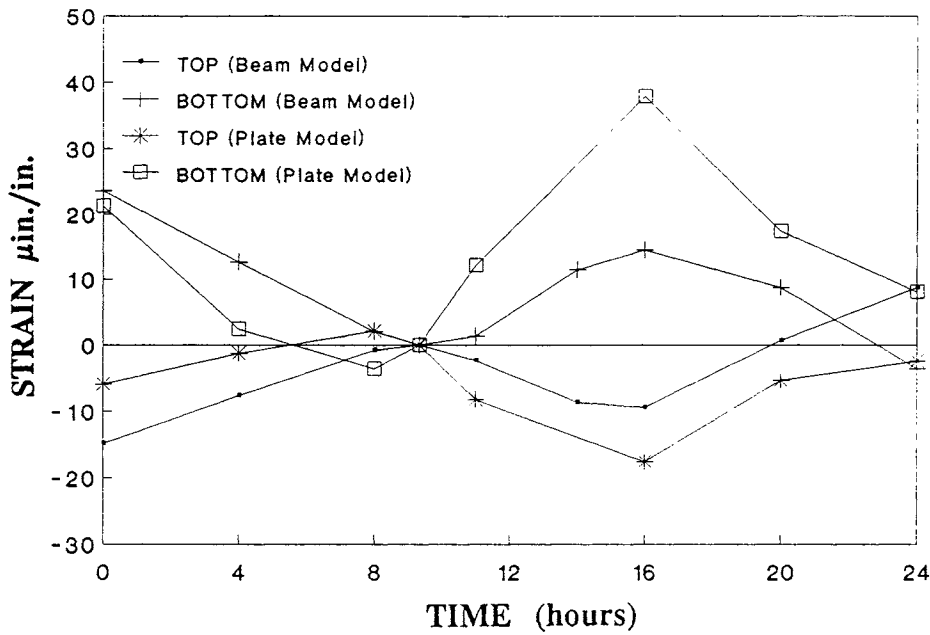


Figure 53. Comparison of Predicted Strain Variations, Beam and Plate Element Models, Segment 33, 11/17/89.

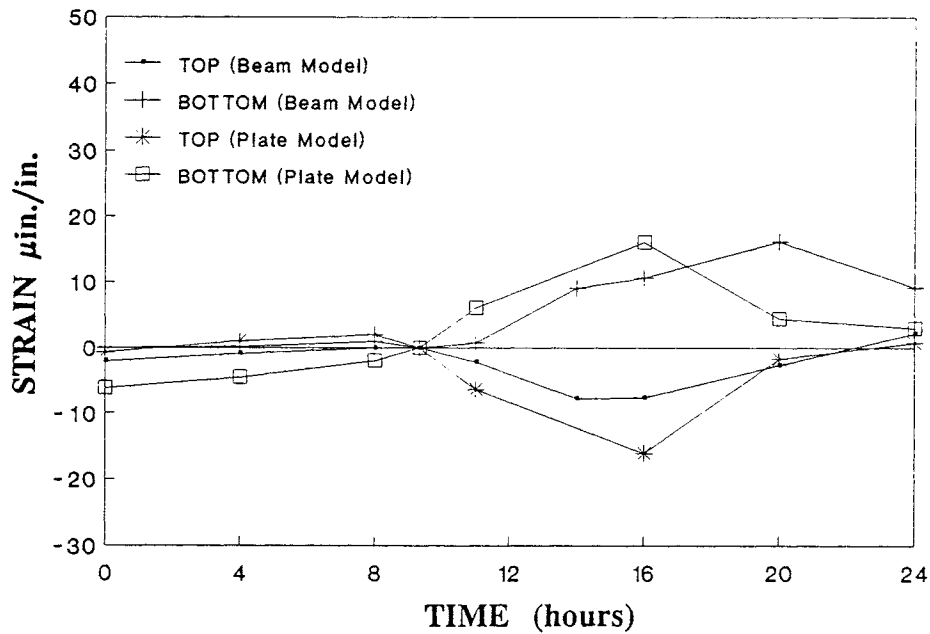


Figure 54. Comparison of Predicted Strain Variations, Beam and Plate Element Models, Segment 48, 11/17/89.

relative strain magnitude were evident between the results of the two models, the overall trends in strain response are similar. Considering the great difference between the two analysis approaches, it must be concluded that the calculated strain variations were the best estimates of bridge response that could be obtained through available analytical means.

The large differences between the measured and predicted strain responses prompted a critical evaluation of the strain-measuring instrumentation and the experimental procedure in general. The measured strains clearly indicate a temperature-driven axial response, so efforts were made to determine if the strains measured by the gages reflected the actual response of the bridge or some other temperature-induced phenomenon. As discussed previously, corrections were made to account for transverse gage curvature and the mismatch between coefficients of thermal expansion of the concrete and reinforcing steel. Other factors that may have resulted in temperature-induced apparent strains were identified and systematically eliminated from consideration. Changes in gage factor attributable to temperature have been documented, but variations of less than 1 percent would be expected over the temperature range encountered in the study (Measurements Group Inc., 1983). Imperfect temperature compensation resulting from differences between the individual longitudinal and transverse gages of the 90-degree strain rosettes may have been possible, but it is unlikely that such differences would be consistent at all of the gages. Likewise, accidental thermocouple effects in the gages, attributable to the solder connections of the lead wires, would not have led to consistent variations at each gage. The data acquisition system was designed to operate under a wide range of temperatures. Even if there was some thermal sensitivity in the system, relatively small variations in temperature were observed at locations of the individual units and the cyclic nature of the temperature changes were not severe.

Since a reasonable explanation for the measured temperature-induced strains could not be identified, it was concluded that the strains measured by the gages do in fact represent the actual bridge response. The consistency with which strain variations were recorded at the various gages eliminated the possibility of local malfunctions, such as imperfect bonding between the concrete and gaged rebar. The measured data presented in Figures 26 through 37 indicated consistent global and local behavior recorded on each of the 3 days of the study. The similarities between the strain variations recorded in the top and bottom flanges of the instrumented segments suggested the presence of a dominant axial response. During the afternoon hours, large differences were observed between gages, especially those in the top flange. This behavior could be attributed to differential heating effects, such as localized flange bending or local strains attributable to the nonlinear component of the thermal gradient. Such temperature differences were consistently measured at locations within the cross section during the study. The strain response measured at gage 1, in segment 33, and at gage 3, in segment 48, were significantly different from those measured by the other gages in respective flanges, suggesting the possibility that certain portions of the bridge are subject to isolated

thermal variations. Such effects may be influenced by the parapet walls or features within the structure that are not readily apparent.

The large amounts of internal and external prestressing steel within the box girder probably had a significant influence on the overall thermal response of the structure. The internal strands, located in the top flange above the webs, were subject to the same temperature changes as the concrete. Assuming the prestressing steel has a larger coefficient of thermal expansion than the surrounding concrete, a temperature increase would result in a relative tensile strain variation, similar to that observed in the measured data during the afternoon hours. The external prestressing within each of the main-span box girders consists of 24 tendons, each having 12 strands 0.6 in in diameter. These strands are effectively insulated from the surrounding environment, so temperature changes in the box girder would generate significant restraining forces during the prestressing. The thermal effects of the prestressing would be difficult to model analytically, and the accuracy of the results would be limited.

Comparison of the measured and calculated results showed that the computer models were limited in their ability to predict the thermal response of such a complex structure. A number of assumptions were made in the analyses. First, the analysis itself involved integrating piece-wise linear temperature distributions over the cross section, which could not account for local variations in temperature. The actual temperature distributions were shown to vary significantly across the section in Figures 23 and 24. As mentioned previously, approximate cross sections were developed to simplify the calculations for the thermally induced axial strains and curvatures. The thermal strains in the cable stays were assumed to follow the daily temperature variations recorded in the pylon. Analysis results from the beam model yielded average strains at the top and bottom flanges of the box girder and did not account for local effects, such as shear lag.

Although these factors limited the accuracy of the predicted strains, the overall strain response was substantiated by the results of the plate element model. Though this model was considerably more detailed and reflected differences in strain variations across the deck, it was also limited in its ability to predict the measured strain response. Temperature changes were applied uniformly through the depth of the plate elements such that the effects of a thermal gradient through the depth of the top flange were not considered. In order to introduce the variation of thermal strain through the flange, the plate element model would have to be loaded with a curvature induced by the linear part of the strain gradient. The finite element model used for this study precluded the incorporation of such a loading.

## Pylon Segments

### Measured Temperature Variations with Time

Temperature data recorded by the thermocouples in pylon segment D6 are shown in Figures 55 through 58. The variations in temperature are plotted over

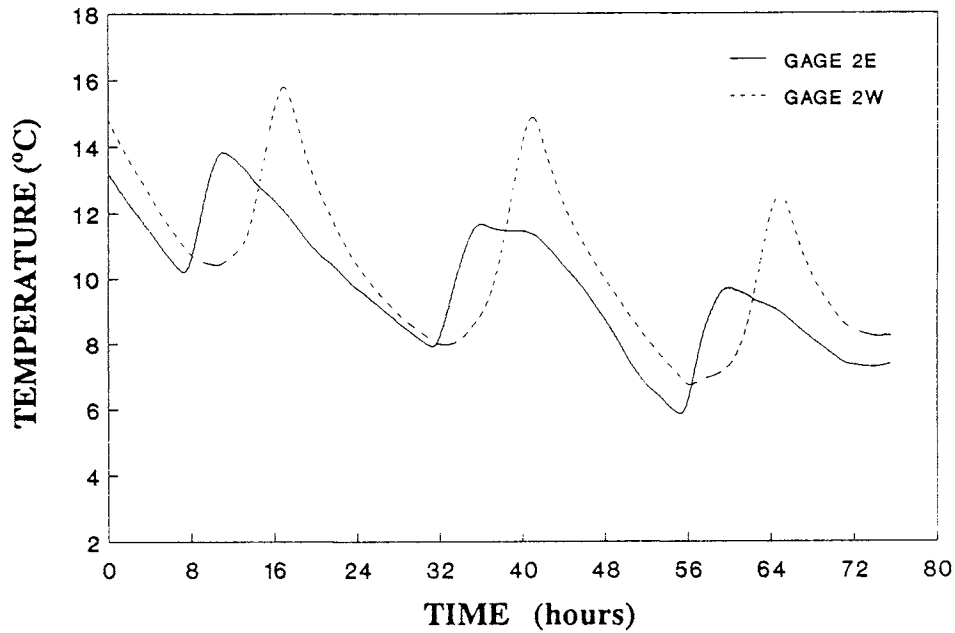


Figure 55. Measured Temperature Variations, Pylon Segment D6, Gages 3N & 3S.

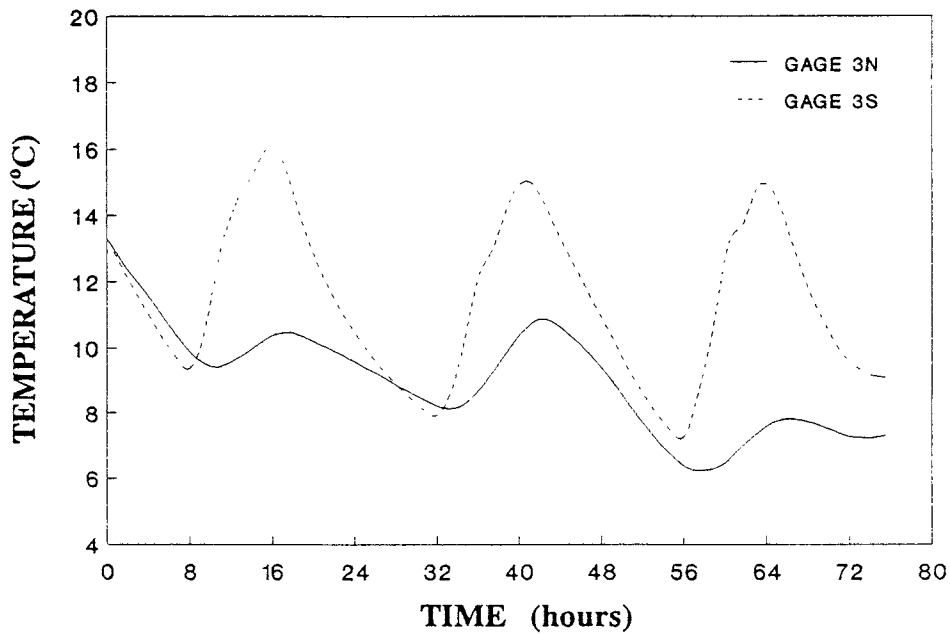


Figure 56. Measured Temperature Variations, Pylon Segment D6, Gages 2E & 2W.

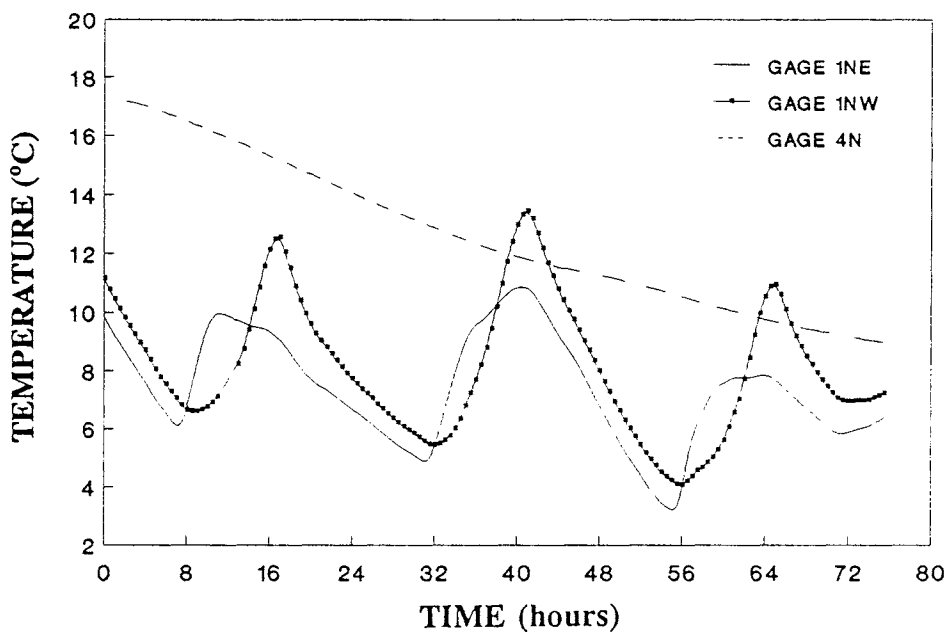


Figure 57. Measured Temperature Variations, Pylon Segment D6, Gages 1NE, 1NW, & 4N.

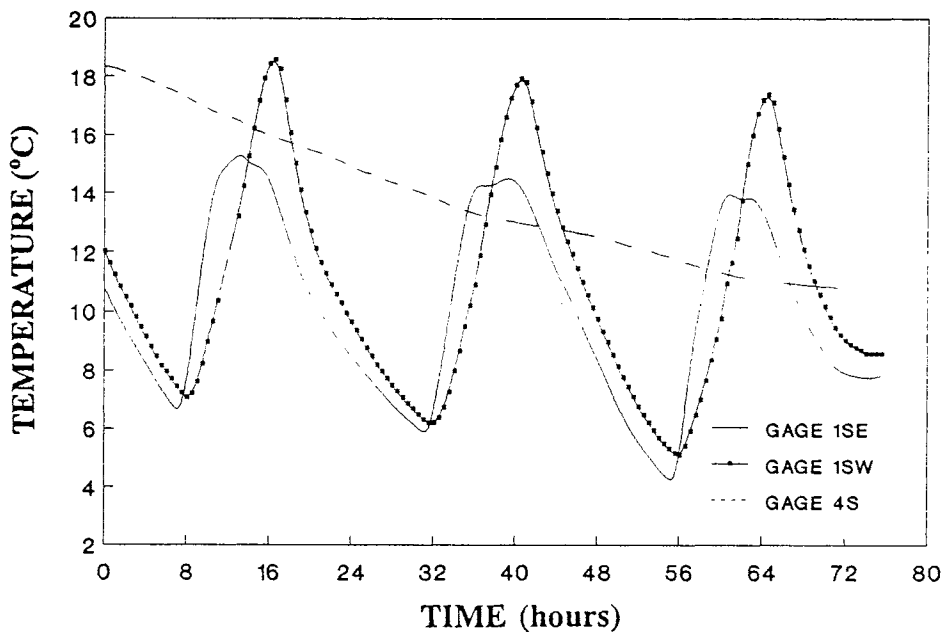


Figure 58. Measured Temperature Variations, Pylon Segment D6, Gages 1SE, 1SW, & 4S.

the same period as previously shown for the box girders. Figure 55 presents the temperatures recorded at the east and west faces of the segment, and Figure 56 shows temperatures recorded at the north and south ends (see Figure 13 for thermocouple locations). From Figure 55 it is seen that daily temperature variations of approximately 4 degrees C were recorded at the eastern side of the segment and variations between 5 and 8 degrees C were recorded at the western side. Daily temperature extremes occurred at the eastern exposure at approximately 6:00 and 12:00 hr, and temperature extremes at the western exposure occurred at 7:00 and 15:00 hr, respectively. The large slopes of the curve representing the temperature variation recorded at gage 2W indicates that rapid heating and cooling occurred at this location. Figure 56 shows the difference between temperatures measured at the north and south ends of the pylon. Daily temperature variations on the order of 6 degrees C were measured by gage 3S, at the south end, and smaller variations of approximately 2 degrees C were measured at the north end.

Similar pylon thermal response information is presented in Figures 57 and 58. These figures present temperatures recorded at the four corners and the interior of the precast pylon segment. An examination of Figure 57 shows that temperature variations of approximately 6 to 8 degrees C were observed at gage 1NW, in the northwest corner of the segment, and smaller temperature changes of 4 to 6 degrees C were observed at gage 1NE in the northeast corner. In contrast to the temperatures recorded near the exterior faces, the thermal response measured at gage 4N, located in the interior of the section, did not exhibit diurnal variations. In fact, the temperature decrease observed at this location and at gage 4S, shown in Figure 58, is indicative of the overall cooling trend that took place during the study. Figures 56 and 58 show that the largest variations in temperature occurred at locations having southern exposures. Daily changes in temperature on the order of 8 to 10 degrees C were recorded at gages 1SE and 1SW. Although larger temperature variations were recorded at the south-facing locations, a comparison of the thermal data presented in Figures 57 and 58 indicates that these points cooled to approximately the same temperature as the northern portions of the segment. The sharp peaks in the temperature variation curves indicate the areas of the pylon subject to rapid heating and cooling.

### Measured Temperature Distributions Across the Pylon

To facilitate the visualization of the temperature variation across the pylon, color contour plots of the measured temperatures were constructed. Two of the measured temperature distributions for the pylon are shown as contour plots in Figures 59 and 60. Figure 59 represents the temperature distribution recorded at 8 A.M. on November 17, and Figure 60 presents the distribution recorded at 4 P.M. the same day. These times correspond to the approximate times at which the minimum and maximum temperatures were measured in the pylon section at thermocouple 1SW. As with the box girder temperature distributions, temperature contours were generated using a finite element model of the cross section in which the node points corresponded to the location of the thermocouples in segment D6.

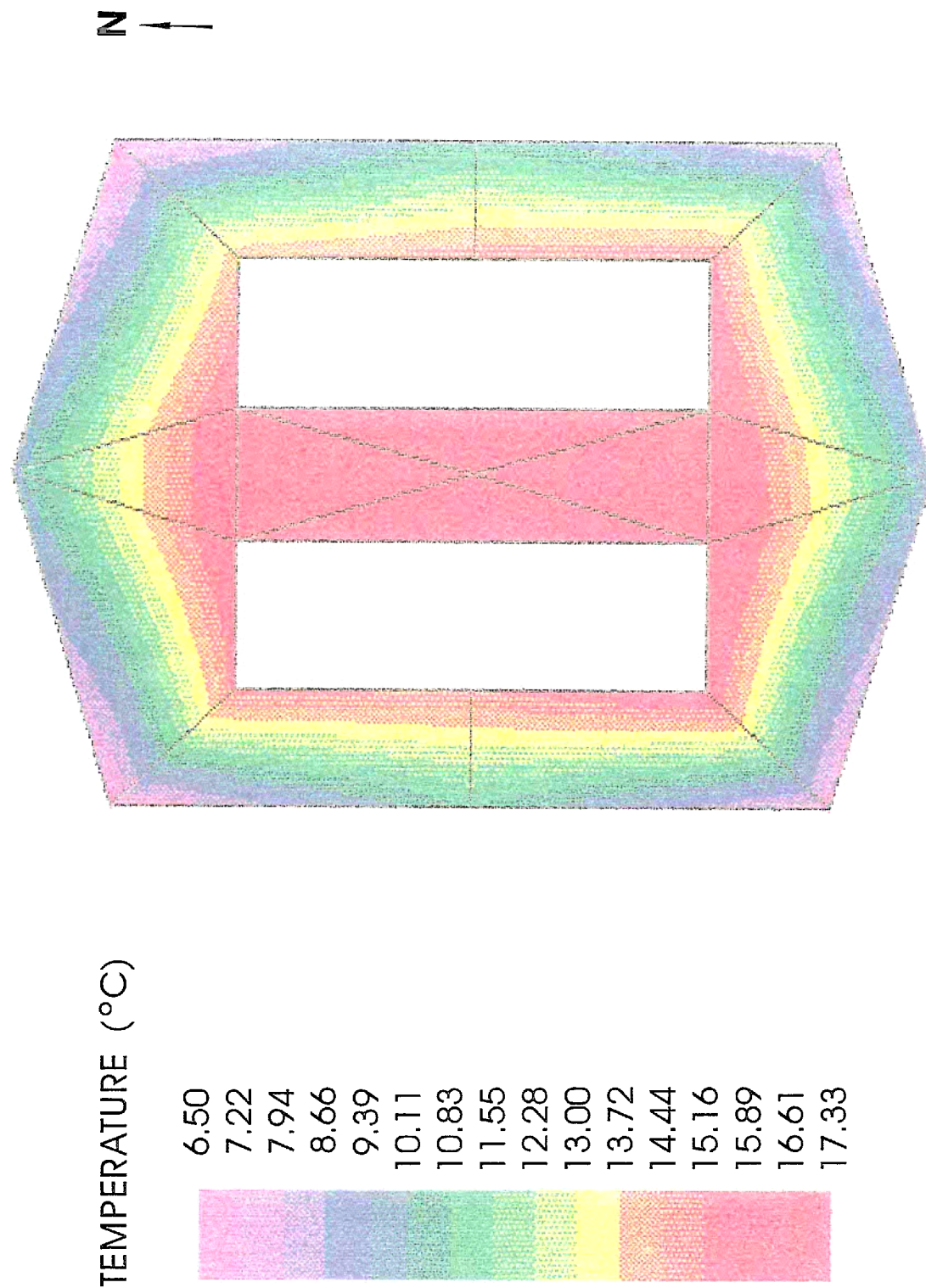
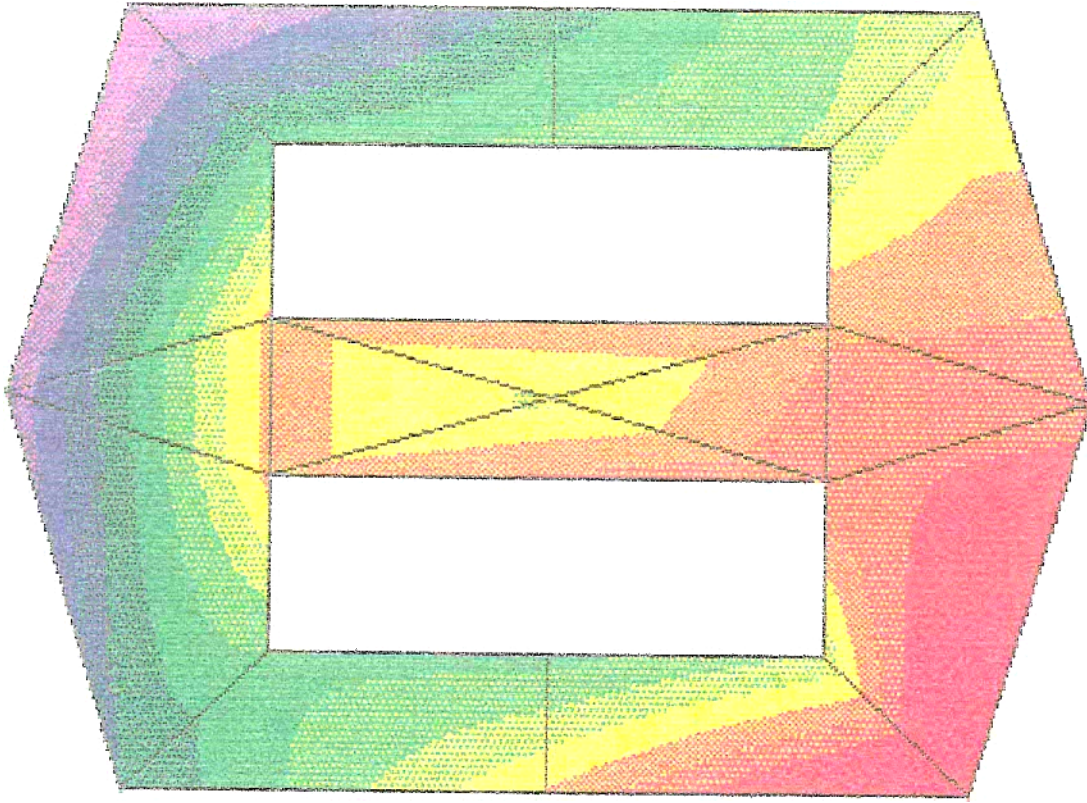


Figure 59. Measured Pylon Temperature Distribution, 11/17/89, 8:00 A.M.

N ↑



TEMPERATURE (°C)

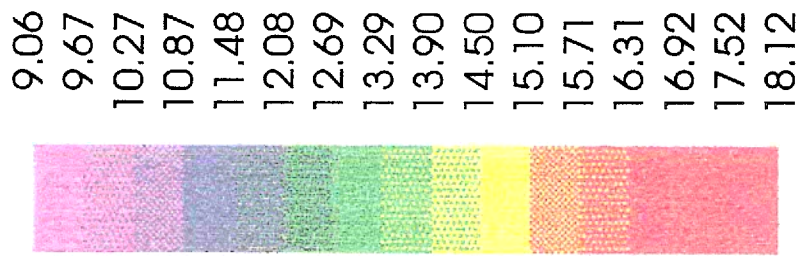


Figure 60. Measured Pylon Temperature Distribution, 11/17/89, 4:00 P.M.

Because of the limited number of thermocouples through the thickness, the intermediate contours are quite approximate.

The temperature distribution data presented in Figure 59 show that, at 8 A.M., the four corners of the pylon were at approximately the same temperature and a fairly uniform thermal gradient existed through the section's walls. Temperatures of approximately 6 degrees C were recorded at the exterior corners, and temperatures of approximately 15 degrees C were measured at the interior, near the inner walls. The highest temperature, about 17 degrees C, was recorded at the center of the section. As shown in Figure 60, the temperature distribution changed significantly by 4 P.M. Consistent with the data presented in Figures 57 and 58, the maximum temperature of approximately 18 degrees C was measured at the southwest corner, and the minimum temperature of approximately 9 degrees C was recorded in the northeast. At the center of the cross section, a temperature of about 14 degrees C was measured, and temperatures of approximately 16 degrees C were recorded at locations near the interior walls corresponding to thermocouples 4N and 4S. During the early afternoon hours, significant warming occurred in the pylon, and as seen from Figure 60, large temperature differences existed through the entire cross section.

### Measured Thermal Strains

Examination of the data recorded at the pylon sections indicated that only a few of the strain gages were not operational. Gages 1NW and 4N, in segment D6, and gages 3B and 4, in the cast-in-place section, appeared to be inoperative (see Figure 12 for gage locations). Representative thermal response data from precast segment D6 and the cast-in-place section are shown for the period of November 17 through 19 in Figures 61 through 66. As with the strain data from the box girder, the measured pylon strains are plotted as daily variations relative to the times at which the minimum temperatures were recorded in the box girder.

Figure 61 presents the measured strain data recorded at segment D6 on November 17. Referring to Figure 12, it is seen that gages 1NE and 1SE were located in the northeast and southeast corners of the section, respectively, and gage 4S was located at the interior of the segment, near the south end. Strain data from the cast-in-place section are plotted for November 17 in Figure 62. Gages 2C, 1A, and 2A were located along the western face of the section. Strain data recorded on November 18 are presented for segment D6 and the cast-in-place section in Figures 63 and 64, respectively. Similarly, pylon strain data recorded on November 19 are shown in Figures 65 and 66.

An examination of the strain data obtained from segment D6, shown in Figures 61, 63, and 65, indicated that similar relative strain variations were recorded on each day of the study. Prior to 8 A.M., decreasing relative strains were measured by the gages. After that time, relative tensile strains were recorded at each location for the remainder of the day. From these figures it may be seen that considerable variation between strain gages was observed between 8:00 and 24:00 hr. The largest relative tensile strains, ranging between 50 and 80 microstrains, were

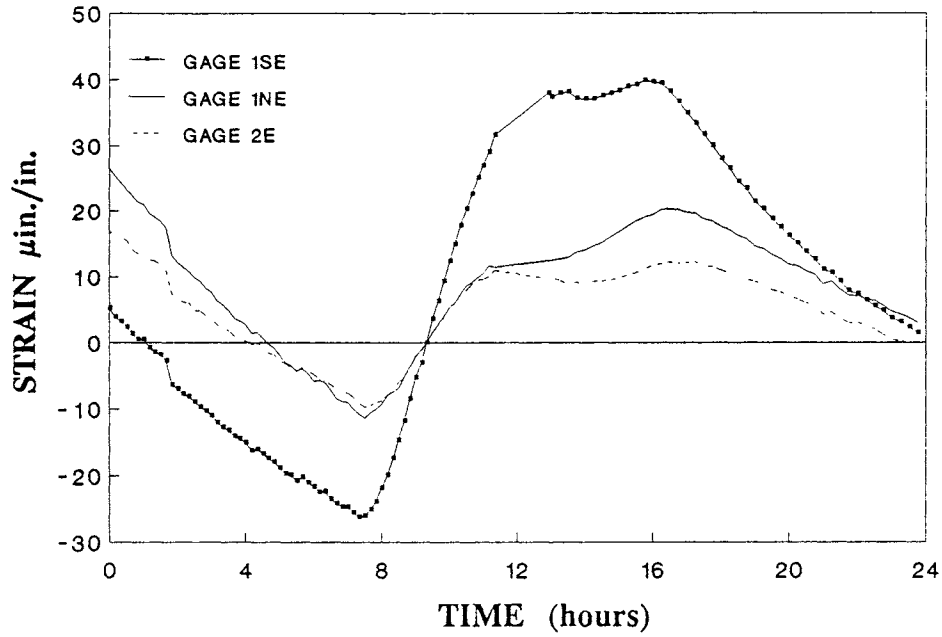


Figure 61. Measured Strain Variations, Pylon Segment D6, Gages 1SE, 1NE, & 2E, 11/17/89.

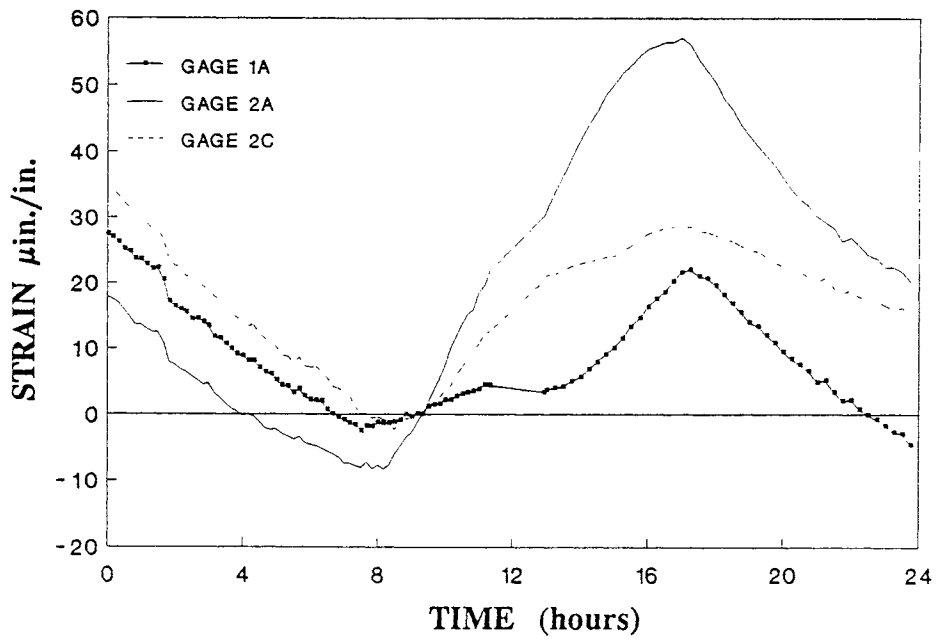


Figure 62. Measured Strain Variations, Cast-in-Place Pylon, Gages 1A, 2A, & 2C, 11/17/89.

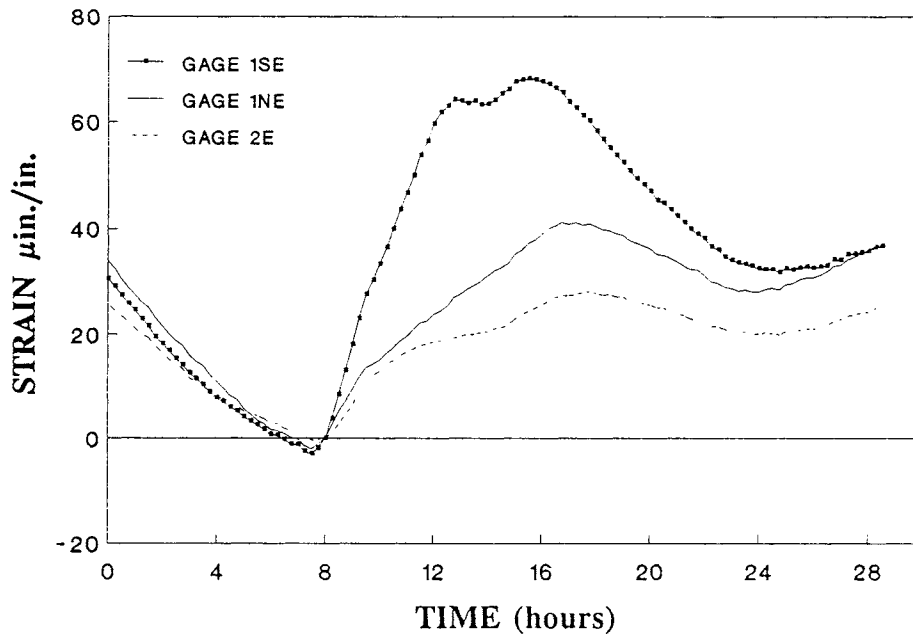


Figure 63. Measured Strain Variations, Pylon Segment D6, Gages 1SE, 1NE, & 2E, 11/18/89.

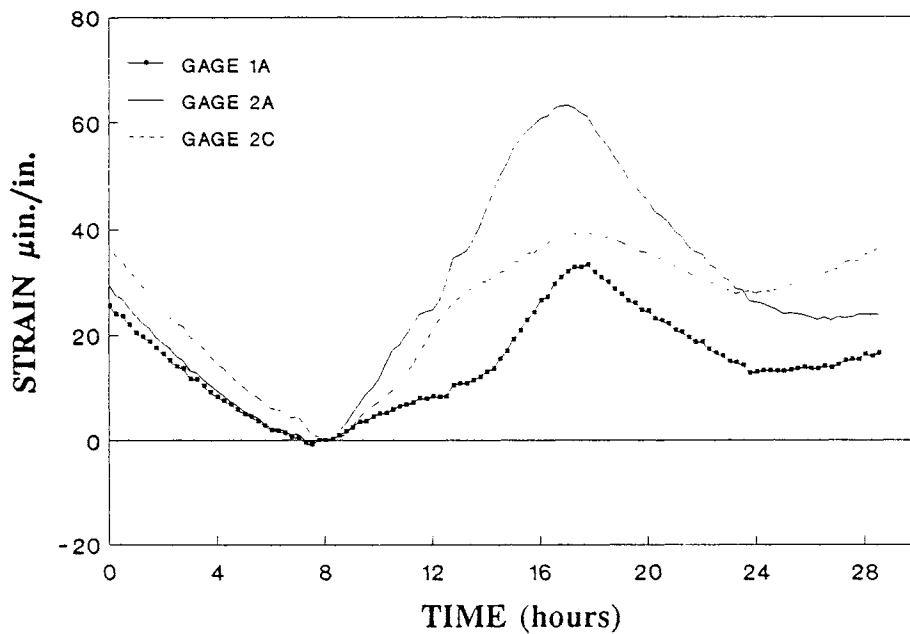


Figure 64. Measured Strain Variations, Cast-in-Place Pylon, Gages 1A, 2A, & 2C, 11/18/89.

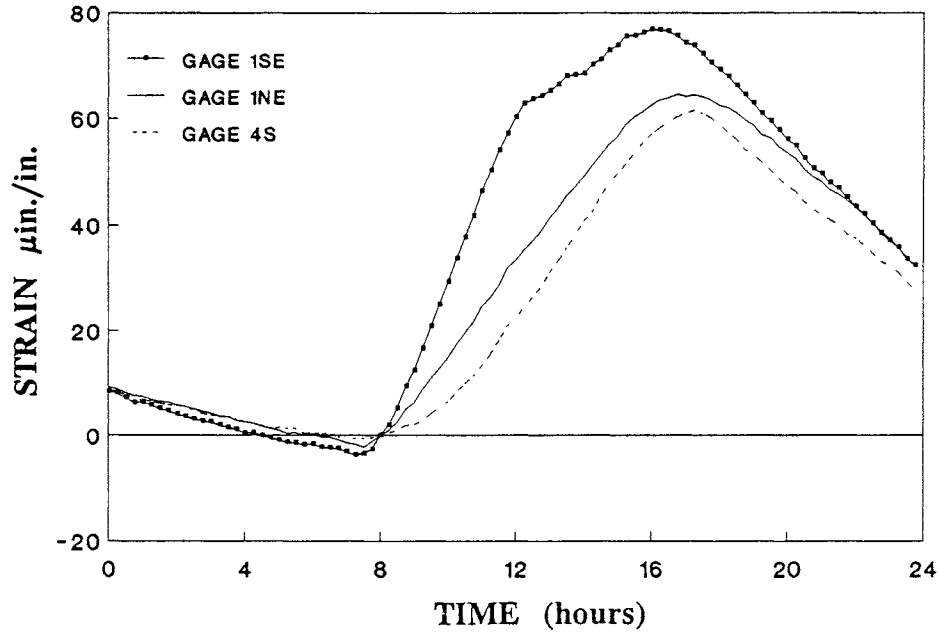


Figure 65. Measured Strain Variations, Pylon Segment D6, Gages 1SE, 1NE, & 2E, 11/19/89.

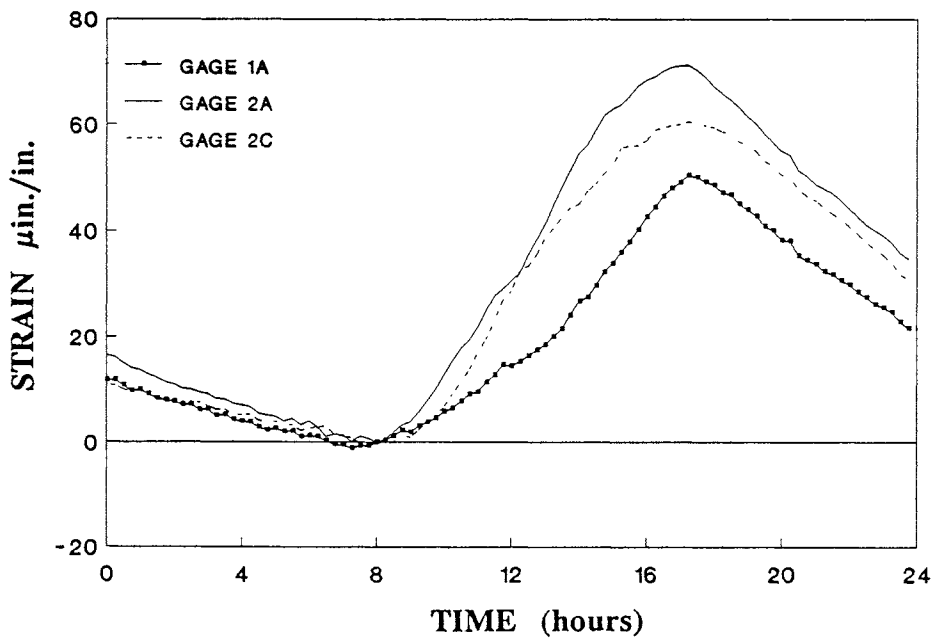


Figure 66. Measured Strain Variations, Cast-in-Place Pylon, Gages 1A, 2A, & 2C, 11/19/89.

consistently recorded at gage 1SW, at approximately 18:00 hr. Peak values of relative tensile strains, recorded at gage 1NE, were on the order of 20 to 65 microstrains, and those measured at gage 2E were only between 10 and 40 microstrains.

Similar strain variations were recorded by the strain gages in the cast-in-place section, as shown in Figures 62, 64, and 66. Relative tensile strains ranging between approximately 10 to 40 microstrains were recorded by each of the gages during the early morning hours. The relative tensile strain variations decreased until approximately 8 A.M., after which a substantial increase in relative tensile strain was observed. Smaller variations in measured strain response were observed between gages during the early morning hours than in the latter half of the day. Peak values of relative tensile strains were consistently recorded at 18:00 hr each day, and the largest magnitudes were measured at gage 2A, located in the southwest corner of the cross section. Maximum tensile strains recorded at gage 2A were approximately 70 microstrains, and the largest relative tensile strains recorded at gages 1A and 2C were on the order of 20 to 50 microstrains.

The strain data recorded at the instrumented pylon sections reflected a cyclic temperature-induced response. The similar strain variations recorded at different locations within each of the sections suggest the presence of a consistent global thermal response. The differences in relative strains recorded between gages during the afternoon hours are indicative of localized effects attributable to differential heating within the cross sections. As was illustrated by the measured data from the box girder, the largest magnitudes of relative tensile strain were recorded at locations subject to direct solar radiation. The peak values of measured strain response occurred roughly at the times at which the highest temperatures were recorded in the pylon section. In contrast to the strains recorded near the exterior surfaces of the sections, the strain data recorded at gage 4S did not resemble the local measured temperature variations. This would seem to indicate that local temperature differentials resulted in differences in measured strains between gages, but the strain variations recorded by the pylon gages reflected the overall thermal response of the structure.

### Comparison of Computed and Measured Thermal Strains

Thermally induced stresses and corresponding strains were calculated for the instrumented pylon sections using measured temperature distributions and the beam element model. Predicted and measured strains for pylon segment D6 and the cast-in-place section are presented in Figures 67 through 72. Again, the strains are plotted as daily variations relative to reference strains recorded during the morning hours of each particular day. Figure 67 compares the measured and predicted strains for November 17 at gages 3N and 3S located at the north and south ends of segment D6. Figure 68 presents a similar comparison of strain variations for gages 3A and 5 in the cast-in-place section. The November 18 strain data for segment D6 and the cast-in-place section are shown in Figures 69 and 70, respectively. Similarly, Figures 71 and 72 present comparisons between measured and calculated pylon strains for November 19.

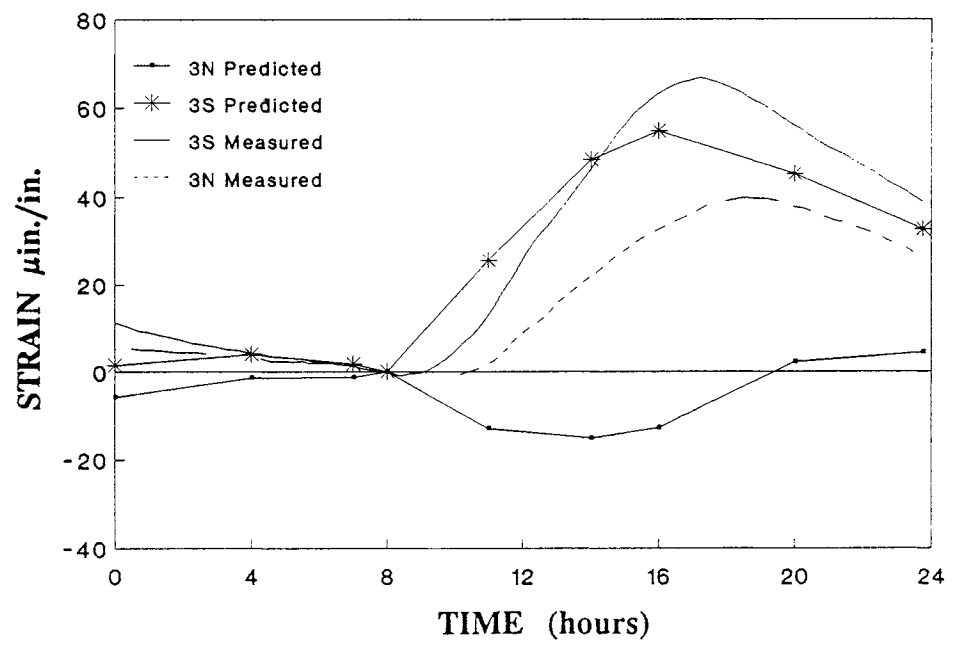


Figure 67. Comparison of Measured and Predicted Strain Variations, Pylon Segment D6, 11/17/89.

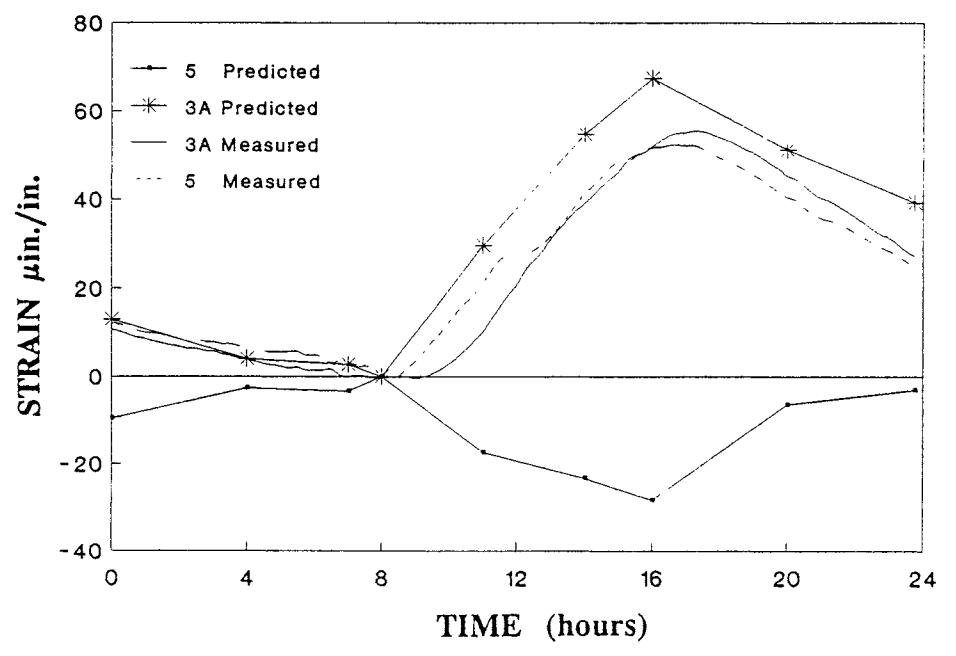


Figure 68. Comparison of Measured and Predicted Strain Variations, Cast-in-Place Pylon, 11/17/89.

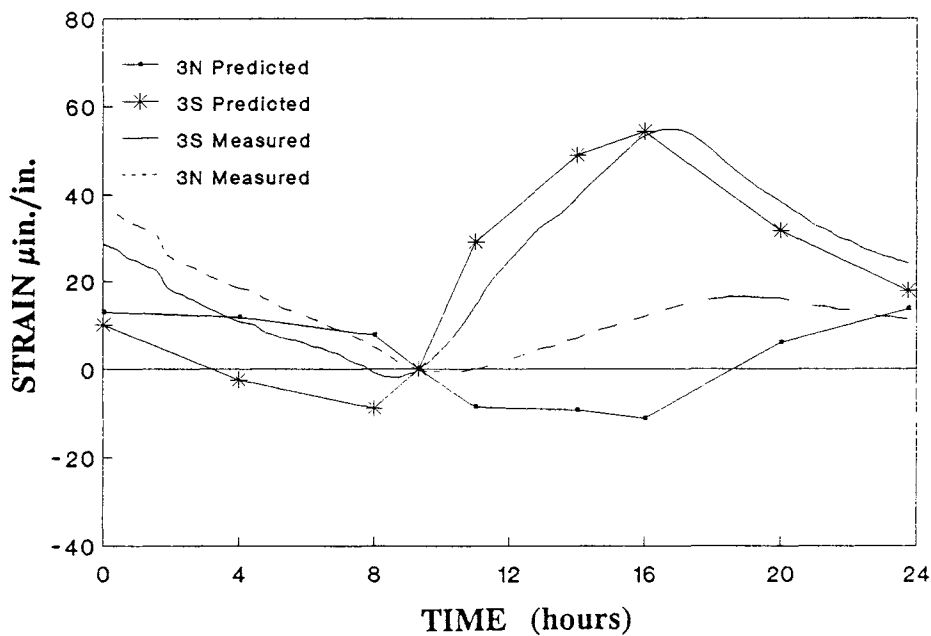


Figure 69. Comparison of Measured and Predicted Strain Variations, Pylon Segment D6, 11/18/89.

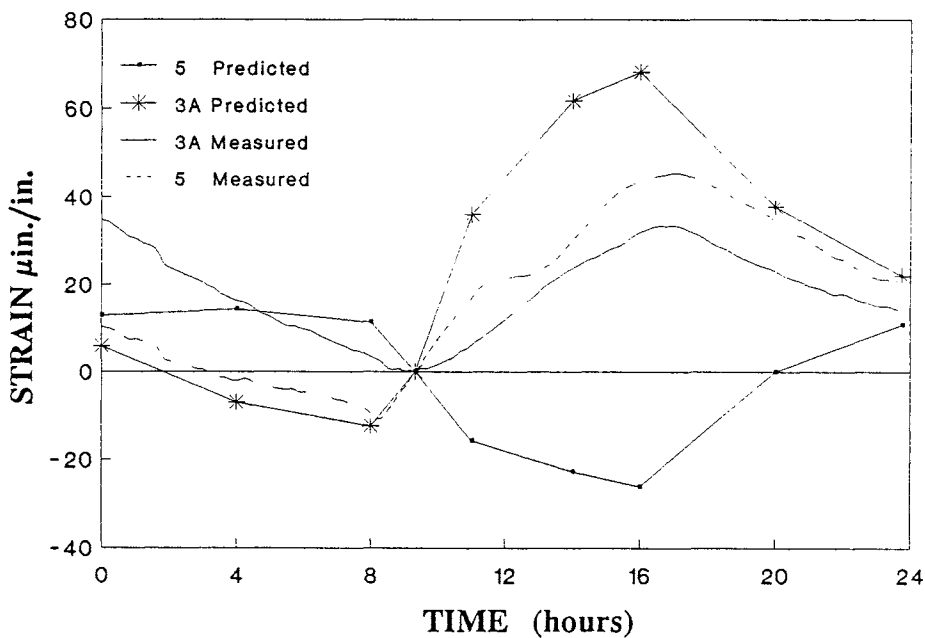


Figure 70. Comparison of Measured and Predicted Strain Variations, Cast-in-Place Pylon, 11/18/89.

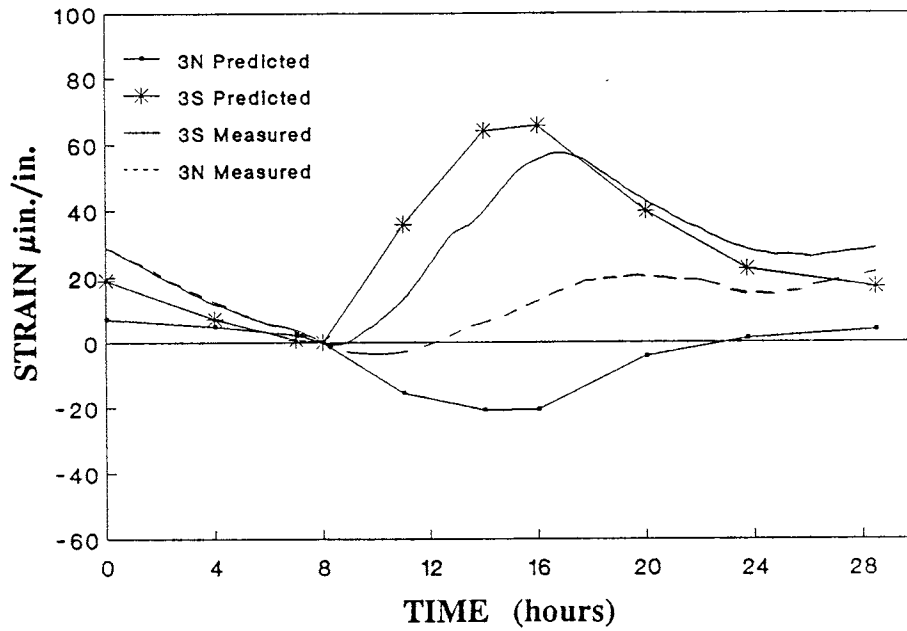


Figure 71. Comparison of Measured and Predicted Strain Variations, Pylon Segment D6, 11/19/89.

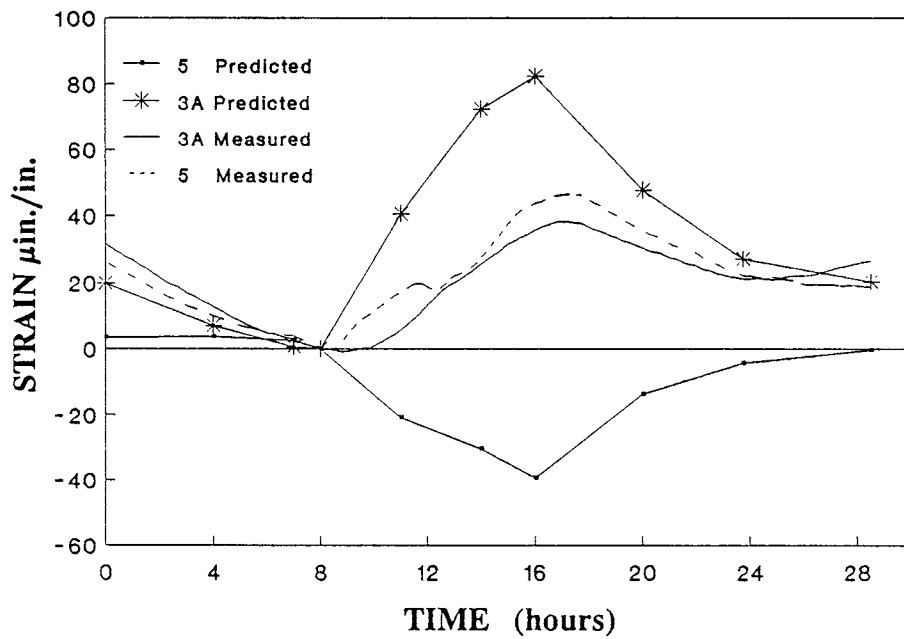


Figure 72. Comparison of Measured and Predicted Strain Variations, Cast-in-Place Pylon, 11/19/89.

The predicted strain variations for segment D6, presented in Figures 67, 69, and 71, indicate that similar relative strain values were calculated for each of the 3 days under consideration. Noticeably different behavior was predicted for the northern and southern portions of the segment. At the south end, the calculated relative strains decreased during the morning, then increased during the afternoon. Peak values of relative tensile strains, on the order of 50 microstrains, were consistently calculated each day at 16:00 hr. Similar trends in predicted response were observed at the north end of the segment prior to 8 A.M. During the afternoon, however, relative compressive strains with magnitudes ranging between 10 and 20 microstrains were calculated. A comparison with the strain data measured at corresponding locations indicated that the strain response was predicted more accurately at the south end of the section. The relative tensile strains measured at gage 3N, between 8:00 and 24:00 hr, were not reflected in the calculated response from the northern portion of the section. The small strain variations observed at the north and south ends of the section prior to 8 A.M. corresponded reasonably well with predicted values.

Similar strain variations were calculated for locations within the cast-in-place section, as indicated in Figures 68, 70, and 72. Again, consistent variations were predicted for the northern and southern portions of the pylon on each of the 3 days. Prior to 8 A.M., calculated values at either location were less than 10 microstrains. During the afternoon, relative tensile and compressive strain variations were calculated for the south and north ends of the cross section, respectively. At 16:00 hr, relative tensile strains of approximately 70 microstrains were predicted at the north end, and relative compressive variations on the order of 30 to 40 microstrains were predicted for the south. A comparison with the corresponding measured data again indicates only limited correlation with the predicted response values. At the south end of the cast-in-place section, the calculated strain variations were consistently larger than those measured at gage 3S. After 8 A.M., the compressive strain variations predicted for the north end of the section did not reflect the relative tensile strains measured at gage 3N.

The predicted strain variations presented in Figures 67 through 72 indicated that the analytical procedure was limited in its ability to predict the measured strain response within the pylon. A comparison of the measured and predicted strain values showed that, although the overall trends in strain variation could be calculated with reasonable accuracy, the analysis was unable to predict the local variations shown by the measured data. In addition to the approximations discussed previously for the box girder, assumptions regarding the temperature distribution within the pylon may have limited the accuracy of the analysis. The temperatures measured by the thermocouples in segment D6 were assumed to represent the temperatures throughout the pylon, resulting in larger differences between measured and calculated strain variations at the cast-in-place section. In addition, the temperature distribution in each section was approximated as a piece-wise linear function between thermocouples, through the center of the cross section, which largely ignored localized temperature differences.

## DISCUSSION

The measured temperature and strain data illustrated the complexity of the thermal response of the structure. The temperatures at locations within the cross section of the box girder and pylon members varied continuously and were significantly influenced by localized climatic conditions. As expected, larger diurnal temperature variations were observed at locations subject to direct solar radiation, such as the top flange of the box girders and the southern portions of the pylon. Significant differences in temperature were also measured between the interior and exterior of the pylon section, especially during the afternoon hours.

Strain variations measured in the instrumented box girder segments reflected the cyclical temperature-induced response of the structure. Comparable strain data were recorded in the two box girder segments, though slightly larger relative strain variations were observed at segment 33. Strains measured in the top and bottom flanges of the box girder were similar in overall trend and magnitude. In general, the strain variations recorded by gages in the box girder segments followed similar daily trends, in which the relative compressive strains observed during the morning hours were followed by relative tensile strains for the latter half of the day. Localized thermal effects in the top flange of the box girder were illustrated by differences in measured response between gages during the afternoon hours. Consistent strain variations were recorded at gages having similar locations within the cross section of the segments.

The strain variations recorded at the pylon segments also reflected the overall thermal response of the structure. Comparable daily strain variations were measured at precast segment D6 and at the top of the cast-in-place portion of the pylon. Similar magnitudes of relative strain were recorded at the two sections, and consistent relative tensile strain variations were observed at locations across each cross section. The measured strain data were indicative of the global response of the pylon as well as localized behavior attributable to differential heating effects.

Measured temperature distribution data from the box girder and pylon sections were used in conjunction with a three-dimensional beam element model to predict average thermally induced strain variations within the structure. Calculated strain results were indicative of significantly dissimilar behavior between the top and bottom flanges of the box girder. The predicted strain variations showed relatively poor correlation with the measured data, however. The assumed thermal strains in the cable stays had a significant effect on the magnitude of calculated strains in the box girder but had little influence on the overall trends of the predicted strain response. The thermal response data obtained from a three-dimensional plate element model were consistent with those from the simpler beam element model and showed variations in strain across the flanges of the box girder. Predicted strain variations for the pylon sections showed more favorable correlation with measured data but did not accurately reflect the relative tensile strain variations observed at the northern portion of the cross section. In general, the analytical procedures were able to predict the thermally induced strains within the same

order of magnitude as those measured in the bridge, but they did not have the sensitivity to account for the local effects observed in the measured data.

This study revealed the many difficulties associated with field instrumentation and testing of structures, especially under construction conditions. The individual bridge segments were formed in the casting yard at the foot of the bridge. Although it was easier to install the instrumentation there, rather than on the structure itself, there were logistical problems with materials and scheduling, which were further compounded by the 90-mile driving distance between the bridge and VTRC. Despite the best efforts of the researchers, it was difficult to protect the equipment from damage caused by construction activities. As a result, a significant number of strain gages and thermocouples were inoperative and constant repairs to the data lines were necessary. Also, the harsh construction and field environment was damaging to the sensitive electronic equipment and has led to serious questions concerning the reliability of the data acquisition system.

Analysis of the measured strain and temperature data indicated a number of deficiencies in the instrumentation and data acquisition system. Malfunctions within the remote scanning chasses were difficult to diagnose and repair and resulted in significant losses of data. Thermal strain corrections were influenced by temperature approximations based on the measured thermocouple data. Large thermal gradients were observed through the flanges of the box girder, and more accurate corrections could be made by installing thermocouples adjacent to each strain gage. Additional thermocouples installed within the webs of the box girders would provide a more detailed temperature distribution within the cross section, thereby improving the accuracy of the predicted thermal response of the structure. Thermocouples installed in a few of the cable stays would eliminate the uncertainties caused by assuming the variations of thermal strain within these members. Additional thermocouple instrumentation would have required a reduction in the number of strain gages installed within the segments, but the reduced amount of strain data would be offset by the improved overall accuracy and reliability provided by more thermocouples.

Large differences between measured and predicted response led to a critical evaluation of each component of the strain-measuring instrumentation. Although the measured data were determined to represent the actual response of the structure, this evaluation raised serious questions regarding the reliability of the data acquisition system. Installation of another system of strain-measuring devices, such as Carlson strain meters, in addition to the strain-gaged rebar, would provide an independent check on the system components. The daily variations of strain recorded indicated that the thermal response of the structure was measurable, though not significantly large. Measurement of the thermal response during the early summer months would yield critical strain variations within the structure.

## CONCLUSIONS

1. The temperature distribution in both the box girders and the pylons of the I-295 bridge is nonlinear. The more massive the element, the more gradual the temperature changes away from the outside surfaces. Thus, the pylon interior temperatures reflected only the long-term mean temperature variation, whereas the box girder elements reflected diurnal changes in temperature throughout the thickness of the elements.
2. Elements of the bridge on the windward side appear to undergo more rapid temperature variation than those away from the wind, as would be expected. Sheltered regions of the bridge, such as the webs between the twin box girders, undergo relatively small diurnal changes that are driven by the ambient air temperature and heat conduction from the other elements.
3. The longitudinal strains measured as a result of diurnal temperature changes form a complex three-dimensional field. The measured strains were of the same order of magnitude as those caused by a fully loaded dump truck traversing the bridge. Even larger strains in the box girders than those measured are anticipated to occur during the summer months, when the angle of solar incidence is higher. On the other hand, the solar incidence on the vertical pylon surfaces is greater during the winter months.
4. Attempts to predict the strain field using finite element models had only limited success. A frame element model was unable to predict the across-bridge variations that were particularly evident on the top flange. The moments applied accounted for only the vertical variation of temperatures. Accurate determination of thermal strains from temperature data must account for the horizontal as well as the vertical variation of temperatures.
5. A plate element model appeared to have some ability to predict the across-bridge strain variations. The plate element model used was designed to account for vertical plane variations only and used a vertical plane of symmetry along the bridge center line, so it did not adequately model the horizontal variation of the strain field.
6. Strain-gaged dummy reinforcing bars did not provide a sufficiently reliable transducer for the measurement of long-term thermal strains. In particular, two deficiencies were noted: (a) the thermal modulus of the steel and the concrete, although nominally the same, actually differ by a sufficient amount to introduce strains of almost the same order of magnitude as the strains being measured, and (b) the half-bridge gages mounted on the curve did not eliminate the temperature dependence of the strain readings. Corrections for these effects were introduced and used in the calculations, but it appears that the corrections are only approximate.

## RECOMMENDATIONS

1. Development of a true three-dimensional finite element with no assumption of symmetry about the center line should be investigated as a means of improving comparison between the predicted and measured thermal strains.
2. Laboratory studies conducted under field temperature conditions are needed to develop further strain-measuring systems that are quick and inexpensive to install but that will perform reliably under field conditions in measuring thermally induced strains. Particular problems that need to be resolved include those encountered with the dummy strain-gaged reinforcing bars on the present instrumentation project. In addition, quick connect (plug in) transducer line connectors need to be investigated for thermal noise contributions since they would greatly facilitate the installation of such systems during construction operations.
3. Little is known of the temperature distribution within cable stays of cable-stayed bridges. A study could be carried out with a relatively short length of stay cable insulated at either end and mounted at the appropriate angle. Such an experiment would be relatively inexpensive to conduct.



## REFERENCES

- Baber, T.T., & Hilton, M.H. (1988). *Field monitoring on the I-295 bridge over the James River: Instrumentation installation and construction period studies*. Charlottesville: Virginia Transportation Research Council.
- Barton, F.W., Baber, T.T., Duemmel, P.S., & McKeel, W.T., Jr. (1991). Field test of a cable-stayed bridge. *Transportation Research Record 1290*. Washington, DC: Transportation Research Board.
- Churchward, A.J., & Sokel, Y.J. (1980). Thermal responses in concrete bridges, Brisbane. *ARRB Proceedings*, 10(3): 87-93.
- Dilger, W.H., Ghali, A., Chan, M., Cheung, M.S., & Maes, M.A. (1983). Temperature stresses in composite box girder bridges. *Journal of Structural Engineering*, 109(6): 1460-1476.
- Duemmel, P.S., Baber, T.T., Barton, F.W., & McKeel, W.T., Jr. (1991). *Field instrumentation and measured response of the I-295 cable-stayed bridge: Part 1—Field study of live load responses*. VTRC Report No. 92-R19. Charlottesville: Virginia Transportation Research Council.
- Elbadry, M.M., & Ghali, A. (1983). Thermal variations in concrete bridges. *Journal of Structural Engineering*, 109(10): 2355-2374.
- Elbadry, M.M., & Ghali, A. (1986). Thermal stresses and cracking of concrete bridges. *Journal of the American Concrete Institute*, 83(6): 1001-1009.
- Hayes, S.W. (1988). *Implementation of the data acquisition system for the I-295 James River Bridge*. Masters thesis. Charlottesville: University of Virginia, Department of Civil Engineering.
- Imbsen, R.A., Vandershaf, D.E., Schamber, R.A., & Nutt, R.V. (1985). *Thermal effects in concrete bridge superstructures*. NCHRP Report No. 276. Washington, DC: Transportation Research Board.
- Mathivat, J. (1983). *The cantilever construction of prestressed concrete bridges*. New York: John Wiley & Sons.
- Measurements Group, Inc. (1983). *Temperature induced apparent strain and gage factor variation in strain gages*. Technical Note No. TN-504. Raleigh, NC.
- Mohr, M. (1989). *The strain gage instrumentation of cables on the I-295 James River cable-stayed bridge*. Masters thesis. Charlottesville: University of Virginia, Department of Civil Engineering.
- Muller, J.M., & McCallister, L.F. (1988). Esthetics and concrete segmental bridges in the United States. *Concrete International*, 10(5): 25-33.
- Podolny, W., Jr. (1985). The causes of cracking in post-tensioned concrete box girder bridges and retrofit procedures. *Prestressed Concrete Institute Journal*, March/April, pp. 82-139.

- Post-Tensioning Institute/Prestressed Concrete Institute. (1978). *Precast segmental box girder bridge manual*. Glenville, IL.
- Potgieter, I.C., & Gamble, W.L. (1983). *Response of highway bridges to nonlinear temperature distributions*. University of Illinois at Urbana-Champaign.
- Priestly, M.J.N. (1978). Design of concrete bridges or temperature gradients. *ACI Journal*, 75: 5.
- Rao, D.S. (1986). Temperature distributions and stresses in concrete bridges. *Journal of the American Concrete Institute*, 83(4): 588-596.
- Waldron, P. (1986). Stiffness analysis of thin-walled girders. *Journal of Structural Engineering*, 112(6): 1366-1384.
- Waldron, P., Ramezankhani, M., & Woodman, N. (1990). Differential temperature effects in concrete box girder bridges. *Proceedings of the Developments in Short and Medium Span Bridge Engineering '90*, Supplement, pp. 1-12. Toronto, Ontario, Canada: Canadian Society of Civil Engineers.
- Yen, Y.-H. (1992). *Modal identification of bridge structures*. Ph.D. dissertation in progress. Charlottesville: University of Virginia, Department of Civil Engineering.